BIOANALYTICAL METHODS DEVELOPMENT FOR DETECTION AND CHARACTERIZATION OF LABILE METAL POOLS IN *ESCHERICHIA COLI*

A Dissertation

by

HAYLEY NICOLE BRAWLEY

Submitted to the Office of Graduate and Professional Studies of
Texas A&M University
in partial fulfillment of the requirements for the degree of

DOCTOR OF PHILOSOPHY

Chair of Committee,	Paul A. Lindahl
Committee Members,	David H. Russell
	Marcetta Y. Darensbourg
	Vishal M. Gohil
Head of Department,	Simon W. North

August 2021

Major Subject: Chemistry

ABSTRACT

Low-molecular-mass (LMM) transition metal complexes are thought to play essential roles in metal ion trafficking, regulation, and signaling in biological systems. Their chemical identities remain largely unknown due to their rapid ligand-exchange rates and weak metal-ligand bonds. Lack of chemical characterization unfortunately precludes biological function. In this dissertation, methods were developed and ameliorated for an integrative approach using LC, ICP-MS, and ESI-MS to investigate the chemical nature of the labile metal pools (LMP) constituting the *E. coli* cytosol.

An *E. coli* cytosol isolation procedure was developed that was devoid of detergents, strongly coordinating buffers, and EDTA. The interaction of metal ions from LMM metal complexes with a SEC column was minimized by pre-loading the column with $^{67}ZnSO_4$. FTSs contained ca. 80 μM iron, 15 μM nickel, 13 μM zinc, 10 μM copper, and 1.4 μM manganese. FTSs chromatographically exhibited 2 – 5 iron, 2 nickel, 2 – 5 zinc, 2 – 4 copper, and 2 manganese species. Endogenous cytosolic salts suppressed ESI-MS signals, making detection of LMM metal complexes difficult. Major LMM sulfur- and phosphorus-containing species were identified, though. These included GSH, GSSG, methionine, cysteine, orthophosphate, and common mono- and dinucleotides such as ATP, ADP, AMP, and NADH. FTSs from cells grown in media supplemented with one of these metal salts exhibited increased peak intensity for the supplemented metal indicating that the size of the LMPs is sensitive to the nutrient metal concentration whereas treatment of the FTS with a metal chelator demonstrated the lability of these LMM metal complexes.

The labile nickel pool (LNP) was selected for further identification efforts based on water-exchanging rates for transition metals. SEC-ICP-MS revealed 4 Ni-containing peaks, which were tentatively assigned to Ni(GSSG), Ni(Asp), Ni(L-His), and Ni(ATP) due to chromatographic behavior of nickel standards and results from exogenous nickel and ligand spiking into FTS. ESI-MS analysis of SEC fractions from FTS revealed Ni(GSSG), suggesting Ni(GSSG) is part of the LNP. HILIC-ESI-MS and HILIC-ICP-MS revealed Ni(GSSG) as the dominant Ni(II) species in the FTS followed by $Ni(L\text{-}His)_2$ and then $Ni(Asp)_2$ and Ni(ATP), showcasing the first molecular description of a LMP in *E. coli*.

DEDICATION

Growing up in a time period when the voices of women have become too loud to dismiss, when women are invited to sit at the table, and when woman are celebrated for their many contributions to society, it is only fitting that this work be dedicated to the influential women who have me given the motivation, support, praise, and above all else, love to mature into the woman, leader, and scientist I am today. I, specifically, want to dedicate a portion of this work to Teresa Sowell, my high school AP statistics teacher – now, lifelong mentor. You ignited me on this research-forward journey, always encouraging me to pursue better but not to get lost in trying to be the best. I also want to dedicate this work to my kind-hearted nana, Norma Heacox. Your relentless support and constant reminders of "things will work out" diminished doubt and instilled confidence, even from hundreds of miles of way. And, indeed, things did always work out. Lastly, I dedicate this work to my late mother, Melody Heacox. Every day you serve as motivation, and your presence is found in many ways around and through me.

ACKNOWLEDGEMENTS

The culmination of work into this dissertation could not have been completed without the guidance, assistance, and support of many persons. The first of which is my PhD advisor, Dr. Paul Lindahl. I cannot thank him enough for the independence and trust he bestowed in me, even in my early days in the laboratory. He gave me the freedom to investigate, tinker, and importantly, fail (and subsequently learn from those failures). He was always enthusiastic about our endeavors, and my thoughts and opinions always felt welcomed and considered. Thank you, Dr. Lindahl, for all of the opportunities you provided and/or allowed that cultivated my personal growth as both a scientist and as a leader. You've been a wonderful advisor, a formidable half-marathon competitor, and a true lifesaver (yes, I made a glovebox joke).

I would like to extend my gratitude to each of my committee members – Dr. David Russell, Dr. Marcetta Darensbourg, and Dr. Vishal Gohil. They always made the time to thoughtfully listen and provide critical feedback and insightful suggestions on my projects. They remained positive and encouraging towards my progress and goals but also stressed the importance of focus and controlled experiments, which was invaluable advice towards this endpoint.

In addition, I would like to thank members of the Lindahl laboratory for their camaraderie and scholarly advice. Specifically, thank you to Dr. Nathanial Dziuba for the LC and ICP-MS training and for fielding my insistent questions on such. Thank you to Dr. Trang Nguyen for training me in standard biological/biochemical techniques and for always asking the nitty-gritty questions during group meetings; these types of questions really encouraged me to understand the 'how' and 'whys' of my research. Thank you to current laboratory members – Joshua Kim, Rachel Shepherd, Waseem Vali, Alexia Kreinbrink, Salvador Fernandez, and Grant Delanoy – for thought-provoking and gut-busting conversation, sharing laboratory chores, and providing morale

(most notably through the candy bowl). Our small, tight-knit group made it feel like we were a (wacky) family. I wish you all the best of luck in your remaining studies and in your journey beyond Texas A&M. Always remember… "it's in the drive."

I would also like to acknowledge the incredible team of Agilent field service engineers (FSE) and application scientists I had the pleasure of working with during my time in the Lindahl laboratory for our LC and ICP-MS systems. My extensive training in HPLC and ICP-MS was only enhanced by these interactions. I would specifically like to call out Graham Oltjen, our HPLC FSE, who repeatedly made himself available to troubleshoot or discuss concepts long past the technical call being closed and the bill paid.

Dr. Yohannes Rezenom of the Department of Chemistry's Mass Spectrometry Facility played an instrumental role in this work by performing ESI-MS analysis and aiding in HILIC method development. Yohannes consistently had a positive attitude no matter the number of samples I brought to him with 'x' number of conditions to test. It was a pleasure to work with him. He, along with many other administrative and support staff (from Mr. James Kirby of the stockroom to Ms. Sandra Horton of the graduate office) were valuable resources to me during my graduate studies.

Additionally, I would like to acknowledge the Graduate Student Association of Chemistry (GSAC) and Phi Lambda Upsilon (PLU) as well as my fellow graduate students who I had the honor of serving alongside or leading in these organizations over the years. Not only were the skills I gained being a part of these organizations invaluable, but these organizations also provided an outlet from the laboratory for socializing, outreach, and professional development. With this, I would also like to thank once again the administrative staff who I had the pleasure of working with through these organizations for your time, service, and professionalism.

Thank you to my doting family, especially, my dad, Mark Heacox. You have been a constant source of encouragement throughout my entire education. Thank you for serving as a tele-therapist for my up-and-down relationship with the LC-ICP-MS. Certainly, thank you for moving closer; I'm glad it only takes a 4-hr drive to have in-person conversation now, even if I did have to move your furniture in return. I would also like to thank my in-laws, Kelli and Tom Brawley for their support. Thank you for both for showing interest in my research and in my well-being. Thank you for all of the comfort you have provided over the years.

To all my friends, those in Texas and those not, thank you for riding alongside me through this process. With all the twists and turns, you all kept me grounded, sane, and well-rounded. I cherish all of the friendships that have lasted and all the new ones that begun.

Last, but certainly not least, I have to thank my husband, Zach Brawley. Thank you for the personal sacrifices you made so that I could succeed and for letting me put my education before you some days. Thank you for also removing me from this mindset and for reminding to 'stop and smell the roses.' You were there every day, for better or worse, to ask questions, to congratulate me when an experiment went well, to comfort me when my instrumentation was down, to provide suggestions, and the list goes on. As a fellow graduate student, you understood the mentality of the process and accepted all the emotions and reactions that come with such. Additionally, thank you, willingly or not, for accepting my wild work schedule. You have consistently pushed me towards betterment. You are my partner, and this dissertation not only represents a culmination of my research efforts, but also represents another chapter in our story. I love you.

CONTRIBUTORS AND FUNDING SOURCES

Contributors

This work was supervised by a dissertation committee consisting of Professors Paul A. Lindahl, David H. Russell, and Marcetta Y. Darensbourg of the Department of Chemistry and Professor Vishal M. Gohil of the Department of Biochemistry and Biophysics.

The *E. coli* K-12 MG1655 wild-type strain and the bacteriophage-containing plasmid pZa31mycR used in Chapters III and IV were generously provided by Professor Ryland Young (Texas A&M University). ESI-MS spectra in Chapters III and IV were collected by Dr. Yohannes Rezenom of the Texas A&M Chemistry Mass Spectrometry Facility.

All other work conducted for the dissertation was completed by the student independently.

Funding Sources

This work was made possible in part by the National Institutes of Health (GM127021), the National Science Foundation (MCB-1817389), and the Robert A. Welch Foundation (A1170). The content of this article is solely the responsibility of the authors and does not necessarily represent the official views of the NIH, NSF, or the Welch Foundation.

NOMENCLATURE

AA	ammonium acetate
ACN	acetonitrile
ADP	adenosine diphosphate
AMP	adenosine monophosphate
ATP	adenosine triphosphate
BPY	2,2-bipyridine
CV	column volume
DP	double peptide
EDTA	ethylenediaminetetraacetic acid
ESI-MS	electrospray ionization mass spectrometry
FTS	flow-through-solution
GSH	reduced glutathione
GSSG	oxidized glutathione
HILIC	hydrophilic interaction chromatography
HPW	high-purity water
ICP-MS	inductively coupled plasma mass spectrometry
LC	liquid chromatography
LMM	low-molecular-mass
LMP	labile metal pool
LNP	labile nickel pool
NADH	reduced nicotinamide adenine dinucleotide
NADPH	reduced nicotinamide adenine dinucleotide phosphate

NMR	nuclear magnetic resonance
OD_{600}	optical density measured at 600 nm
pFTS	pseudo-FTS
phen	1,10-phenanthroline
SEC	size exclusion chromatography
SP	single peptide
V_e	elution volume
V_0	void volume
WC	whole cell

TABLE OF CONTENTS

Page

LIST OF FIGURES

Page

LIST OF TABLES

Page

CHAPTER 1

INTRODUCTION

Metal Ion Homeostasis in Bacteria

The first-row late d-block metal ions, including manganese (Mn), iron (Fe), nickel (Ni), copper (Cu) and zinc (Zn), have unique and exceptional catalytic properties which make them indispensable for life.[1] They are typically installed into the active sites of metalloenzymes where they orchestrate catalytic events, often involving substrate binding, electron transfer, and/or small-molecule activation. It has been suggested that approximately one third of all proteins require metals for their biological roles and almost half of all enzymes must associate with one or more metal ions.[2] The presence of metalloproteins necessitates a tight regulation of metal metabolism and homeostasis to maintain the appropriate metal concentration in the cell while avoiding toxicity, which includes transport, delivery, storage, detoxification, and efflux machineries.[3] This is further substantiated by the fact that many iron and copper complexes react with O_2 or H_2O_2 (via the Fenton or Haber-Weiss reactions) to generate reactive oxygen species that damage DNA, membranes, proteins, and other essential cellular components.[4,5]

Labile Metal Pools

The total metal content of the bacterial cell (atoms/cell) is defined as the quota and reflects the overall demand for metals to support growth, with the majority of metal quotas arising from metalloproteins/metalloenzymes. The labile metal pool (LMP) can be defined as that portion of the total metal quota that is accessible to a chelator *in vivo*.[6] Neither the exact chemical compositions of these metal complexes nor their cellular functions are established.[7] This knowledge-gap is due, in large measure, to their *lability* – i.e. they possess ligands that exchange

rapidly due to the inherent weakness of metal-ligand coordinate bonds. It is hypothesized that nascent proteins acquire their metal cofactors during synthesis from this labile pool of exchangeable metal ions and that metalloregulatory proteins monitor the status of this same pool.[6] The properties of the LMP are determined, in part by the overall avarice with which metals bind to ligands, as described in the Irving-Williams series [Cu(II) > Zn(II) > Ni(II) > Co(II) > Fe(II) > Mn(II) > Mg(II) > Ca(II)] and by the variety and affinity of potential metal ligands in the cytosol.[8,9] Such labile complexes are presumed to have non-proteinaceous ligands composed of metabolites possessing O, N, and/or S Lewis-basic donor atoms, and thus are also referred to as low-molecular-mass (LMM) metal pools.[10]

The Nature of Metal Complexation with Low-Molecular-Mass Ligands

During complex formation in an aqueous medium, two types of stabilities are considered – thermodynamic stability and kinetic stability.[11] The thermodynamic stability of metal complexes is determined by the Gibbs free energy, which has an enthalpic and an entropic contribution. The entropic contribution to complex stabilization derives from the metal ion preference for particular donors while the entropic contribution to complex stabilization derives mostly from the chelate effect and the structure of the LMM ligand when it changes during complexation.[12]

In regard to enthalpy, stabilization derives from the metal ion preference for particular donors.[12] Concepts have been developed that attempt to predict this preference. The first is a concept that groups metal ions into two categories, A and B; this grouping depends on whether the complex is more stable with a donor atom from a member of the first periodic group or with a member of a subsequent group.[13] In the other concept, metal ions and ligands are grouped into soft and hard acids and bases depending on the degree of their polarizability.[14] Many biologically

important metal ions belong to a borderline category of acids with a tendency to form stable complexes with moderately polarizable ligands (bases) such as nitrogen donors. The borderline character of these metal ions is also seen in their tendency to form complexes with both hard oxygen and soft sulfur donors. Additional interactions such as hydrogen bonding and electrostatic interactions within the ligand formed during the complexation may also affect the stability significantly.[12]

The kinetic stability of metal complexes refers to reactivity, and labile and inert are descriptors of this type of stability.[11] Factors that affect rates of ligand substitution reactions can also affect thermodynamic stability; however, it is incorrect to assume that stability is always correlated with certain reaction rates.

All biologically important molecules such as amino acids, peptides, metabolites, carbohydrates, nucleotides, DNA and RNA, and vitamins contain atoms that can serve as electron pair donors for metal coordination and therefore can be considered as potential ligands. The most commonly proposed LMM ligands include metabolically relevant carboxylic acids (pyruvate, malate, citrate, etc.), amino acids (histidine, glutamate, cysteine, and aspartate), nucleotides (AMP, ADP, and ATP), and redox buffers (reduced and oxidized glutathione).[10] The cellular concentration of LMM ligands is in excess (hundreds of micromolar to millimolar range) as compared to the coordinated metal's concentration (hundreds of nanomolar to micromolar range).[12]

Metalloregulation

In bacterial cells, a panel of DNA binding transcriptional regulators, termed metalloregulatory proteins or metallosensors, collectively manage the bioavailability of transition

metals in the cell cytoplasm.[3] They do this by forming coordination complexes with a specific metal, and in turn, coordination allosterically activates or inhibits binding to a DNA operator that often overlaps with the promoter. Metalloregulatory protein binding here regulates either physical access or the activity of RNA polymerase, thus controlling the expression of downstream genes. Downstream genes typically encode metal transporters, metallochaperones, metal-storage proteins, or metal efflux systems, thus connecting metallosensor metal binding to transcriptional control of the adaptive response to too little or toxic concentrations of a specific metal. Cognate metal ion binding can drive transcriptional derepression (mediated by allosteric inhibition of DNA operator binding by metal), transcriptional activation (mediated by metal-dependent conformational changes on the bound DNA), or transcriptional co-repression (mediated by allosteric activation of DNA binding) of downstream genes.[3]

Based on metalloregulator affinities, Hellman and coworkers proposed that the LMP serves as a buffer such that the LMP is in equilibrium with metal ions at a thermodynamically defined concentration of hydrated metal ions.[6] For example, when aqueous metals exceed the dissociation constant (K_d) of the metalloregulator, the cell responds appropriately by repression of uptake or derepression of efflux and storage functions as stated above. The equilibrium concentration of aqueous metals in the cell varies over many orders of magnitude, once again based on the Irving-Williams series.

Metal Ion Homeostasis in *Escherichia coli*

In this section, we overview metal trafficking (the translocation of a metal from the plasma membrane where it enters the cell to the site of installation into its "client" apo-protein) and regulation (the transcriptional repression and de-repression of metal import and export systems)

for manganese, iron, nickel, zinc, and copper (biologically relevant metals pertinent to this dissertation) in the model gram-negative bacterium, *Escherichia coli*, with pertinent insight into the role of LMPs and metallochaperones in these cellular functions.

Manganese

E. coli employs manganese to activate a variety of enzymes, but only does when iron is unavailable or when the cell is assaulted by oxidants.[15] Manganese homeostasis in *E. coli* constitutes a Mn-dependent transcriptional regulator, MntR, which upregulates the Mn efflux pump, MntP, and downregulates the Mn importer, MntH. MntS is a small protein (ca. 5031 Da) that is synthesized when manganese levels decline. Specifically, MntS helps to increase the bioavailable Mn(II) by acting as inhibitor of MntP. Additionally, it has been proposed that MntS serves as a chaperone in *E. coli*.[15]

Spectroscopic and kinetic modeling insights provide strong support for the proposal that specific LMM Mn(II) complexes are catalytically competent and functionally important in clearing superoxide from *E. coli* in a way that supplements SOD-dependent mechanisms.[16] For example, simple $Mn(phosphate)_n$ and $Mn(carbonate)_n$ complexes are efficient catalysts of superoxide disproportionation, and this catalysis occurs at physiologically relevant rates and metabolite concentrations, which may explain studies that connect oxidative stress resistance to phosphate accumulation and/or changes in phosphate metabolism. Additionally, manganese carbonate complexes have been shown to catalyze the decomposition of H_2O_2 suggesting that other small molecule Mn(II) complexes can potentially function downstream of superoxide, although this reaction has not been thoroughly investigated.[17]

Iron

Iron is required for the growth of *E. coli* as it is present in heme proteins, iron–sulfur cluster proteins, and di-iron and mononuclear enzymes among others.[18] The Fur (ferric uptake regulator) system regulates cellular iron by binding Fe(II) ions, likely from the labile cytosolic iron pool, and regulating transcription of more than 100 genes involved in iron import, trafficking, and storage as well as in iron-dependent enzyme catalysis and cellular metabolism.[19] However, iron-bound Fur has never been isolated from any bacteria.[20] Recently, Fontenot *et al*. reported that Fur instead senses the intracellular "free" iron content via reversible binding of a [2Fe-2S] cluster.[20]

Under iron-deplete conditions within *E. coli*, the loss of Fur DNA-binding activity results in expression of the RyhB, a small RNA, that represses translation of non-essential iron-enzymes[21], while triggering synthesis of iron uptake systems such as the high-affinity Fe(III)-chelating siderophore, enterobactin, and its cognate import system and the Fe(II) import system, Feo, predominantly expressed under anaerobic conditions.[22] Fe(II) can additionally enter the cell via MntH. Under iron-replete conditions, Fur positively regulates expression of iron storage functions (including heme-containing bacterioferritins, ferritins, and Dps-family mini-ferritins) as well as the iron efflux system, FieF (or Yiip).[21]

Wofford *et al.* isolated two LMM Fe(II) complexes from *E. coli*, which they concluded constituted the labile iron pool.[19] They determined that the concentration of this pool varied inversely with oxygen exposure during cell growth such that the labile iron pool increased with anaerobicity as previously observed by Beauchene *et al*.[23] Additionally, Wofford *et al.* examined this pool via Mössbauer spectroscopy and found that the isomer shift, δ, and quadrupole splitting, ΔE_Q, parameters for the labile iron pool corresponded to a non-heme high-spin Fe(II) complex coordinated by O/N-containing ligands.[19] They hypothesized that this pool is involved in iron

trafficking and/or regulation and that it may also serve as a feedstock for building iron-sulfur clusters as the iron donor for such remains elusive.[24]

Nickel

Nickel is utilized by *E. coli* among other prokaryotes and simple eukaryotes in the active sites of various enzymes for catalysis in systems such as carbon monoxide and carbon dioxide metabolism, hydrogen uptake and production, and urea hydrolysis.[25] A hydrogenase-specific nickel transporter, NikABCDE, is synthesized under anaerobic growth conditions in accordance with the nickel-requirement.[26] Its expression is positively regulated by the global Fumarate Nitrate Reductase regulator (FNR) when the oxygen concentration drops below 0.5%, and repressed by the metalloregulator NikR in the presence of excess nickel.[27] Nickel is inserted into this cluster by a dedicated metallochaperone complex that is composed of HypA, HypB, and SlyD.[28] Based on the ability of SlyD to bind multiple metal ions, it is thought that SlyD contributes to Ni(II) storage and is a possible source for Ni(II) ions during [Ni-Fe]-hydrogenase assembly in *E. coli*.

Assembly of the hydrogenase active site [Ni-Fe] metallocluster must compete with NikR for Ni(II) ions to ensure optimal NikABCDE expression for the prevailing growth condition.[26] However, genetic data indicates that NikR function is independent of NikABCDE function[29], suggesting the presence of a second nickel transporter in *E. coli*. The enzymatic nickel requirement for glyoxalase I (Glx I) activity[30] (under aerobic and anaerobic conditions) further supports this notion.

RcnR is an additional regulatory protein that when nickel-bound, activates transcription of RcnAB, a nickel efflux pump consisting of a membrane permease (RcnA) and a periplasmic protein (RcnB). RcnAB not only prevents accumulation of toxic nickel levels but also blocks

premature activation of NikR through competition for Ni(II), allowing nickel ions to be trafficked to the hydrogenase enzymes.[26] The Ni(II) substrate for the regulatory proteins, NikR and RcnR, and for Glx I is currently unknown. Lebrette *et al.* reported a crystal structure of Ni(L-His)$_2$ bound to NikA, the periplasmic nickel-binding portion of NikABCDE, *in vitro*. Furthermore, addition of L-histidine increased the rate of nickel uptake *in vivo* (anaerobically)[31]. Despite these findings, the physiological relevance of Ni(L-His)$_2$ is unestablished.

Zinc

Nearly all bacteria employ tripartite, high affinity ABC zinc transporters consisting of a periplasmic or extracellular solute-binding (lipo)protein (subunit A), a transmembrane-spanning permease (subunit B), and a cytoplasmic ATPase (subunit C).[3] In addition to the high-affinity zinc uptake system, *E. coli* possess subsidiary, low-affinity zinc importers (ZupT, PitA, and MntH).[32] *E. coli* possess three types of zinc exporters: a P-type ATPase, ZntA, a cation diffusion facilitator (CDF) family transporters, ZitB, and YiiP, and the periplasm-spanning "efflux guns" CzcD and CzcBCA.[3]

The flux of zinc, like other metals mentioned thus far, in and out of the cell is controlled at the transcriptional level by several types of zinc-responsive transcription factors. For *E. coli,* these include members of the Fur family (Zur) to up-regulate zinc import via transcriptional repression and members of the MerR (ZntR) to increase zinc export and/or intracellular sequestration via transcriptional activation.[33,34] Both Zur and ZntR manifest femtomolar sensitivity to zinc in vitro. Therefore, it has been postulated that the concentration of internal aqueous zinc is approximately femtomolar even though the total zinc quota for an *E. coli* cell is approximately 200 μM.[35] It is

important to note that a cytosol virtually devoid of aqueous zinc does not imply a cytosol devoid of a pool of LMM zinc complexes.

The mechanism by which zinc, and the aforementioned transition metals, is trafficked to various client proteins once imported into *E. coli* cells is poorly understood. The rates of zinc transfer would be low on a biologically meaningful time scale at the reported very low concentrations, pM – fM range, of zinc ions prevailing in the cytosol based on half-life time for reconstitution of zinc proteins.[12,36] Two pathways are envisioned to overcome this dilemma. The first is the direct associative transfer between proteins through metallochaperones. Small proteins in *E. coli* that have been proposed as potential zinc metallochaperones include an unidentified 20-kDa periplasmic protein that is only produced when cells are incubated with millimolar concentrations of Zn(II)[37], YdaE, a protein with structural similarity to SmtA (the cyanobacteria metallothionein)[38], and ZraP, a 20.4-kDa membrane-associated protein that undergoes a specific Zn(II)-induced cleavage under Zn stress to release a 12-kDa carboxy-terminal Zn(II)-binding region into the periplasm.[39] The second pathway is that of labile, LMM pools that facilitate zinc transfer by serving as the substrate for zinc proteins. The role of a labile, LMM zinc pool gains support when considering multiple zinc metallochaperones would need to be employed to provide specificity for interaction with the tens of *E. coli* zinc-requiring proteins.[12,40]

Copper

Only a small repertoire of bacterial cuproenzymes is known, with most located in the periplasmic space[41]. Although the function of these enzymes is well understood, the mechanisms underlying their metallation and Cu(I) trafficking in this compartment as well as in the cytosol is poorly understood. However, unlike the metals previously discussed, copper chaperones are

suspected to play a greater role in copper trafficking due to copper's redox properties and ability to form thermodynamically stable complexes.

Similar to other members of the MerR family of proteins previously mentioned, CueR is a cytosolic Cu(I) sensing transcriptional regulator and is one of three Cu(I) metalloregulators in *E. coli*.[42] Cu(I) binds to CueR with a strong affinity (10^{-21} M)[43] and in doing so (under high concentrations of cytosolic Cu(I)), activates the transcription of CopA, a Cu(I) efflux P-type ATPase, CueO, a multi-copper oxidase, and various Cu(I) chaperones (CopZ, CueP, etc).[41] CopZ is involved in cytoplasmic Cu(I) trafficking. Extensive studies have shown CopZ interacts with the regulatory N-metal binding domain of CopA, exchanging Cu(I) with a $K_{eq} \sim 1$.[44] This interaction appears mediated by metal-dependent electrostatic interactions as CopZ loads Cu (I) substrates into transmembrane transport sites of CopA. Recently, it was discovered that in *E. coli*, CopZ is synthesized by programmed ribosomal frameshifting (PRF) out of the *CopA* gene.[45] The interaction of the CopZ chaperone with the efflux enzyme, CopA, implies the absence of a cytosolic labile Cu(I) pool. A similar conclusion was reached in *Saccharomyces cerevisiae* such that the intracellular "free" (free meaning chelatable) copper was calculated as less than one "free" copper ion per cell, and thus, a pool of "free" copper ions could not be used in physiological activation of metalloenzymes.[46]

The two-component system CusRS regulates the *cusCFBA* Cu(I) efflux system under anaerobic conditions and controls periplasmic Cu(I). The Cus complex is composed of a plasma membrane energy-providing channel, CusA; an outer membrane pore, CusC; a periplasmic protein linking CusA and CusC, CusB; and a soluble periplasmic Cu(I) chaperone, CusF. Specifically, CusF interacts with and delivers Cu(I) to CusB.[47]

The *pcoABCDE* cluster is also regulated by a two-component system, PcoRS. The Pco proteins, whose function is not fully understood, appear to contribute to the control of periplasmic Cu(I) in *E. coli* and other Gram-negative bacteria, perhaps under aerobic conditions.[47] Sequence analysis and experimental evidence suggest that PcoA is a periplasmic multicopper oxidase. PcoB may function as the outer membrane transporter while PcoD appears to be the inner membrane transporter that drives Cu(I) entry from the periplasm to the cytoplasm. PcoC and PcoE are putative periplasmic Cu(I) chaperones, and less is known about the Pco Cu (I) chaperones as compared to CopZ and CusF.[41] The presence of these two efflux clusters, *cusCFBA* and *pcoABCDE*, with their respective Cu(I) chaperones, suggest that the presence of a periplasmic labile Cu(I) pool is also unlikely.

Although the major Cu(I) efflux systems have been identified and are well characterized, Cu(I) influx mechanisms are poorly understood. Early characterization of the *E. coli ompB* porin mutants showed a Cu-resistant phenotype, suggesting that Cu(I) may enter the cells through these outer membrane proteins. Only recently has the participation of members of the major facilitator superfamily and TonB-dependent transport system in Cu import been proposed.[41]

Evaluation of Current Strategies Towards Detection and/or Identification of Labile Metal Pools

Both spectroscopic and non-spectroscopic methods exist for probing labile metal pools in various mediums. Each technique offers their own advantages and disadvantages, with certain methods more advantageous towards quantification of LMPs and others towards identification of LMPs. Therefore, many of these methods are complementary to one another. Four predominant strategies for investigating LMPs with their respective pros and cons are discussed herein.

Chelator Probes

The most popular strategy for studying labile metal pools in cells is to expose intact cells to custom-designed chelator probes.[48,49,50,51] These chelator probes enter cells and change their optical properties (fluorescence, phosphorescence, luminescence, or magnetic resonance imaging) upon binding labile metals as demonstrated in figure I-1. Quantifying these changes allows the size of labile metal pools to be quantified. In addition to quantification, these probes allow for visualizing metal distribution and dynamics in living specimens.[52] This approach has an advantage over strategies in which cells are disrupted, thereby potentially altering the endogenous LMPs. Fluorescence-based chelator probes are the most popular and these types of probes have been used to quantify the labile Zn(II)[48], Cu(II), Fe(III), and Ni(II) pools in *E. coli*[53], however, the majority of this metal imaging has been performed in eukaryotic cells.[54]

Despite the imaging and quantification advances in recent decades, chelator probes are not without fault. First, the chelator-based approach destroys the sought-after metal complexes, making it unlikely that this approach could ever be used to chemically identify metal trafficking complexes. Moreover, chelators are not completely specific for a particular metal, much less for a particular metal complex, and different chelators and reaction conditions yield different estimates of the size and properties of labile metal pools.[7] For example, estimates of the labile iron pool concentration in aerobically-grown bacteria, including both Gram positive and Gram negative, have been reported as 1 μM[55], 10 μM[56,57] , 26 μM[23], 15 – 30 μM[58] and 140 μM[59]. One final caveat of these probes has recently been explored by Marszałek *et al.* with regards to the labile zinc pool.[60] Their work describes the capability of these probes to form ternary Zn(II)−probe−LMM ligand complexes and compete for Zn(II) ions with said probes under physiological conditions. Such

interactions could significantly affect the Zn(II) ion availability to the probe (competition) and/or modulate its fluorescence (ternary complex formation). Probes are routinely calibrated against Zn(II) ions added as inorganic salts in non-coordinating or weakly coordinating buffers. This may yield unreliable aqueous zinc concentrations in the presence of LMM ligands, compared to the calibrations.

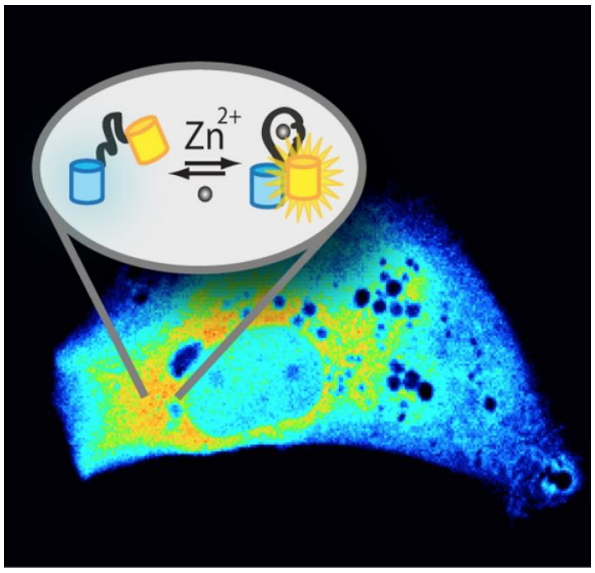

Figure I-1. Demonstration of a fluorescence resonance energy transfer (FRET)-based probe for Zn(II) detection. A Zn(II)-binding domain exists between two fluorescent proteins. Zinc binding induces a conformational change that leads to a change in FRET ratio (blue = no Zn(II); yellow = Zn(II)). Used with permission from (54) https://pubs.acs.org/doi/10.1021/cr400546e

Kinetic and Thermodynamic Simulations of Metal-Ligand Complexes

Potentiometric and spectrophotometric titrations of metal salts with various LMM ligands under physiological conditions (concentration and pH) have been performed over the years to establish affinity constants, all in an effort to predict the major components of these labile metal

pools. Hider and Kong have led this effort in the iron community.[61] Specifically, they investigated citrate, hydrogen sulfide, cysteine, and reduced glutathione (GSH) as potential ligands for the labile iron pool; their simulations suggested that the major cytosolic Fe(II) species are $Fe(II)(GSH)_n$ and hexaaqua-Fe(II) with $Fe(II)(citrate)_n$ being a minor component (< 3%). This group additionally evaluated the speciation of manganese at physiological conditions using published affinity constants. They reported that citrate was the dominant ligand and that GSH failed to bind under these conditions.[62]

Affinity constants and speciation plots afford hypothetical endogenous labile metal pools; however, uncertainties exist in both the calculation of the affinity constants as well as in the subsequent speciation derivation. First, binding constants are subject to variation based on conditions of the experiment – pH, ionic strength, and temperature.[12] To add, comparison of binding ability can be only performed for apparent constants of complexes with the same stoichiometry; this can be circumvented by comparing competitivity indices.[63] In speciation plots, a limited number of potential ligands are competitively tested in addition to employing the assumption that the buffers/reductants of choice have little to no affinity for the metal, which is not always true. Furthermore, in the absence of knowledge of the coordination mode of the metal in these labile metal pools, virtually all experiments employ metal salts in biological buffers without recognizing that the species of metal in such solutions most likely are not the biological substrates.[12]

Density functional theory (DFT) has become a useful tool for probing the coordination properties of LMM ligands to different transition metal ions. In this method, the interaction between metal ions and organic molecules in the gas phase is simulated; however, this ignores the effect of solvent, which is a key component when trying to model biological systems. Liu *et al.*

explored the coordination behavior of metal cations (Cr(II), Mn(II), Fe(II), Co(II), Ni(II), Cu(II), Zn(II), Cd(II), and Hg(II)) with GSH in a 1:1 stoichiometry, producing nine optimized electronic structures of these metal complexes based on the ion potential, the electron configuration, and the coordination numbers of the metal ions as well as the chelate site and type of heteroatom of GSH. These nine optimized structures featured mono-, bi-, tri-, tetra-, and penta-coordinated metals, with the absolute binding energy highest for all metals mono-coordinated to the sulfur of GSH.[64]

Nuclear Magnetic Resonance

In addition to potentiometric studies, nuclear magnetic resonance (NMR) has been utilized to assess coordination of metals to various LMM ligands. Briefly, in this technique, the binding constant for metal-ligand complex can be measured by a change in linewidth or chemical shift of the peaks corresponding to the free ligand upon binding to a metal. Typically, NMR is performed with diamagnetic compounds; paramagnetic compounds induce signal broadening and a wide chemical shift, which limits the utility of the method.[65] Krężel *et al*. has investigated the coordination of Zn(II) with GSH, GSSG, and L/D-histidine using 1-D ^{1}H NMR.[63,66] Interestingly, when L-His and GSH were competitively tested, the solution structure, as determined by NMR, revealed a ZnH(GSH)(L-His)(H_2O) complex at pH 6.8, which included tridentate L-His, monodentate (sulfur) GSH, and weak inter-ligand interactions. Calculations of competitiveness of this complex for Zn(II) binding at pH 7.4 indicated that it could be formed *in vivo* under conditions of GSH depletion. Otherwise, GSH alone emerged as the sole Zn(II) ligand.[63] Despite the progress made towards determining metal-ligand interactions, this technique is sensitive to concentration and the complexity of proton assignment increases exponentially when analyzing a biological medium versus standards.

Chromatography-based Approach

An emerging strategy involves isolating and then separating labile metal pools from a complex biological matrix on a liquid chromatography (LC) system. LC is an effective bioanalytical technique that offers several different mechanisms of chemical separation. Further, different types of LC can be combined to yield separations with higher degrees of purity.

Size exclusion chromatography (SEC) columns and hydrophilic interaction chromatography (HILIC) columns have been utilized to separate labile metal complexes within various organisms (plants, *Saccharomyces cerevisiae*, and more) with varying degrees of success, highlighted below. Traditionally, the mechanism of steric exclusion warrants the observed relation between elution and the hydrodynamic volume, or size, of a molecule for SEC, with larger biomolecules eluting more quickly as compared to smaller biomolecules. However, secondary interactions, ionic and hydrophobic, can skew this relation.[67] HILIC columns operate similar to normal-phase columns such that they retain moderate to highly polar compounds. The HILIC stationary phases are highly polar and hydrophilic, which causes them to absorb water from the mobile phase to form a thin layer of water on the surface. Increasing the aqueous content of the mobile phase reduces the partitioning effect of the sample in the mobile phase with the stationary phase; when this partitioning is eliminated (typically, at $\geq$50% aqueous mobile phase), polar compounds are no longer retained on the column. HILIC relies on a highly organic mobile phase, thus, if the analyte is not compatible with this mobile phase, solubility issues may arise.[68]

Equally as important as separation is detection. The application of inductively coupled plasma mass spectrometry (ICP-MS) allows for sensitive detection of various transition metals, including isotopes, in complex sample matrices over a dynamic concentration range, in some cases

down to ppt. Briefly, liquid samples are first nebulized in the sample introduction system, creating a fine aerosol that is subsequently transferred to the argon plasma. The high-temperature plasma atomizes and ionizes the sample, generating ions. ICP-MS is therefore considered a 'hard' ionization technique because it completely atomizes most molecules in the sample. Furthermore, the ionization energy of argon primarily dictates which elements can be analyzed (i.e., sufficiently ionized in the plasma) – those with an ionization energy close to that of argon (H, C, N, O, etc.) cannot be observed. The ions are then extracted through the interface region and into a set of electrostatic lenses referred to as the ion optics. The ion optics focuses and guides the ion beam into the quadrupole mass analyzer. The mass analyzer separates ions according to their mass-charge ratio (m/z), and these ions are measured at the electron multiplier detector.[69]

While ICP-MS can provide information on the metal-portion of these labile metal pools of interest, this destructive technique yields limited (if the ligands are P- or S-containing) to no information on the ligands. Electrospray ionization mass spectrometry (ESI-MS) has risen to popularity for the identification of metal complexes in a wide range of samples because of its high selectivity and sensitivity.[70] ESI uses electrical energy to assist the transfer of ions from solution into the gaseous phase before they are subjected to mass spectrometric analysis. The transfer of ionic species from solution into the gas phase by ESI involves three steps: (1) dispersal of a fine spray of charge droplets, followed by (2) solvent evaporation and (3) ion ejection from the highly charged droplets.[71] This method of ionization is comparatively 'softer' than that of ICP.

For a metal-ligand complex, ESI-MS typically generates singly charged metal-ligand spectra that can be identified based on relative isotopic abundance corresponding to the naturally occurring metals. Furthermore, ESI-MS instruments allow for optimization of efficient detection conditions (e.g., positive and negative ionization mode) for the metal complexes of interest across

a range of solvents and pH conditions.[70] The main caveat of utilizing ESI-MS to identify metal complexes in a biological matrix is the necessity to de-salt the sample prior to introduction into the system. Nonvolatile salts can cause signal suppression by either peak splitting by adduct formation or by peak ion suppression from a reduction in the vapor pressure, thereby increasing the surface tension of the charged droplets.[72]

Online SEC-ICP-MS, HILIC-ICP-MS, and HILIC-ESI-MS have all been utilized to probe metal-ligand complexes from various biological matrices. The Lindahl laboratory has been employing SEC chromatography with online ICP-MS to detect LMM metal complexes in *Saccharomyces cerevisiae* cytosol[73], mitochondria[7], and vacuoles[74], with progress in identifying the LMM sulfur and phosphorus pools in some of these organelles.[73] Ouerdane *et al.* was able to determine the speciation of non-covalent nickel species in plant tissue extracts by ESI-MS after isolation by 2-D SEC-HILIC monitored by ICP-MS.[75] LMM Fe(II), Cu(II), Zn(II), and Mn(II) complexes were identified in coconut water by Alchoubassi *et al*. using HILIC-ICP-MS and HILIC-ESI-MS.[76]

A major drawback of the chromatography-based strategy is that the structural integrity of cells and organelles are compromised during the isolation of metal complexes. As a result, cellular contents are mixed together, which can promote side reactions involving these labile metals, giving rise to artifacts. Thus, LC peaks observed in chromatograms might be artifacts of the isolation procedure. Metal complexes are undoubtably difficult to isolate, separate, and detect because of their lability and low concentrations.

Objectives

The identity of labile metal pools, whether it be Mn(II), Fe(II), Ni(II), Zn(II), or Cu(I) coordinated, in the cytosol of *E. coli*, has never been reported while many hypothetical pools have been suggested based on stability constants. This dissertation will present the first molecular-level description of a labile metal pool in bacteria, specifically that of Ni(II), in *E. coli* in chapter IV.

The main objectives of this dissertation were to develop and refine analytical methods for isolating, separating, detecting, and identifying labile, LMM metal pools in the *E. coli* cytosol. The simple, Gram-negative bacterium, *E. coli*, possesses quick doubling times and lacks organelles, which allows for ease in isolating cytosolic components of interest. The chromatography-based approach is the most direct method for characterizing these metal complexes. When coupled to ICP-MS and ESI-MS independently, the results presented illustrate the potential for elucidating these elusive labile metal pools. The method development described herein provides the foundation for separation and detection of labile metals pools in more complex biological systems such as the organelles of *S. cerevisiae* or the blood and tissues of mammals.

CHAPTER 2

METHODOLOGY

Strains and Growth Conditions

A derivative of *E. coli* K-12, MG1655, was transformed with bacteriophage-containing plasmid pZa31mycR.[77] MG1655-pZa31mycR cells were cultured in 50 mL of M9 minimal media containing 0.4% (w/v) glucose, 1 mM chloramphenicol (Sigma Aldrich), and 10 μM (n = 12) of natural-isotopic-abundance $Fe(III)_2(citrate)_3$ overnight at 37 °C with 200 rpm shaking. We determined by ICP-MS that M9 media contained 0.9 ± 0.6 μM Fe, 4 ± 1 μM Zn, 0.09 ± 0.01 μM Mn and 1 ± 1 μM Cu. Once grown, cultures were transferred to 1.0 L of growth media. Independent 1.0 L batches of cells were grown and harvested at early (OD_{600} ~0.6), mid- (OD_{600} ~1), or late (OD_{600} ~2) exponential phase by centrifuging at 4,000×*g* for 15 min, with the predominant number of replicates grown to mid-exponential phase. Pellets (ca. 3 (1) g wet cells for aerobically (anaerobically)-grown cells) were washed in high-purity trace-metal-free double distilled-deionized water (HPW) and re-centrifuged at the same speed for 10 min. Pellets were resuspended in 5.0 mL of 20 mM ammonium bicarbonate (Sigma Aldrich) buffered at pH 7.2. The suspension was transferred to a 15 mL polypropylene falcon tube, quickly frozen in liquid N_2 and stored at -20 °C. Additional batches of MG1655-pZa31mycR cells were cultured in which no $Fe(III)_2(citrate)_3$ was supplemented in the growth media (n = 8); there was essentially no change in the growth rates, α, between this supplementation or lack thereof ($\alpha = 0.0106\ min^{-1}$ (0 μM) vs. $\alpha = 0.0097\ min^{-1}$ (10 μM)).

For anaerobic growths, MG1655-pZa31mycR cells were cultured in 50 mL of the same M9 media (0.4 % glucose, 1 mM chloramphenicol, and 0 μM $Fe(III)_2(citrate)_3$) (n = 2) and grown aerobically as described above. Once grown, cultures were transferred to 1.0 L of growth media

in a round bottom flask, N_2 gas was bubbled into the culture, and the culture was incubated at 37 °C with 100 rpm shaking. The cells were harvested anaerobically once grown to mid-exponential phase (OD_{600} ~ 0.2), and the whole cell (WC) pellet resuspension was quickly frozen in liquid N_2 and stored at -20 °C. Logarithmic growth curves for aerobically- and anaerobically grown MG1655-pZa31mycR *E. coli* are shown in Figure II-1.

Additional batches were grown aerobically, unless otherwise denoted, in which the medium was supplemented with metal salts, an amino acid, or both. The metal salts included: 100 µM (n = 6) of natural-isotopic-abundance $Fe(III)_2(citrate)_3$, 100 µM (n = 5) $Zn(acetate)_2$, 100 µM $MnCl_2$ (n = 1), 1 µM $CuSO_4$ (n = 1), and 1 µM $NiSO_4$ (n = 1, + O_2; n = 2, -O_2). The amino acid was 400 µM L-histidine (n = 1, -O_2). These batches were harvested in mid-exponential phase and the WC pellet was treated in accordance with previous samples.

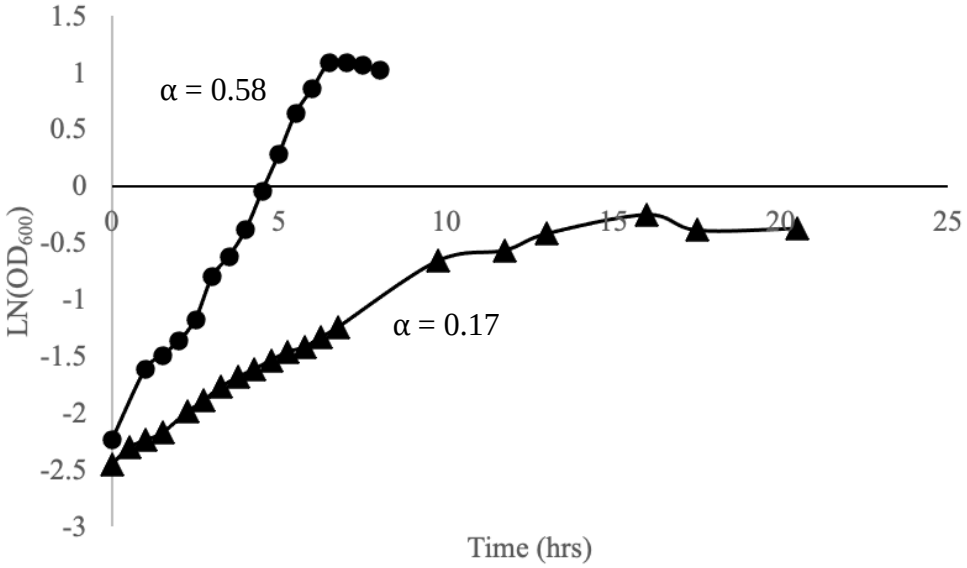

Figure II-1. Logarithmic growth curves of aerobically- (circles) and anaerobically-grown (triangles) MG1655-pZa31mycR *E. coli* cultured in M9 minimal growth media with 0.4% glucose with growth rates (α) in hr^{-1} overlaid.

Isolation of Cytosol and Flow-through-solution (FTS)

Frozen cells, both aerobically- and anaerobically-grown, were thawed at 37 °C with 100 rpm shaking for 30 min. The lysate was centrifuged at 10,000 ×*g* for 5 min, transferred to a new 15 mL Falcon tube, and incubated with 20 µL of 1.12 mg/mL DNase (Sigma Aldrich) and 10 mM $MgCl_2$ (Acros Organics) for 30 min at 37 °C with 100 rpm shaking. Following DNA hydrolysis, the lysate was centrifuged at 100,000 ×*g* for 60 min with a Beckman-Coulter SW 32 Ti rotor in an Optima L-90K Ultracentrifuge. The resulting supernatant, defined as the cytosol, was brought into a chilled anaerobic glove box (MBraun Labmaster 120, 1 – 10 ppm O_2, 4 – 8 °C) and passed through an Ultracel regenerated cellulose 3 kDa ultrafiltration disc (EMD Millipore) using an Amicon filtration system; the solution that passed through the membrane was defined as flow-through-solution (FTS).

Metal and Ligand Standards

Stock solutions of $Fe(II)SO_4$ (Fisher chemical), $Zn(II)(acetate)_2$ (Acros Organics), $Mn(II)Cl_2$ (Sigma Aldrich), $Cu(II)SO_4$ (Acros Organics), and $Ni(II)SO_4$ (Sigma Aldrich) (1.0 mM each) were prepared in HPW. Similar stock solutions, ranging from 1.0 – 1000 mM, of reduced glutathione, GSH, (Sigma Aldrich), oxidized glutathione, GSSG, (Sigma Aldrich), cysteine (Sigma Aldrich), methionine (MP Biomedicals), Na_2HPO_4 (Sigma Aldrich), $NaH_3P_2O_7$ (Sigma Aldrich), Na_4NADPH (Sigma Aldrich), Na_2NADH (Sigma Aldrich), Na_2AMP (Sigma Aldrich), NaADP (Sigma Aldrich), Na_2ATP (Sigma Aldrich), L-histidine (MP Biomedicals), glutamic acid (Acros Organics), aspartic acid (Fisher Scientific), and Na_3citrate (Fisher Chemical) were prepared in HPW. All stocks were stored at 4 °C. For LC-ICP-MS or ESI-MS analysis, stock standards were diluted (day-of) to the desired final concentration in mobile phase or HPW *(see LC-ICP-MS*

analysis and ESI-MS analysis). Na(polyphosphate) (Sigma Aldrich) was prepared at 1.1 g/mL and filtered through the 3 kDa membrane; the filtrate was diluted in mobile phase prior to LC-ICP-MS analysis.

A "ligand cocktail" consisting of the most likely metal-binding ligands present in the *E. coli* cytosol was prepared in 20 mM ammonium acetate (AA) pH 6.5. This cocktail was comprised of the following standards (final concentration) based on reported values for the *E. coli* cytosol: 2 mM citrate[78], 5 mM GSH[79], 500 µM GSSG[80], 5 mM ATP[81], 500 µM ADP[81], 200 µM AMP[81], 100 µM cysteine[82], 50 mM glutamate[78], 5 mM aspartate[78], 70 µM L-histidine[78], 5 mM phosphate[83], and 3 kDa-filtered polyphosphate[83].

LC-ICP-MS Analysis

SEC-ICP-MS

Primary LC-ICP-MS analyses were performed on a single Superdex® Peptide 10/300 GL (GE Life Sciences) SEC column. Additional analyses were performed on two such columns linked in series. To assess metal adsorption to the SEC columns, a "ghost column," which consisted of PEEK tubing, was employed. The mobile phase passed through the column at 0.6 ml/min for the single and 0.25 ml/min for the double column using an Agilent 1260 bio-inert quaternary pump (G5611A) with diode array (G4212B), fraction collector (G5664A), and multisampler (G5688A). The entire LC system was located inside the glove box. Eluate flowed to an ICP-MS (Agilent 7700x) located outside of the box where ^{23}Na, ^{39}K, ^{31}P, ^{34}S, ^{55}Mn, ^{56}Fe, ^{57}Fe, ^{60}Ni, ^{63}Cu, ^{65}Cu, ^{66}Zn, ^{67}Zn, and ^{68}Zn were detected. The mobile phase was either 20 mM or 50 mM AA pH 6.5 for LC-MS (Sigma Aldrich) (*see Appendix I*), which had previously been passed through a 0.22 µm filter using a Stericup vacuum filtration system (Corning) and then degassed using a Schlenk line prior

Table II-1. Standards for molecular mass calibration curve using single SEC column.

Compound	Source	Method of detection	Molecular weight (Da)	Concentration	Log(MW)	Elution volume (mL)	V_e/V_o
$(Na)_2AMP$	see *Metal and ligand standards*	P, UV-260	347	100 µM	2.54	28.53	1.37
Riboflavin	Sigma Aldrich	UV-260	376	1 mM	2.58	26.59	2.65
NaADP	see *Metal and ligand standards*	P, UV-260	427	100 µM	2.63	25.87	1.55
$(Na)_2ATP$	see *Metal and ligand standards*	P, UV-260	507	100 µM	2.71	23.89	2.07
$(Na)_2NADH$	see *Metal and ligand standards*	P, UV-260	663	50 µM	2.82	24.67	2.44
$(Na)_4NADPH$	see *Metal and ligand standards*	P, UV-260	744	50 µM	2.87	22.74	2.57
Cyanocobalamin	Fisher Bioreagents	Co	1,355	50 µM	3.13	19.26	2.78
Insulin (bovine)	Sigma Aldrich	UV-280	5,734	50 µM	3.76	14.46	3.06
Cytochrome C (equine)	Sigma Aldrich	Fe	12,384	20µM	4.09	12.74	2.86
Thyroglobulin	Sigma Aldrich	UV-210	660,000	0.1 mg/ml	5.82	9.31	1.00
NaH_2PO_4	see *Metal and ligand standards*	Fe	95	20 µM	1.98	21.92	2.35
Cysteine	see *Metal and ligand standards*	S	121	500 µM	2.08	22.15	2.38
Methionine	see *Metal and ligand standards*	S	149	500 µM	2.17	21.19	2.28
GSH	see *Metal and ligand standards*	S	307	100 µM	2.49	21.09	2.27
ZnEDTA	Acros Organics/Sigma Aldrich	Zn	354	1/10 µM	2.55	19.74	2.12
Fe(Bipy)3	Fisher Chemical/Alfa Aesar	Fe, UV-523	524	2/20 µM	2.72	18.44	1.98
Fe(Phen)3	Fisher Chemical/Acros Organics	Fe, UV-510	597	2/20 µM	2.78	21.19	2.28
GSSG	see *Metal and ligand standards*	S	613	100 µM	2.79	20.03	2.15
Zn acetate (hexaaqua Zn)	see *Metal and ligand standards*	Zn	172	1 µM	2.24	44.89	4.82
$FeSO_4$ (hexaaqua Fe)	see *Metal and ligand standards*	Fe	164	1 µM	2.21	22.40	2.41
$MnCl_2$ (hexaaqua Mn)	see *Metal and ligand standards*	Mn	163	1 µM	2.21	20.71	2.22
$NiSO_4$ (hexaaqua Ni)	see *Metal and ligand standards*	Ni	166	1 µM	2.22	24.98	2.68

to import into the box. AA was selected as the mobile phase buffer due its volatility and compatibility with both ICP-MS and ESI-MS. Samples (50 - 150 µL) were injected automatically using the multisampler (*see appendices 2 and 3 for ICP-MS tuning* and *LC-ICP-MS operational instructions*). Peak elution volumes (V_e) were calibrated to molecular masses using standards listed in Table II-1. Designated peaks were simulated with Fityk software (fityk.nieto.pl) employing the Levenberg-Marquardt algorithm with a built-in Gaussian function (*see Appendix IV for LC-ICP-MS data analysis instructions*).

^{67}*Zn Loading of SEC Column*

Prior to loading, the column was cleaned by one of two methods. The first cleaning method entailed passing 500 µL of a chelator cocktail (10X) through it. The cocktail included 500 µM each of ethylenediaminetetraacetic acid (EDTA) (Sigma Aldrich), ethylene glycol-bis(β-aminoethyl ether)-N,N,N′,N′-tetraacetic acid (EGTA) (Sigma Aldrich), 1,10-phenanthroline (phen) (Acros Organics), 2,2-bipyridine (BPY) (Alfa Aesar), bathocuproinedisulfonic acid (Sigma Aldrich), deferoxamine (END Millipore), (N,N,N′,N′-tetrakis(2-pyridinylmethyl)-1,2-ethanediamine (TPEN) (Sigma Aldrich), and 1 mM ascorbic acid (Acros Organics). Three separate aliquots of the cocktail were injected onto the column with alternating injections of 500 µL HPW. A column volume (CV = 24 mL) of the mobile phase 50 mM AA (Sigma Aldrich) pH 6.5 was passed between injections. In the second method, chelator cocktail (1X) was passed through the column for 3 CVs as the mobile phase with no injection, followed by a rinsing of the column with 3 CVs of HPW as the mobile phase. The second method is the current laboratory standard as the concentrated amount of ascorbic acid in the 10X chelator cocktail undergoes oxidation more rapidly.

Three methods were used to load the column with ^{67}Zn. In the first method, > 10 CVs of 10 µM $^{67}ZnSO_4$ (90%; Isoflex USA) in HPW was passed as the mobile phase through the column, and then the mobile phase was changed to 50 mM AA pH 6.5 to rinse-off unbound ^{67}Zn. This method eventually contaminated the LC system with ^{67}Zn, which was painstakingly removed by excessive flushing with dilute HCl pH 3. In the second method, 500 µL of 10 µM $^{67}ZnSO_4$ was injected onto the column. After passing 1 CV of 50 mM AA pH 6.5 mobile phase, 500 µL of HPW was injected, followed by another CV of mobile phase. These injections were repeated 4× more. The column was then rinsed with 50 mM AA pH 6.5 until a flat baseline for ^{66}Zn was attained. In the third method, 5 CVs of a mobile phase consisting of 5 (or 10) µM $^{67}ZnSO_4$ in 50 (or 20) mM

AA pH 6.5 was passed through the column, followed by 50 (20) mM AA pH 6.5 until a flat ^{66}Zn baseline was achieved. Due to heavy use, the loading procedure was repeated monthly (*see Appendix III*).

HILIC-ICP-MS

HILIC-ICP-MS analyses were performed on a SeQuant® 4.6 x 150 mm (3.5 µm) ZIC®-HILIC column (Merck KGaA, Darmstadt, Germany). The column was equilibrated in 90% acetonitrile (ACN) (HPLC grade)/10% 10 mM AA (LC-MS grade) pH 6.5 for 30 minutes at a flow rate of 0.5 ml/min prior to analyses. Both mobile phases were filtered and degassed as previously described. Samples were diluted 5-fold and standards were diluted 10- or 20-fold in ACN prior to injection (20 µL) onto the column. Applying a gradient of 90% ACN to 40% ACN in 20 minutes (~2.5% / min) was sufficient for the elution of polar compounds.

For detection via ICP-MS, the ICP-MS was configured in organic mode, which includes both hardware and software adjustments. In terms of hardware, the ICP-MS must be outfitted with platinum sampler and skimmer cones (more inert towards O_2 than classic nickel cones), a brass lens base (for conductivity capability with the Pt cones), and a 1.5 mm diameter torch (to reduce solvent load to keep the plasma stable). Additionally, the auxiliary gas must have oxygen incorporated to prevent carbon deposition on the cones. 20% O_2/80% Ar was utilized in these experiments to supply 25% O_2 optional gas. In terms of the software, the ICP-MS was operated at higher forward power (1600 W vs. 1550 W for aqueous analysis) and the spray chamber was cooled to -5 °C. The ICP-MS was tuned in organic mode with tune solution prepared according to Appendix I with ACN as the organic solvent.

Elemental Analysis

In ICP-MS, notorious spectral interferences can severely affect measurement accuracy for some elements and the stability of the ICP as an ion source can result in inferior precision values (as reported by relative standard deviation, RSD)[84]. The source of spectral interferences can come from the sample matrix, the solvent medium, or the plasma gas[85]. To overcome these interferences, we have developed and/or employed a number of strategies.

Addressing Interferences via Sample Preparation

To determine the concentration of trace-metal grade nitric acid, HNO_3, (Fisher Scientific) needed to sufficiently digest a cellular lysate while limiting metal contamination from the acid, two experiments were performed. The first experiment evaluated the digestion efficiency of 5% (v/v) HNO_3 vs. 100% HNO_3 at either 70 or 80 °C for either 24 or 48 hrs on *E. coli* WC lysates, cytosol, and FTS. There was no significant difference between 5 (pH ~ 0.08) and 100% HNO_3 (pH ~ -1.2). There was, however, a significant effect of time and temperature on digestion. Thus, it was concluded that digestion of samples would occur at 80 °C and for protein-concentrated samples (WC lysates), proper digestion took approximately 2 days (48 hrs) whereas less protein-concentrated samples (cytosol and FTS) were sufficiently digested after approximately 24 hours. This experiment was complemented by investigating the limit of detection (LOD) for Fe, Zn, and Cu in 5% (standard), 0.5%, 0.05%, 0.005%, and 0.0005% HNO_3 blanks in HPW. The LOD for all metals was reach by the 0.5% HNO_3 blank, indicating the lowest background metal counts was achieved in this blank. Therefore, the final concentration of HNO_3 in all blanks, standards, and samples for elemental analysis would be 0.5%.

Addressing Interferences with Instrumental Parameters

A collision/reaction cell (CRC) prior to the quadrupole mass analyzer of the ICP-MS offers the ability to remove spectral interferences either through collision or reaction mode. Collision mode uses a non-reactive gas, such as He, and a process called kinetic energy discrimination (KED) to selectively attenuate all polyatomic interferences based on their size. KED exploits the fact that all polyatomic ions are larger than analyte ions of the same mass, so they collide with the cell gas with a higher frequency as they pass through the cell, emerging with lower residual energy. These low energy ions are excluded from the ion beam by a bias voltage at the cell exit. Reaction mode uses specific reaction gases, such as H_2, to remove known, reactive interferences from each analyte isotope. Collision mode with He is best suited for P, S, Mn, Co, Ni, Cu, and Zn analysis whereas reaction mode with H_2 is best suited Fe analysis. Additionally, no gas mode (i.e., no CRC) is best for alkali and alkali earth metal analysis.

Prior elemental analysis in the Lindahl lab operated the CRC in collision mode with a He flow rate of 3.6 (standard) – 4.2 mL/min. To optimize the He flow rate for P, S, Mn, Co, Ni, Cu, and Zn, the He flow rate was ramped from 3.5 to 10 mL/min, stepping 0.5 mL/min for both a blank of 0.5% HNO_3 and a level 3 standard from TEXASAM-15REV3 (Inorganic Ventures) in 0.5% HNO_3. During these ramps, the counts per second (CPS) was determined for each isotope of each element selected. The background equivalent concentration (BEC) is a quantitative measure of the background and should be minimized for each element of interest. BEC was minimized for P, Mn, Ni, and Zn under low He flow conditions (He flow rate = 3.6 mL/min) whereas BEC was minimized for S, Co, and Cu under a higher He flow rate (8.0 mL/min). The same ramping experiment was performed for Fe isotopes but with H_2 as the reaction gas. BEC was minimized at a H_2 flow rate of 5.0 mL/min.

In addition to accurate isotope measurements, high precision is necessary too. The two main parameters affecting precision are the statistics of ion counting (i.e., the detector) and the stability of the ion current.[86] Simultaneous detection of the ion currents of the isotopes of interest is the only way to eliminate the time-dependent variation in the ion current. Unfortunately, a quadrupole mass analyzer does not possess quick enough scan rates for such, and thus, this is a limitation of our instrumental setup. However, two strategies have been employed to ensure efficient ion counting by the electron multiplier detector.

First, it is important to note that the Agilent 7700x ICP-MS has a 9-order dynamic range of the detector such that CPS > 10^6 are analyzed in analog mode and CPS $\leq 10^6$ are analyzed in pulse mode. While these two modes may have individual linear characteristics, they are not well correlated, which means that a calibration curve for an analyte of interest would have a large undesirable break from one mode to the other. To prevent this, we have implemented a weekly detector cross calibration (i.e., a P/A factor tune) to align these modes into a single linear signal response, thereby allowing the full linear, dynamic range of the instrument to be exploited. Secondly, in any pulse counting system there is a specific time interval after which no new events can be counted; this interval is defined as the dead time. The dead time of the detector is, thus, one of the factors that may contribute to uncertainty in isotope measurements when in pulse mode. A dead time calibration was performed using two standard solutions of erbium. The improvement in accuracy and precision in a set of TEXASAM-15REV3 standards upon these implementation strategies is demonstrated for ^{56}Fe in Table II-2.

Table II-2. Fe-56 calibration curve from TEXASAM-15REV3 standards in 0.5% HNO_3 pre- and post-P/A factor tuning and dead time calibration of the electron multiplier detector.

Standard level	Expected [Fe-56], nM	Observed (pre) [Fe-56], nM	Observed (pre) RSD, %	Observed (post) [Fe-56], nM	Observed (post) RSD, %
0	0	0	5	0	2.1
1	1.6383	1.7850	4	1.614	2.6
2	16.383	18.722	1.1	16.215	0.5
3	163.83	183.69	0.6	160.29	0.5
4	1638.3	1839.3	0.6	1611.8	0.7
5	16383	16117	1	16131	0.3

Standard and Sample Preparation

A series of calibration standards was prepared with the following stock metal solutions: TEXASAM-15 (Inorganic Ventures) (Chapter III), TEXASAM-15REV3 (Chapter IV), or ICP-MS-ISC-2 (High-purity Standards) for nickel analyses (Chapter III and IV); each standard was a 10-fold dilution of the previous standard (5 total). The final concentration of trace-metal grade HNO_3 in each of these standards was 0.5 % aside from the stock (standard level 5), which was 2% (as prepared by the company). Two blanks of 0.5% HNO_3 accompanied this standard set (*see Appendix V for ICP-MS standard/sample preparation*). Additionally, an internal standard solution, IV-ICPMS-71D (Inorganic Ventures) was prepared in 0.5% trace-metal grade HNO_3. This solution, specifically elements Sc-45 and Y-89, was independently monitored through elemental analysis through peristaltic pump introduction. This internal standard assisted in assessing instrument instability, matrix effects, and signal drift, all evident through RSD values (*see Appendix I for internal standard preparation*).

For elemental analysis, denoted as ‘offline’ ICP-MS analysis, of samples, three aliquots (50 - 100 µL) of lysate, cytosol, and FTS from the independent batches were transferred into 15

mL polypropylene falcon tubes. Either 150 µL of trace-metal grade HNO_3 (prior to optimization) or 500 µL of 5% trace-metal grade HNO_3 was added to each tube. Tubes were capped, sealed with electrical tape, vortexed, and incubated at either 70 °C for ~ 15 hrs (prior to optimization) or 80 °C for 24 - 48 hrs, depending on sample type. Samples were cooled to room temperature and then diluted to a final volume of 3 or 5 mL with HPW followed by ICP-MS analysis (*see Appendix VI for offline ICP-MS operational instructions*). For back-calculating the metal concentration of the various samples, the cell pellet mass and density of an *E. coli* cell[87] were used for calculating the packing efficiency[88] and the cytosolic fractional volume of 0.61 was assumed[89,90].

ESI-MS Analysis

Direct Injection

Electrospray ionization mass spectrometry (ESI-MS) was performed using a Thermo Scientific Q Exactive Focus (Waltham, Massachusetts) instrument. FTSs, LC fractions, and standards (GSH, ATP, etc.) were diluted 2× or 20× (5 µL sample + 5 µL CH_3OH for 2×; 10 µL sample + 200 µL CH_3OH for 20× using LC-MS grade methanol (Thermo Fisher Scientific)), depending on metal and salt concentrations in the sample. Samples were injected into a 10 µL loop, using methanol as a mobile phase at a flow rate of 300 µL/min. The Q Exactive Focus HESI source was operated in full MS (66 – 1000 m/z) in positive and negative modes. The mass resolution was tuned to 70,000 full-width half-max (FWHM) at m/z 200. Spray voltage was 3.5 kV for positive mode and 3.3 kV for negative mode. Sheath gas and auxiliary gas flow rates were 7 and 0 AU, respectively. Transfer capillary temperature was held at 270 °C and the S-Lens RF level was set at 50 V in both polarities. Exactive Series 2.11/Xcalibur 4.1 software was used for data acquisition and processing.

HILIC-ESI-MS

Sample and standard analysis was performed using a Thermo Scientific Q Exactive Focus coupled with LC unit (ultimate 3000 RS). Samples were separated by injecting 20 µL of sample into a SeQuant® 4.6 x 150 mm (3.5 µm) ZIC®-HILIC column (Merck KGaA, Darmstadt, Germany). The mobile phase consisted of 10 mM AA (eluent A) (LC-MS grade) and acetonitrile (eluent B) (LC-MS grade). The flow rate was set at 0.5 mL/min with the following gradient: 0 – 20 min 90 - 40% B and back to 90% B in 20.1 min, with a hold at 90% B 20.1 - 30 min. The Q Exactive Focus HESI source was operated in full MS (100 – 1000 m/z) in positive and negative modes. The mass resolution was tuned to 70000 FWHM at m/z 200. The spray voltage was set to 3.75 kV for positive mode and 2.80 kV for negative mode. The sheath gas and auxiliary gas flow rates were set to 35 and 10 AU, respectively for positive mode. For negative mode, the sheath gas and auxiliary gas flow rates were set to 40 and 10 AU, respectively. The transfer capillary temperature, and the auxiliary gas heater temperature were held at 275 and 320 °C, respectively for positive mode. Similarly, in negative mode the transfer and auxiliary gas heater temperature were set to 320 and 350 ^{o}C, respectively. The S-Lens RF level was set at 50 V in both polarities. Exactive Series 2.8 SP1/Xcalibur 4.1 software was used for data acquisition and processing.

Troubleshooting

A troubleshooting guide for LC, LC-ICP-MS, and ICP-MS operational and instrumental errors has been developed and can serve as a tool prior to calling the Agilent call center for technical assistance (*see Appendix VII*).

CHAPTER 3

LOW-MOLECULAR-MASS LABILE METAL POOLS IN *ESCHERICHIA COLI:* ADVANCES USING CHROMATOGRAPHY AND MASS SPECTROMETRY*

Introduction

Transition metals have unique and exceptional catalytic properties which make them indispensable for life.[1] They are typically installed into the active sites of metalloenzymes where they orchestrate catalytic events, often involving substrate binding, electron transfer, and/or small-molecule activation. Ironically, the same properties that make them indispensable for life also make them dangerous. Many iron and copper complexes react with O_2 or H_2O_2 (ala the Fenton reaction) to generate reactive oxygen species that damage DNA, membranes, proteins, and other essential cellular components.[4,5] The mismetallation of zinc and manganese into protein sites designed for other metals is also problematic.[91,92] For this reason, metal ion *trafficking* – the translocation of a metal from the plasma membrane where it enters the cell, to the site of installation into its "client" apo-protein, is not only critical for the cell's survival but must take place in a manner that protects the cell from the metal and avoids toxic side-reactions.[12,93] In many cases, metals are passed from one protein chaperone to the next[94], but in others, low-molecular-mass (LMM) metal complexes are likely involved[93]. Such labile metal complexes or pools also appear to be involved in metal ion homeostasis and signalling.[95–99] Metal-associated diseases often involve metal ion dysregulation, altered trafficking patterns, and/or increased oxidative damage.[16,100] A more chemical-level understanding of labile metal trafficking would improve the understanding of such biological processes and lead to new strategies for treating metal-associated diseases.

*Reprinted with permission from Paul A. Lindahl and Hayley N. Brawley. Low-Molecular-Mass Labile Metal Pools in *Escherichia coli*: Advances using Chromatography and Mass Spectrometry, *JBIC* **2021**. Copyright 2021 Springer.

Neither the exact chemical compositions of these trafficking metal complexes nor their cellular functions are established.[93] This knowledge-gap is due, in large measure, to their *lability* – i.e. they possess ligands that exchange rapidly due to the inherent weakness of metal-ligand coordinate bonds. Ligand exchange rates can be slowed by increasing the denticity of the ligands, employing certain metal oxidation or spin states, or by using particular donor atoms and coordination geometries. We hypothesize that the rate of lability has been adjusted, through evolutionary pressures, to be slow enough for such complexes to "hold together" during transit (to avoid arbitrary deleterious reactions) yet fast enough to release the metal efficiently to its client apo-protein. Such trafficking complexes are presumed to have non-proteinaceous ligands composed of metabolites possessing O, N, and/or S Lewis-basic donor atoms.

The most popular strategy for studying labile metal pools in cells is to expose intact cells to custom-designed fluorescence-based chelators.[49,54,101–103] These chelators enter cells and change their fluorescence properties upon binding labile metals. Quantifying these changes allows the size of *labile metal pools* to be quantified. This approach has an advantage over strategies in which cells are disrupted. Conversely, the chelator-based approach *destroys* the sought-after metal complexes, making it unlikely that this approach could ever be used to chemically identify metal trafficking complexes.[4] Moreover, chelators are not completely specific for a particular metal, much less for a particular metal complex, and different chelators and reaction conditions yield different estimates of the size and properties of labile metal pools.[93]

We are developing a complementary approach to study labile metal complexes in which cells are disrupted and soluble lysates are passed through an ultrafiltration membrane.[19,73,104,105] The resulting flow-through-solution (FTS) is passed down a size-exclusion chromatography (SEC) column, and the eluate is sent to an online ICP-MS. The column resolves species with molecular

masses between ca. 100 and 7000 Da. One challenge of this LC-ICP-MS approach is that endogenous metal trafficking complexes might be altered during sample preparation or during migration through the column; the advantage is the potential for collecting and identifying endogenous metal trafficking complexes and ultimately for establishing cellular roles.

We have attempted to identify labile metal complexes in the cytosol of *E. coli* but have encountered problems along the way. These include unwanted effects of a common chelator, unwanted secondary interactions of labile metals on the column, unwanted ligand-exchange reactions, and the unwanted suppression of ESI-MS signals due to salts present in the cytosol. Here, we describe our efforts to overcome these problems. Using the lessons learned, we then examined the labile metal content of the cytosol from *E. coli* and detected numerous LMM labile metal complexes. Although we have not established the chemical identity or cellular function of these complexes, we are closer to doing so than ever before.

Results

Our long-term objective is to determine the chemical composition of the LMM labile metal pools in *E. coli* and other biological systems. We previously detected LMM metal complexes in *E. coli* and *Saccharomyces cerevisiae*[19,73,105] but did not identify them; the main objective of those studies was to establish reproducibility. We initially focused on zinc because of its redox inactivity and ability to form stable coordination complexes, properties that increased our likelihood of success. We selected the Gram-negative model bacterium, *E. coli*, because much supporting mechanistic information was known about metal ion metabolism in this organism. FTS, which should exclusively contain species with masses < 3 kDa, was subjected to SEC. Eluates were sent directly to an ICP-MS for detection of metals, sulfur, and phosphorus. The LC was located in a

refrigerated inert atmosphere glove box to avoid oxidation of metal ions and sulfhydryl groups and to minimize ligand-exchange reactions.

A Holin/Endolysin-containing Strain Allowed Cell Lysis Without EDTA

We became acutely concerned with the chelator EDTA in our buffers when we noticed that the LMM Zn(II) species previously detected in FTSs (Figure III-1A, trace a) co-migrated with Zn(EDTA) (Figure III-1A, trace b). To investigate further, we lyophilized the Zn(II)-containing fractions that eluted from the column and rehydrated the dried material in minimal D_2O. ESI-MS of the resulting solution (Figure III-1B) demonstrated the presence of Zn(EDTA), including the pattern expected from the natural isotope distribution (49% ^{64}Zn; 28% ^{66}Zn; 4% ^{67}Zn; 18% ^{68}Zn). We removed EDTA from all buffers but discovered that removing it from the lysis buffer decreased the effectiveness of cell lysis. We switched to a custom strain of *E. coli* (MG1655+pZa31mycR) in which lysis occurred via canonical phage lysis. The strain contained a plasmid encoding two phage proteins, holin and endolysin, which upon freezing and thawing initiated cell lysis. These cells were used for the remainder of the study.

EDTA-free Cytosolic FTS Contained 2 – 5 Labile LMM Zinc Species with a Collective Concentration of ~13 µM

We isolated cytosolic FTSs from 10 independent batches of *E. coli* cells in the absence of EDTA and passed them through a ^{67}Zn-loaded column (see below). The cells contained an average of 400 ± 200 µM Zn(II), whereas isolated cytosol contained 200 ± 100 µM Zn(II), and FTS contained 13 ± 3 µM Zn(II) (determinations were back-calculated to concentrations within the cell). EDTA-free FTS displayed a different chromatogram that included, on average, 5 partially

resolved LMM Zn(II) peaks (Figure III-1A, trace c). The green lines simulated these peaks using parameters given in Table III-S1. A few individual traces exhibited just 2 of those Zn(II) peaks (Figure III-S1). We considered that the growth phase at harvest (early, mid, or late exponential) might reveal significant differences, but none was evident and so traces were averaged. Traces were obtained using 50 mM AA pH 6.5, the default mobile phase for the entire study. When EDTA-free FTS was treated with EDTA, the major peak in the resulting trace (Figure III-1A, trace e) migrated with Zn(EDTA) (Figure III-1A, trace f). Clearly, Zn(II) peaks obtained in the absence of EDTA more accurately represented the labile zinc pool in *E. coli*. Under these growth conditions, this pool constituted about 3% of the total Zn(II) in the cell. We concluded that the detected Zn(II) species were labile towards EDTA, and that the LMM Zn(II) complex previously reported[19] was probably Zn(EDTA). All other FTSs described in this manuscript were isolated in the absence of EDTA.

Supplementing the growth medium with 100 μM $Zn(acetate)_2$ led to large increases in the LMM Zn(II) pool, to an average of 200 ± 100 μM (range from 70 – 320 μM). Most of the additional Zn(II) eluted as an intense broad peak at ca. 40 mL (Figure III-1A, trace d) which likely arose from hydrated Zn(II) ions that interacted strongly with the column. Such peaks were only observed when the growth medium was supplemented with $Zn(acetate)_2$. Curiously, the Zn(II) peak with V_e ≈ 21 mL in traces from un-supplemented FTS was absent in supplemented FTS whereas the other 4 peaks were present under both conditions, and with similar relative intensities. See Table III-S1 for parameters used to simulate these and other peaks.

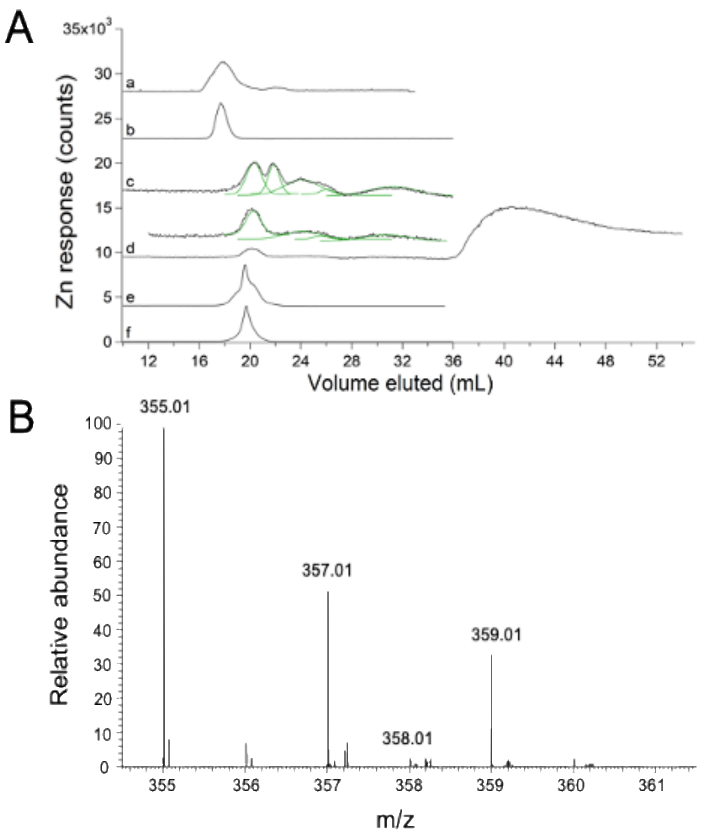

Figure III-1. Zn-detected LC-ICP-MS chromatograms (A) and ESI-MS spectrum (B) of *E. coli* FTS. Panel A: (a), average of 3 traces of cytosolic FTS isolated from MG1655 *E. coli* cells using EDTA. (b), 1 µM $ZnCl_2$ + 1 µM EDTA ÷ 4. The mobile phase for (a) and (b) was 20 mM ammonium bicarbonate pH 8.5. (c), average of 8 independent traces of FTS from RYMG1655+pZa31mycR *E. coli* cytosol (black) overlaid with simulations (green). Unless specified otherwise, no EDTA was used during isolation, the default mobile phase was 50 mM AA pH 6.5, and the cells were MG1655+pZa31mycR. (d), average of 2 traces from independent FTSs of cells grown in 100 µM $Zn(acetate)_2$ supplemented growth medium. Offset is (d) ×5. (e), FTS as in (c) but incubated with 500 µM EDTA ÷20. (f), 1 µM $Zn(acetate)_2$ + 20 µM EDTA ÷10. Panel B**:** Positive mode spectra of Zn-containing LC fractions from FTSs isolated as in (a), then lyophilized and resuspended in D_2O. Lines with indicated masses reflect the 1+ charge state of Zn(EDTA) and showed the expected isotope pattern. ×# and ÷# refer to an #-fold multiplication/division of the detector response in the plotted trace.

Zinc-loading Minimized Metal Interaction with Columns

We previously reported that labile LMM metal complexes partially adsorbed onto, and desorbed from, the SEC column.[73,104] Metal ions likely participated in secondary ionic interactions with basic groups on the solid support such as carboxylates.[106] Previously, we cleaned the column regularly and extensively using a chelator cocktail, and on occasion, with dilute acid and base. However, low detector response and spurious metal peaks remained problematic. The latter effect was due to "injection-initiated" metal ion desorption in which simply injecting a sample perturbed the column sufficiently to dislodge small quantities of metal ions.

We developed three methods (see Chapter II) to minimize adsorption/desorption problems further – namely by saturating basic sites on the column with a particular isotope of zinc (^{67}Zn) and then detecting two different isotopes (^{66}Zn and ^{68}Zn) in subsequent analyses of samples containing natural-abundance isotopes of zinc. Zinc-loading by method 2 caused ~ 0.1% of the sites on the solid support to coordinate ^{67}Zn(II) ions. Loading by method 3 caused binding of ~ 2.5% of sites. Although fewer sites were bound by method 2, blocking them was enough to minimize the interaction of hydrated metal ions with the column. We suspect that the affinity of the sites to Zn(II) was variable and that the strongest binders caused most of the problem. Method 3 provided the best reproducibility and largely eliminated spurious LC peaks. Regardless of method, loaded ^{67}Zn(II) ions gradually desorbed, such that the column had to be reloaded periodically.

The behavior of Zn-loading is illustrated in Figure III-2. The grey ^{66}Zn-detected traces in Figure III-2A, traces a – c were obtained by passing 5, 2, and 1 µM natural-abundance Zn(acetate)$_2$ through an unloaded column. Peaks were extremely broad and showed severe tailing. Distorted peak shapes likely reflected binding interactions with the column that were strong enough to hinder

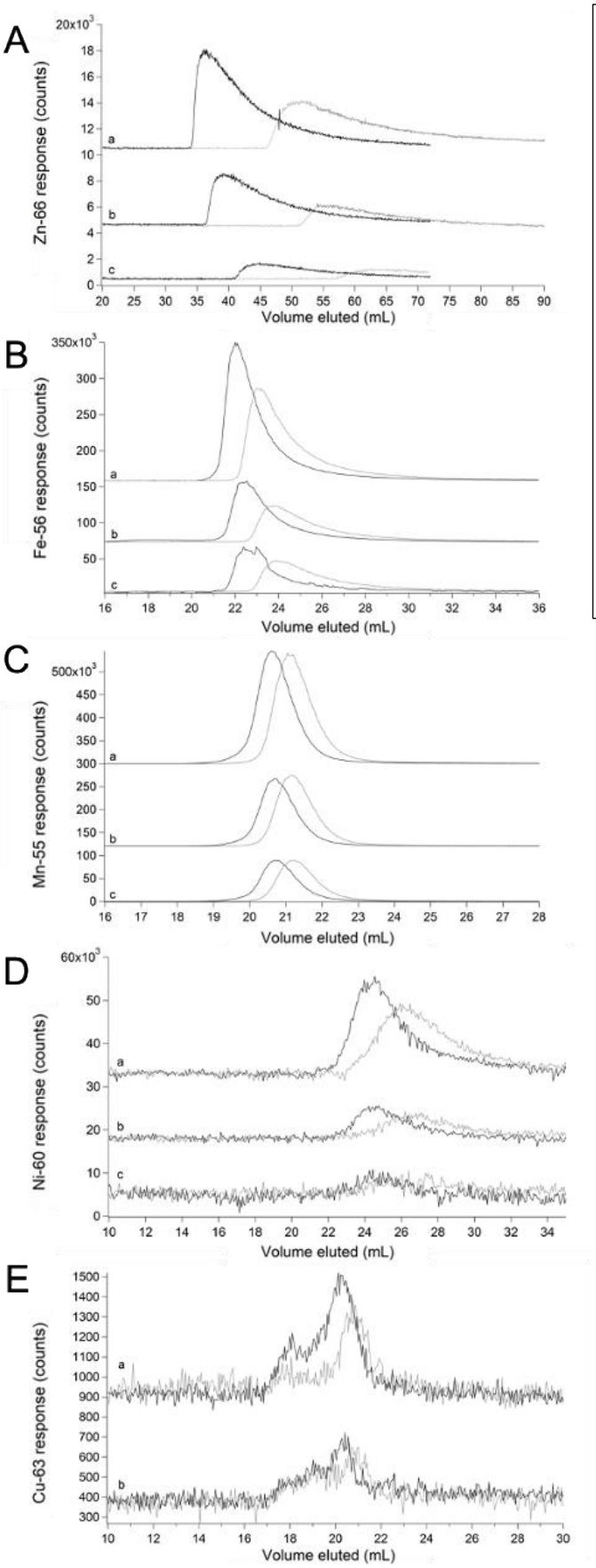

Figure III-2. **Chromatograms of aqueous zinc (A), iron (B), manganese (C), nickel (D), and copper (E) on an unloaded (grey) and $^{67}ZnSO_4$-loaded single SEC column (black).** A (a - c), 5, 2, and 1 µM Zn acetate, respectively; B (a – c), 5, 2, and 1 µM $FeSO_4$. C (a – c), 5, 2, and 1 µM $MnCl_2$; D, (a – c), 5, 2, and 1 µM $NiSO_4$. E (a – b), 5 and 1 µM $CuSO_4$.

passage but weak enough to allow passage within the timeframe of the experiment. As the concentration of Zn(II) increased (c → a), the elution volume (V_e), tailing, and peak-width all decreased. We conclude that as the concentration of Zn(II) in the sample increased, column interactions declined, requiring less elution volume and affording greater homogeneity. The same phenomenon was evident in the corresponding black ^{66}Zn(II) traces of Figure III-2A, which were obtained by passing the same solutions through a ^{67}Zn-loaded column. Elution volumes were reduced further when the loaded column was used, and linewidths were narrower, indicating diminished column interactions. We used a "ghost column" (consisting of PEEK tubing that replaced the actual column) and peak-fitting software to show that > 90% of injected Zn(II) in samples eventually eluted from *both* loaded and unloaded columns.

A similar though less severe phenomenon was evident by passing aqueous iron, nickel, and manganese ions through the column. The grey traces in Figure. III-2B, obtained by passing 5, 2, and 1 μM $FeSO_4$ through the column, exhibited broad peaks with some tailing. As the concentration of iron increased (c → a), V_e, linewidths, and tailing all decreased. The corresponding black traces, obtained by injecting the sample solutions onto a loaded column, exhibited sharper peaks and lower V_e. Again, this illustrated a decline in column interactions due to ^{67}Zn-loading. Nearly 100% of the injected iron eventually eluted from the column regardless of whether it was loaded. Two effects might have been involved, including an interaction with the column that delayed elution and caused tailing, and an "overloading" effect in which disproportionately more metal ions bound to the column when higher concentrations were injected, thereby causing injector-initiated spurious metal peaks. The same trend was observed when passing 5, 2, and 1 μM $NiSO_4$ through the columns (Figure III-2D). Passing manganese ions through the column afforded sharp and nearly Gaussian peaks (Figure III-2C) regardless of

whether the column was loaded. Of the metals tested, manganese ions probably interacted least with the column.

The opposite situation was found with aqueous Cu(II) ions, as little of the injected Cu(II) eluted from the column (Figure III-2E). More Cu(II) eluted from the ^{67}Zn-loaded column than from an unloaded column, but peak shapes were similar. Only 1% of the Cu(II) injected onto the Zn-loaded column eluted; the rest must have been adsorbed, accounting for the poor signal-to-noise ratio. The observed signal is likely due to a contamination in the mobile phase. We suspect that aqueous Cu(II) ions bound the column so strongly that they displaced bound ^{67}Zn ions; however, we were unable to detect Cu-dependent ^{67}Zn elution. Reassuringly, the different behaviors observed followed the Irving-Williams series[107] in which the order of binding strengths (to classical O-, N-, and S–based ligands) varies in the order (weakest) Mn(II) < Fe(II) < Ni(II) < Zn(II) < Cu(II) (strongest).

Chromatographic Behavior of Iron and Zinc Standards Reflected the M-L Binding Strength of the Complex

At this point, we shifted focus to iron, as its interaction with the ^{67}Zn-loaded column was weaker than zinc's, yielding sharper peaks that were easier to study. Iron(ATP) is a candidate cytosol trafficking complex[108], and so we examined its chromatographic properties by mixing 1 μM $FeSO_4$ with increasing concentrations of ATP. Both iron and phosphorus signals were monitored. In the absence of ATP, iron migrated as a broad tailing peak with $V_e \approx 24$ mL (Figure III-3A, trace a). As ATP concentrations increased (and with [$FeSO_4$] fixed at 1 μM), the iron peak shifted left and sharpened, ultimately eluting at ca. 23 mL. This behavior indicated that Fe and ATP formed a complex at sufficiently high concentrations of ATP but that the complex dissociated

as it migrated through the column such that the iron eluted at different mobile phase volumes depending on the ATP concentration. The chromatographic behavior of ATP was independent of iron but was unexpectedly complicated nevertheless (Figure III-S2, panel A). ATP migrated as 3 peaks, including a major peak at 23.5 mL and two low-intensity "satellites" at 22 mL and 25.5 mL. The satellite peaks did not comigrate with inorganic phosphate or ADP, which would have indicated hydrolysis of the standard. They may have been due to impurities in the ATP standard.

The chromatographic behavior of Fe(ATP) changed when the concentration of AA in the mobile phase was lowered from 50 to 20 mM. Using 20 mM AA, the 1 μM $FeSO_4$ sample lacking ATP eluted as a broad trailing iron peak at ca. 27 mL (Figure III-3B, trace a), a downstream shift of ca. 2 mL relative to the peak obtaining using 50 mM AA. We interpreted this as indicating a stronger interaction between aqueous Fe(II) and the column. As the ATP concentration increased, the broad tailing peak remained until the ATP concentration was $\geq$ 500 μM. At such high ATP concentrations, the broad tailing peak was replaced by a sharper peak with a more Gaussian lineshape ca. 23 mL (Figure III-3B, traces f and g). This peak shifted and sharpened with increasing ATP concentration. We conclude that an Fe(ATP) complex formed more tightly when 20 mM AA was used in the mobile phase but that the interaction between iron and the column was also stronger, giving rise to the broad tailing and lack of comigrating iron and phosphorus signals. The corresponding phosphorus traces using 20 mM AA followed the same general trend as with 50 mM AA, including the two satellite peaks (Figure III-S2, panel B)

Traces of two tight-binding iron complexes, $[Fe(phen)_3]^{2+}$ and $[Fe(BPY)_3]^{2+}$, where phen = 1,10-phenanthroline and BPY = 2,2'-bipyridine, were simpler to interpret. Reported logβ values for these complexes are 21.2 and 17.5, respectively.[108] Our LC-ICP-MS system included an online diode-array UV-vis spectrometer. This allowed the intact colored complexes and the metal to be

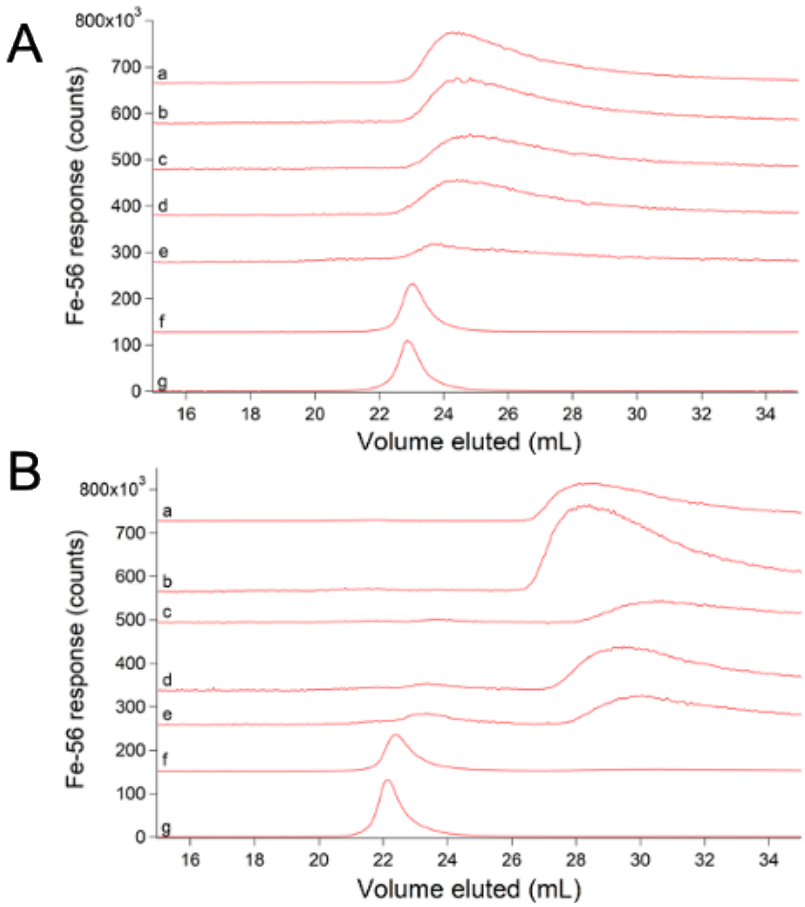

Figure III-3. Iron-detected chromatograms of Fe(ATP) using 50 mM (A) and 20 mM (B) AA pH 6.5 mobile phases. All traces are from samples containing 1 µM $FeSO_4$ + the following (final) µM concentrations of Na_2ATP. Panel A: (a), 0; (b), 5; (c), 10; (d), 25; (e), 50; (f), 500; (g), 1000. Panel B: (a), 0; (b), 5; (c),10; (d), 25; (e), 50; (f), 500; (g), 1000.

monitored simultaneously and independently as they eluted from the column. Both iron and UV-vis traces of $[Fe(phen)_3]^{2+}$ and $[Fe(BPY)_3]^{2+}$ exhibited single comigrating peaks (Figure III-4A, traces a and b), establishing that these complexes remained intact as they migrated through the column.

The column was calibrated by plotting the logarithm of the standard molecular mass *vs.* the ratio of V_e to void volume (V_e/V_0) where V_0 was determined to be 9.3 mL using thyroglobulin. The best-fit linear-regression line was $\log(MM) = -0.920(V_e/V_0) + 5.197$ with an R^2 of 0.96. We expected that species would migrate through the column with V_e inversely proportional to the logarithm of molecular mass of the species, but this was not always the case (Figure III-4B, triangles). For example, $[Fe(phen)_3]^{2+}$ has a higher molecular mass than $[Fe(BPY)_3]^{2+}$ (570 vs. 524 Da), but it migrated as though it had a lower mass (Figure III-4B, yellow vs. dark red triangle). This problem was exacerbated for weakly coordinated metal complexes in which V_e shifted with changes in the concentration of the ligand, mobile phase, and the extent of interaction with the column.

Iron GSH is another candidate cytosol trafficking complex[62,109], and so we examined the chromatographic properties of 1 μM $FeSO_4$ solutions mixed with increasing concentrations of GSH in hopes of generating the complex. Each solution was passed down the column (using 50 mM AA mobile phase), and the eluate was monitored for iron and sulfur (Figure III-5A). The experiment was repeated using 20 mM AA mobile phase (Figure III-5B). GSH migrated with $V_e \approx 21$ mL regardless of mobile phase whereas V_e for the iron peaks shifted depending on the GSH concentration and mobile phase. At low GSH concentrations, iron migrated as a broad tailing peak at $V_e \approx 23$ mL (Figure III-5A, trace a) and 29 mL (Figure III-5B, trace a), depending on mobile phase. These peaks were nearly identical to those observed with $FeSO_4$ alone. In solutions

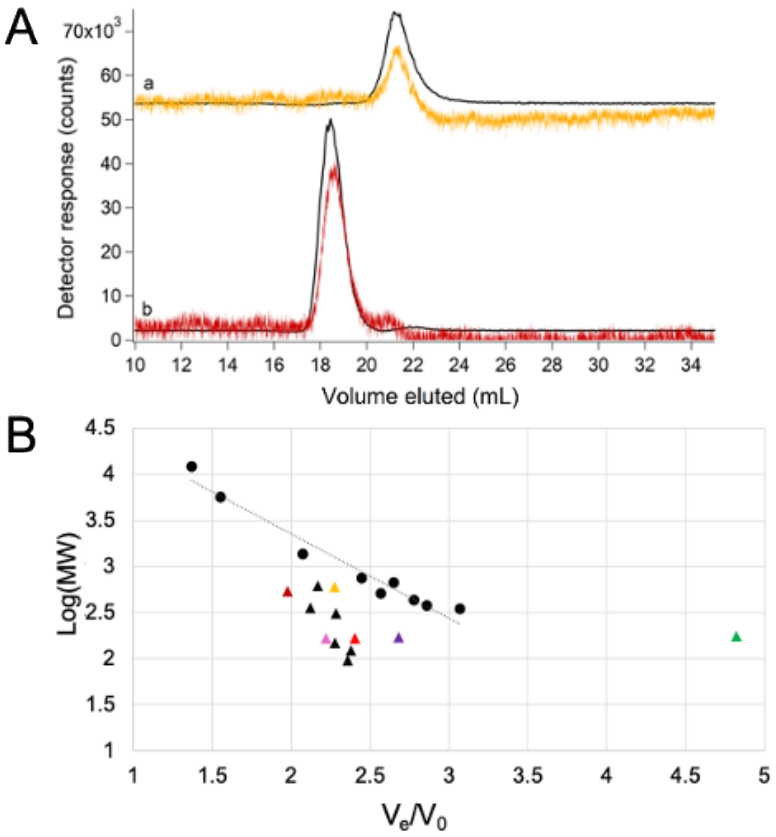

Figure III-4. Chromatograms of $[Fe(phen)_3]^{2+}$ (orange) and $[Fe(BPY)_3]^{2+}$ (red) (Panel A) and deviations from expected molecular mass trend line (Panel B). Panel A: (a), 2 µM $FeSO_4$ + 20 µM phen detected by iron ICP-MS (black, ÷1.33) and at 510 nm (orange, $\times 10^4$); (b), 2 µM $FeSO_4$ + 20 µM BPY detected by iron ICP-MS (black, ÷2) and at 523 nm (red, $\times 10^4$). Panel B: molecular mass calibration curve and trendline ($\log(MW) = -0.9204(V_e/V_0) + 5.1971$; $R^2 = 0.9575$) using standards from Table S1 (circles) and a Zn-loaded single column. Deviant standards are shown as triangles. $[Fe(phen)_3]^{2+}$ and $[Fe(BPY)_3]^{2+}$ are color-coordinated to UV-vis traces in Panel A. Aqueous metal standards were Zn acetate (green), $FeSO_4$ (bright red), $MnCl_2$ (pink) and $NiSO_4$ (purple).

containing intermediate concentrations of GSH, the iron peak shifted left and sharpened (Figure III-5A, trace b and 5B, trace b). The traces of solutions containing 50 or 100 mM GSH had a broad peak that migrated at about the same V_e as peaks present in solutions containing 0.1 and 1 mM GSH (red dashed lines). In addition, the traces involving 50 or 100 mM GSH contained an intense Fe peak at ca. 22 mL (Figure III-5A, trace c) and at ca. 26 mL (Figure III-5B, trace c), simulated in the dashed black lines. Also, trace c of Figure III-5B exhibited a minor Fe peak at ca. 22 mL which partially overlapped the dominant sulfur peak centered at 21 mL. We regard both iron peaks (at 22 mL using 50 mM AA and 26 mL using 20 mM AA) as Fe(GSH) candidates. This behavior (shifting due to changing the concentration of the coordinating ligand, and development of new peaks when high concentrations of the ligand are used) indicated weaker binding for Fe(GSH) than for either $[Fe(phen)_3]^{2+}$ or $[Fe(BPY)_3]^{2+}$. Consistent with this assessment, reported stability constant for Fe(GSH) is $\log\beta = 5.1 - 5.6$.[62]

Despite zinc's strong interaction with the ^{67}Zn-loaded column, we assessed its chromatographic properties by mixing 2 μM $Zn(acetate)_2$ solutions with either 0.1, 1, or 100 mM GSH (Figure III-S3). Each solution was passed down the column (using 50 mM AA mobile phase), and the eluate was monitored for zinc and sulfur. Direct comigration of zinc and sulfur peaks at ca. 21 mL was only observed when GSH concentration was 100 mM (Figure III-S3, trace D); complexation of Zn(GSH) was confirmed via positive mode ESI-MS (m/z = 370.00, 372.00, 373.00, 374.00) for the fraction containing the standard peak. As with the Fe(GSH) standards, when increasing amounts of GSH was mixed with $Zn(acetate)_2$, a shift in the Zn(II) trace was observed. This demonstrated weak binding of Zn(GSH).

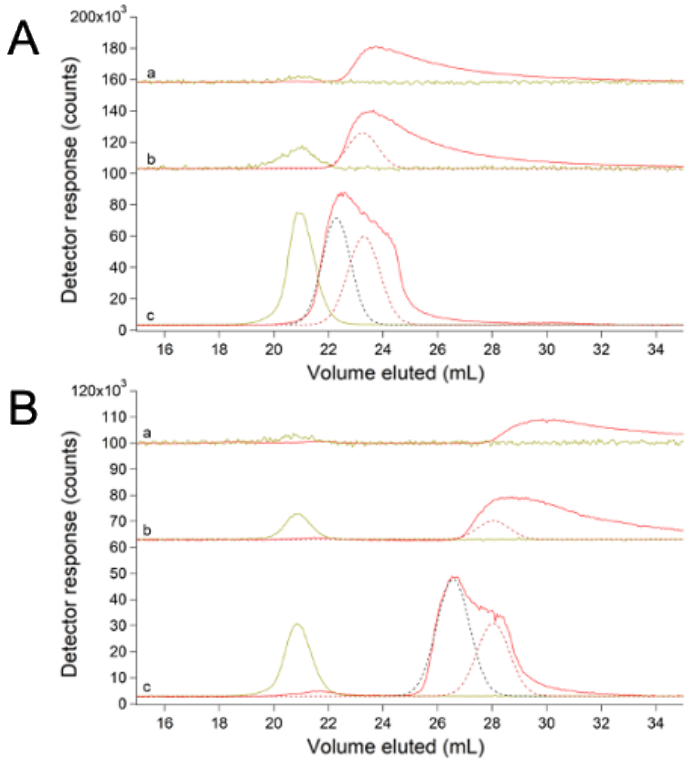

Figure III-5. Chromatograms of $FeSO_4$ (red) and GSH (yellow) using 50 mM (A) and 20 mM (B) AA mobile phase buffers. Panel A: (a), 1 µM $FeSO_4$ + 100 µM GSH ×5; (b), same as (a) but with 1 mM GSH; (c), same as (a) but with 100 mM GSH ÷10. Panel B: (a), 1 µM $FeSO_4$ + 100 µM GSH ×5; (b), same as (a) but with 1 mM GSH ÷10; (c), same as (a) but with 50 mM GSH ÷10. Dashed lines are simulations.

The LMM Sulfur Pool Consisted of GSH, GSSG, Methionine and Cysteine

The averaged sulfur-detected trace of cytosolic FTSs exhibited a broad unresolved peak suggesting multiple contributing species (Figure III-6A, trace a). Individual sulfur traces of FTS are given in Figure III-S4. Cysteine, methionine, GSH, and GSSG standards migrated in this region (Figure III-6A, traces b - e), suggesting that they might contribute to the observed broad FTS peak. Peaks from each species were simulated (color-coded lines in Figure III-6A, trace a) and combined to recreate the overall experimental trace (black line). To better resolve each contribution, FTS was passed through the double ^{67}Zn-loaded column. Sulfur-detected traces exhibited 4 resolved species (Figure III-6B). The ESI-MS spectra of fractions collected when FTS eluted from the double column (Figure III-S5) included peaks at m/z = 613.16, 308.09, 150.06, and 122.03 Da for LC peaks e, d, c, and b, respectively in Figure III-6B. This confirmed the presence of the GSSG, GSH, methionine, and cysteine as predicted by fitting the unresolved peak obtained with the single column. The intensity of each contributing simulation was converted into absolute concentration using calibrated intensities of standard peaks, and those concentrations were multiplied by the dilution factors involved in isolating FTS. Accordingly, the concentrations of GSH, GSSG, methionine, and cysteine in *E. coli* cytosol were calculated to be 3000, 400, 800, and 200 µM, respectively. The concentration for GSH was similar to previous reports, but lower concentrations have been reported for oxidized glutathione, methionine, and cysteine (5, 150, and 20 - 100 µM, respectively).[62,78,82,110] No other LMM sulfur species were evident, suggesting that if any were present in cytosol their concentrations must be < 200 µM.

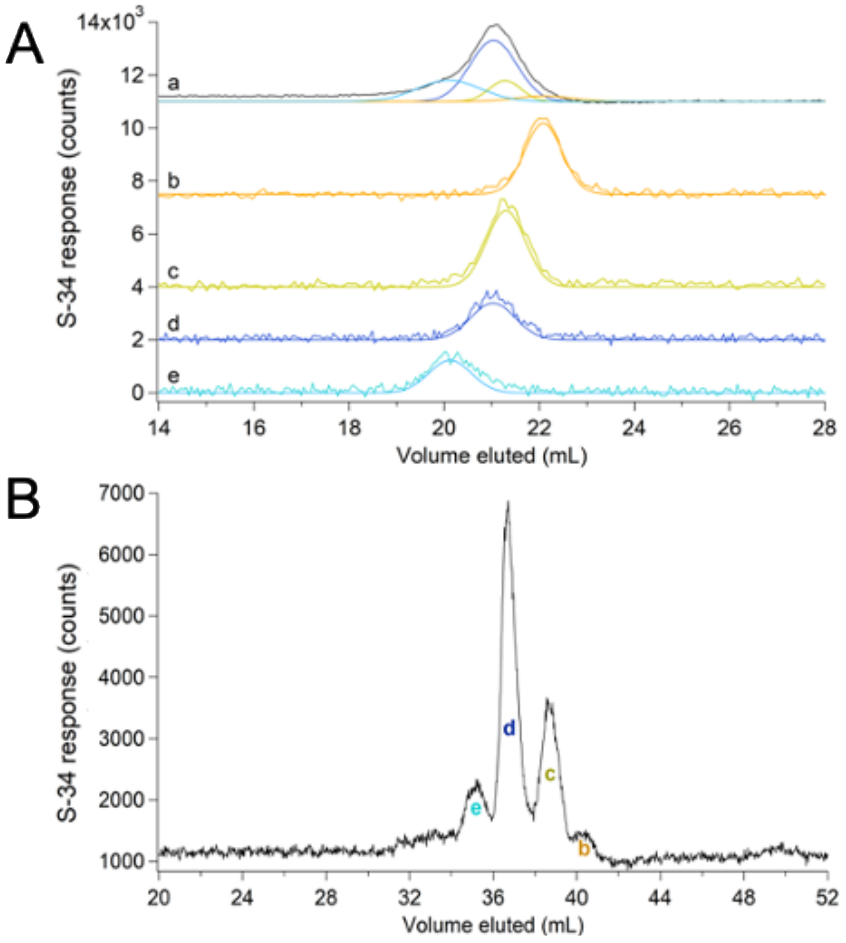

Figure III-6. Sulfur-detected chromatograms of FTS and standards on single (A) and double (B) SEC columns. Panel A**:** (a), averaged FTS trace (black) and simulations (colored lines coded with standard simulations below). (b), 500 µM cysteine; (c), 500 µM methionine; (d), 250 µM GSH; (e), 250 µM GSSG. Panel B: FTS replicate with peaks (b) – (e) correspond to standards in Panel A that were identified by positive-mode ESI-MS.

FTS Included Many LMM Phosphorus-containing Metabolites

The FTS exhibited one intense LMM phosphorus peak (with $V_e \approx 22$ mL) and ca. 6 minor-intensity peaks (Figure III-7, trace a). Individual traces are given in Figure III-S6. Solutions of phosphorus standards Na_2HPO_4, $NaH_3P_2O_7$, Na(polyphosphate) after ultrafiltration, NADPH, NADH, AMP, ADP, and ATP exhibited peaks (Figure III-7, traces c – h), some of which comigrated with those in the FTS traces (color-coded lines in Figure III-7b). Phosphate and pyrophosphate/polyphosphate traces are presented in Figure III-7c. The peaks from these standards were simulated and the same parameters were used to simulate the peaks in the FTS traces. Negative mode ESI-MS of fractions from FTS eluate established the presence of phosphates (m/z= 96.97; 194.95; 292.92), pyrophosphate (m/z = 176.94), AMP (m/z = 346.06), ADP (m/z = 426.02), ATP (m/z = 505.99) and NADH (m/z = 664.11) (Figure III-S7). Inorganic phosphate ions and nucleotides were the main LMM phosphorus species in *E. coli* cytosol. The total phosphorus concentration in *E. coli* cytosolic FTS was 140 ± 40 mM. The intracellular inorganic phosphate concentration is 1 – 10 mM.[83] *E. coli* cells accumulate excess phosphate ions as polyphosphate in millimolar quantities. Based on our simulations, the ATP and ADP concentrations are 1000 and 200 µM, respectively, similar to reported concentrations (1300 – 2000 µM and 450 µM, respectively).[78,81] Reported concentrations of AMP (ca. 70 µM) were dramatically lower than we observed (1000 µM). Although ESI-MS analysis established the presence of pyrophosphate, inorganic phosphates, GSSG, GSH, and other potential ligands (citrate, glutamic acid, etc.) in FTSs, no metal-ligand complexes were detected

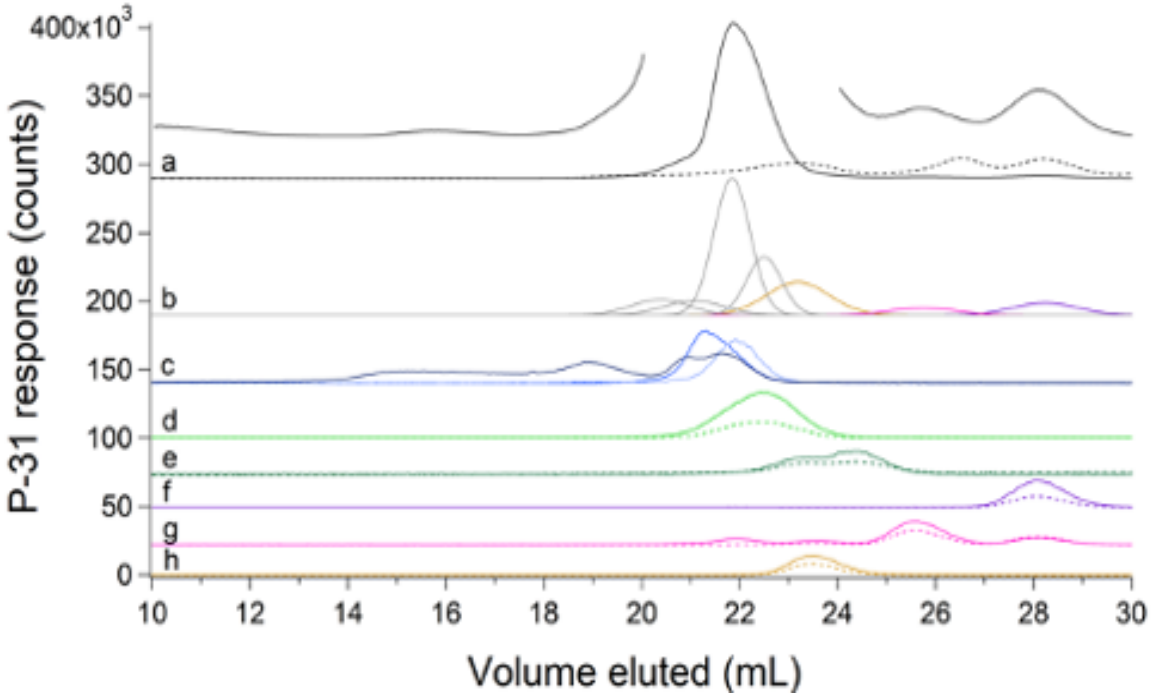

Figure III-7. Phosphorus-detected chromatograms of FTS and standards. (a), average traces of FTS detected by ICP-MS (solid black line ÷10) and at A_{260} (dashed black line ×20). The offset line is the ICP-MS data magnified ×2 excluding the dominating peak. (b), simulations of the FTS attributed to any standard listed below. (c), polyphosphate after ultrafiltration (darker blue); 500 µM $NaH_3P_2O_7$ ÷2 (dark blue), 500 µM Na_2HPO_4 ×5 (light blue); (d), 100 µM NADPH ÷2 (solid line) and A_{260} ×20 (dashed line); (e), 100 µM NADH ×5 (solid line) and A_{260} ×200 (dashed line); (f), 100 µM AMP ×3 (solid line) and A_{260} ×20 (dashed line); (g), 100 µM ADP and A_{260} ×20; (h), 100 µM ATP and A_{260} ×30.

Salts in FTSs Suppressed ESI-MS Signals

We hypothesized that our inability to detect metal complexes by ESI-MS arose from the presence of salts in the FTS; "salt suppression" is a well-known mass spectrometry phenomenon.[111] To investigate, we obtained ESI-MS spectra of 0.5 mM GSH in water containing 25 mM of each salt present in the growth medium (Figure III-S8). The GSH peak was uniformly observed in all samples by ESI-MS, but its intensity in salt solutions relative to that in HPW was strongly diminished. Simple inorganic salts were not well resolved from the GSH peak using the single column (Figure III-8A); however, passing *E. coli* cytosolic FTS through the double column resolved these species nicely (Figure III-8B). The improved resolution of the double column was recognized late in our study, and so the single column remained the default. Also, there was a major disadvantage of the double column, namely that processing a sample was 5× slower than using a single column (200 min *vs*. 40 min).

FTS Consisted of 2 – 5 LMM Iron Species with a Collective Concentration of ~ 80 μM

Under the growth conditions used, *E. coli* cells contained 1000 ± 300 μM iron; isolated cytosol contained 400 ± 200 μM iron, and the cytosolic FTS contained 80 ± 20 μM iron. Thus, the labile iron pool in these *E. coli* cells accounted for 8% of the iron in the cell and 20% of the iron in the cytosol. When the medium was supplemented with 100 μM $Fe(III)_2(citrate)_3$, the average concentration of iron in the FTS increased to 200 μM. The range of concentrations determined in 4 independent batches was unusually large (65 μM to 500 μM) perhaps due to subtle differences in aerobicity during cell growth.[19,23] It is also possible that some supplemented iron may not have been fully removed despite extensive washing of cells during harvesting.

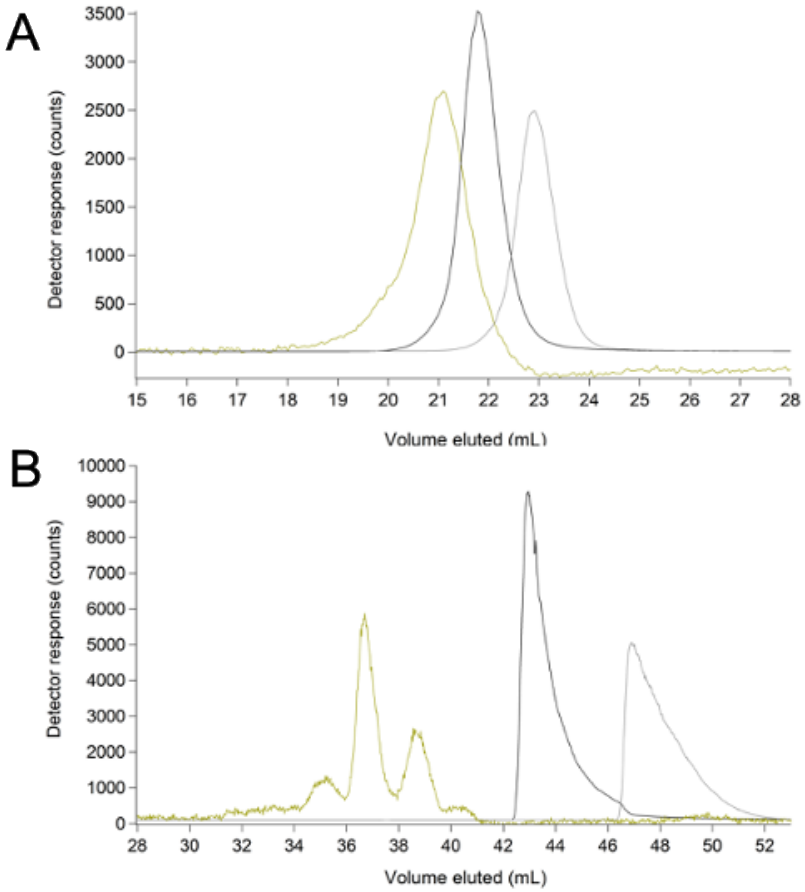

Figure III-8. Chromatograms of FTS on single (A) and double (B) SEC columns monitoring sulfur (yellow), sodium (black) ÷5×10^5, and potassium (grey) ÷10^4.

The average iron-detected trace of FTS revealed 5 partially overlapping peaks (Figure III-9, trace a). Some individual traces (Figure III-S9) exhibited as few as 2 iron species. The FTS from Fe-supplemented cells exhibited similar LC peaks but with different relative intensities (Figure III-9, trace c). There was some variation in iron speciation, possibly dependent on the stage of growth during harvest. Trace b in Figure III-9 was of FTS isolated from cells harvested at mid-exponential phase. The same harvest conditions were used for supplemented growth in Figure III-9c; the shapes of the two curves were closer to each other than to the average trace. BPY was added to one FTS batch; the formation of $[Fe(BPY)_3]^{2+}$, and the loss of ~ 70% intensity relative to the original peaks (Figure III-9 trace d and Figure III-4A, trace b) demonstrated the lability of the original detected LMM Fe-containing complexes.

We inadvertently demonstrated the lability of these complexes in another way, namely by treating FTS with acid phosphatase (PPX), which catalyzes the hydrolysis of polyphosphate chains.[112] The LMM metal species present before treatment were replaced with an increase in metals bound to PPX in the void volume (Figure III-S10). This suggests that PPX chelated the LMM metal species in *E. coli* cytosol. We performed similar experiments previously to evaluate whether LMM metal species in the cytosol of *S. cerevisiae* were coordinated by polyphosphate ions.[73] At that time, we had difficulty interpreting our results (because metal polyphosphate complexes were not expected to be in the cytosol), but they can now be explained by assuming that PPX chelated metals from LMM metal complexes in the cytosol; PPX-sensitive species probably do not coordinate polyphosphate ions.

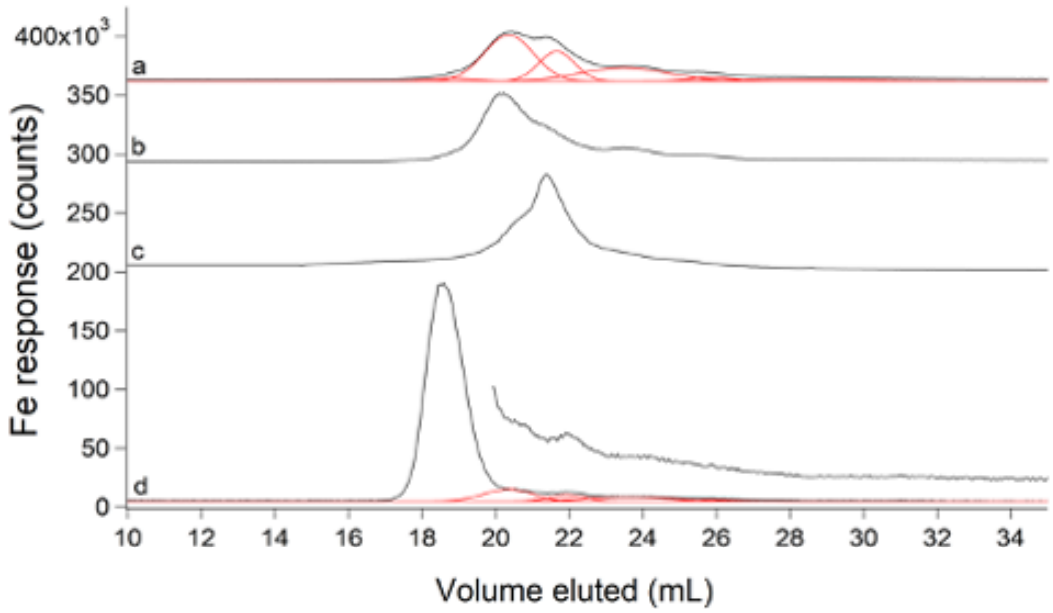

Figure III- 9. Iron-detected chromatograms of FTSs. (a), average of 8 FTSs (black) and simulations (red); (b), average of 4 FTSs harvested during mid-exponential growth; (c), average of 4 FTS from cells supplemented with 100 µM $Fe(III)_2(citrate)_3$ and harvested during mid-exponential growth; (d), un-supplemented FTS replicate incubated with 500 µM BPY and simulations for remaining peaks from (a) in red. Offset in (d) is the same trace but ×3.

FTS Contained 2 – 4 LMM Copper Complexes with a Collective Concentration of ~ 10 µM

The average copper FTS trace consisted of 4 partially overlapping LMM species with V_e between 15 – 22 mL (Figure III-10, trace a). These species became more intense during late stationary phase. Some individual traces (Figure III-S11) exhibited as few as 2 LMM copper species. The modest elution volumes and relatively strong peak intensities suggested that these copper species are *not* aqueous copper ions, as such ions adsorbed strongly to the column (Figure III-2E) in contrast to the apparent undeterred passage of these species. We supplemented the growth medium with 1 µM $CuSO_4$ (higher concentrations could not be used because they were toxic). Doing so increased the concentration of the LMM copper pool from 7 ± 1 µM to 9.3 ± 0.2 µM Cu (comparison made for mid-exponential growth phase) and it shifted the relative intensities of the LMM peaks (Figure III-10, trace c). Again, we matched the growth phase of Cu-un-supplemented cells during harvest; the control FTS exhibited in trace b in Figure III-10. Copper concentrations in whole cells and cytosol were 8 ± 2 µM and 6 ± 2 µM, respectively. The lability of the LMM copper species was established using the chelator TPEN. LC traces of TPEN-treated FTS exhibited a single peak (Figure III-10, trace d) that comigrated with a Cu(TPEN) standard (Figure III-10, trace e). We conclude, surprisingly, that *E. coli* contains a LMM *labile copper pool,* and that this pool represents the vast majority of the copper (roughly 80%!) in the cell. Some of this copper may be located in the periplasm, since this is the major site of copper metabolism in *E. coli*.[47]

FTS Contained LMM Manganese and Nickel Complexes

E. coli FTS exhibited two LMM Mn(II) peaks with $V_e \approx 20$ and 21 mL (Figure III-11, trace a). Individual traces, shown in Figure III-S12, were highly reproducible. The peak at 21 mL was

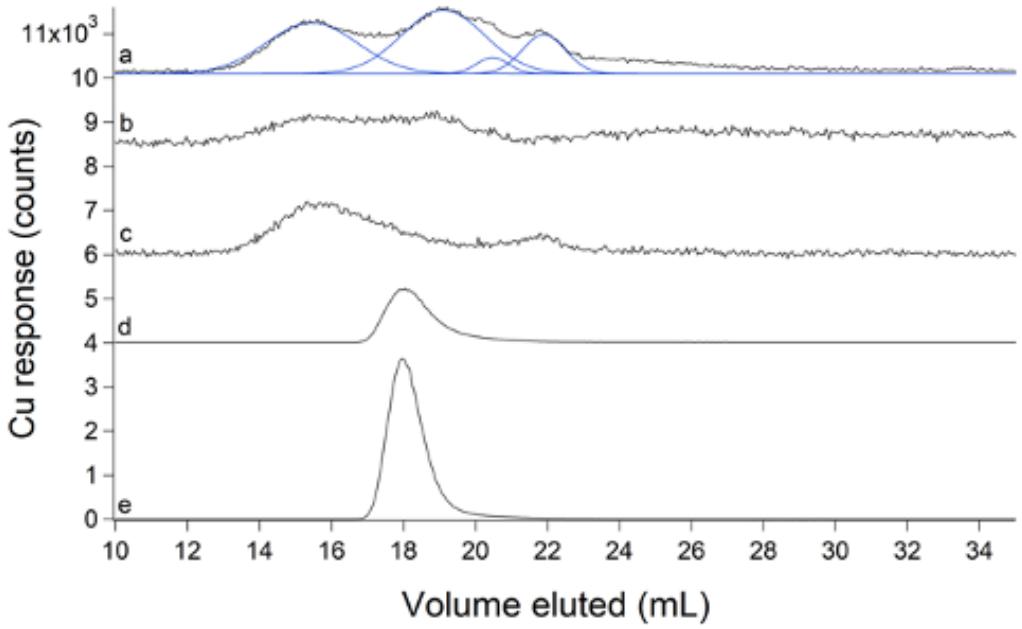

Figure III-10. Copper-detected chromatograms of FTSs (a - d) and standard (e). (a), average of 8 FTSs (black) with simulations in blue; (b), average of 4 FTSs from mid-exponential growth harvest; (c), FTS from cells supplemented with 1 µM of $CuSO_4$ and harvested in mid-exponential phase; (d), un-supplemented FTS replicate incubated with 50 µM TPEN ÷100; (e), 1 µM $CuSO_4$ + 10 µM TPEN ÷200.

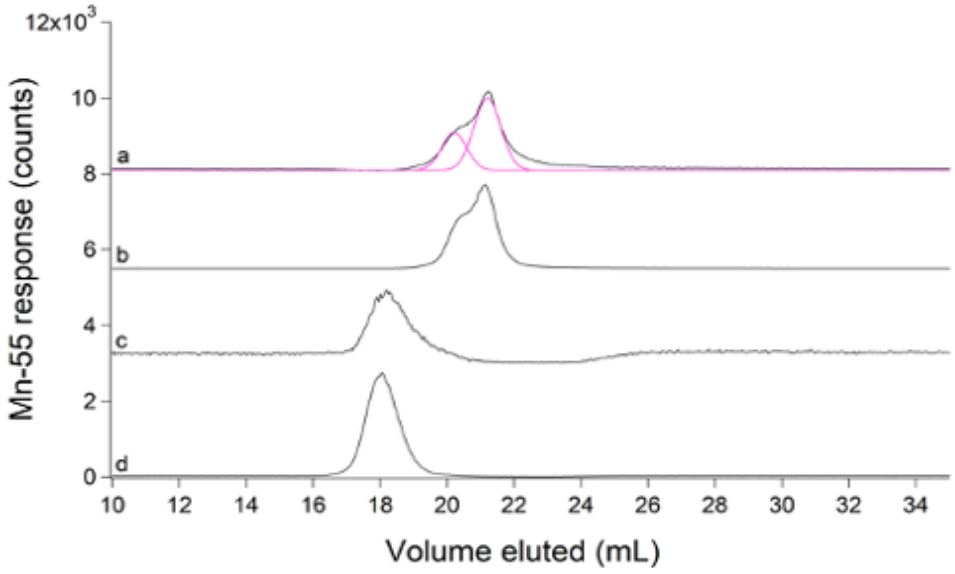

Figure III-11. Manganese-detected chromatograms of FTSs (a – c) and standard (d). (a), average of 8 FTSs (black) and simulations (pink); (b), FTS from cells supplemented with 100 µM of $MnCl_2$ ÷100; (c), FTS incubated with 50 µM TPEN; (d), 1 µM $MnCl_2$ + 10 µM TPEN ÷20.

about twice as intense as that at 20 mL. Under our growth conditions, *E. coli* cells and cytosol contained 7 ± 2 μM and 4 ± 1 μM Mn(II), respectively. The concentration of Mn(II) in FTS was 1.4 ± 0.7 μM. Supplementing the growth medium with 100 μM $MnCl_2$ increased the concentration of the labile Mn(II) pool to 115 ± 9 μM – a 70-fold increase! The Mn(II) trace for this batch was significantly more intense relative to un-supplemented FTSs but peak positions and relative intensities were about the same (Figure III-11, trace b). The lability of the two LMM Mn(II) species was demonstrated using TPEN (Figure III-11, c and d).

We did not focus on nickel until late in our study, but a retrospective analysis revealed two LMM Ni(II) species in *E. coli* FTS, with $V_e \approx 20$ (minor) and 21 (major) mL (Figure III-S13). The concentration of Ni(II) in FTS was 15 ± 2 μM. The corresponding sulfur trace comigrated with the Ni(II) peaks, raising the intriguing possibility of 1-2 LMM Ni-S complex(es).

Discussion

E. coli and probably all/most prokaryotic and eukaryotic cells contain non-proteinaceous low-molecular-mass metal complexes that are used in metal ion trafficking, regulation, and signalling. Although the existence of these complexes has been recognized for decades, the number of species involved, their chemical composition, and their specific roles in cellular physiology remain enigmatic. The fundamental problem is that metal complexes are labile such that their ligands dissociate and reassociate rapidly. The most popular approach to study these "labile metal pools" has been and continues to be using custom-designed fluorescence-based chelator probes. Much progress has been made using chelator probes, but they destroy the complexes of interest during detection, raising doubts that such an approach can ever identify such complexes or

establish their cellular roles. We are developing a complementary approach using an LC-ICP-MS system in conjunction with ESI-MS. In this study, we overcame several problems and have set the stage for future advances.

Proper sample preparation is critical for probing labile metal pools; metal chelators and buffers that coordinate metals and/or interfere with ESI-MS analysis should be excluded. EDTA is a common metal chelator that was difficult to eliminate; we did so by using a strain of *E. coli* that could be lysed by a simple freeze/thaw cycle. Metals tend to interact with size-exclusion columns which contain basic sites (carboxylate groups) that bind metals. Typically, the ionic strength of the mobile phase is increased to minimize secondary column interactions, but doing so here would have been problematic for ESI-MS and ICP-MS. Thus, we invented a new strategy to combat secondary interactions, namely passing a particular isotope of aqueous zinc ions (^{67}Zn) through the column which bind tightly to basic sites. Then when detecting zinc-containing eluents by ICP-MS, different zinc isotopes (^{66}Zn and ^{68}Zn) were monitored. Although the use of a "zinc-loaded" column did not completely inhibit all interactions and the column required periodic reloading, it minimized these problems and afforded greater reproducibility for probing endogenous LMM metal complexes in biological systems.[73]

Using a Zn-loaded column, the chromatographic behavior of metal complexes was found to depend on the binding strength of the complex. Tight-binding complexes like $[Fe(phen)_3]^{2+}$ and $[Fe(BPY)_3]^{2+}$ passed through the column intact whereas intermediate-binding complexes like Fe(ATP) and Fe(GSH) exhibited complex behavior in which the elution profile of the metal varied with the concentration of the coordinating ligand. Weak-binding metal complexes like hexaaqua-iron eluted slowly from the column and exhibited excessive broadening/tailing due to extensive column interactions.

We also assessed the importance of the mobile phase in chromatographic behavior; this was especially important for weak-binding metal complexes that interact strongly with the column. Mobile phase buffers with lower ionic strength promoted metal complexes to remain intact as they pass through the column but also promoted greater column interactions.

Finally, we identified salt suppression as a major problem in identifying labile metal pools by ESI-MS in aqueous cellular solutions, since such solutions contain high concentrations of salts. We found that using two SEC columns linked in series was an effective, albeit time-intensive, strategy for separating LMM non-proteinaceous metal complexes from salt-containing solutions.

With these lessons learned, we assessed the labile iron, zinc, copper, manganese and nickel pools in *E. coli* cytosol as well as LMM pools of sulfur and phosphorus. As expected, the major LMM sulfur species was GSH, followed by GSSG, methionine, and cysteine. The major LMM phosphorus species in the cytosol were inorganic phosphate ions and LMM polyphosphates followed by ATP, ADP, NADH, etc. Due to limited resolving capabilities of the single SEC column, the concentration of inorganic phosphate and LMM polyphosphates could not be determined; however, the calculated concentrations of later-eluting P species (ATP and ADP) were similar to those reported. The increased concentration of AMP observed relative to previous reports likely resulted from the DNA hydrolysis step in our cytosol isolation protocol which generates nucleotide monophosphates. While metal ions are capable of binding monophosphate groups of nucleotide monophosphates, no LMM metal species present in *E. coli* cytosol comigrated with AMP. Thus, the high concentration of nucleotide monophosphates should not have influenced the LMM metal pools.

Outten and O'Halloran concluded that WT *E. coli* cells are devoid of "free" (i.e. aqueous) Zn(II) ions based on experiments in which Zur and ZntR transcription factors were titrated with

aqueous zinc.[35] Zn-bound Zur suppresses Zn(II) import whereas Zn-bound ZntR stimulates Zn(II) export. An aqueous Zn(II) concentration of 10^{-15} M minimized both activities suggesting that *E. coli* cells operate under homeostatically-regulated conditions centered around this concentration. However, this concentration corresponds to less than one atom of aqueous Zn(II) per cell. Using our system, aqueous Zn(II) ions interacted strongly with the column, and they eluted as broad tailing features at large volumes. In contrast, labile LMM Zn(II) complexes with stronger ligands eluted earlier and as sharp peaks, indicating less interaction with the column. The LMM Zn(II) peaks that we detected are in the latter category. We conclude that *E. coli cytosol contains μM concentrations of labile LMM non-proteinaceous Zn(II) complexes but not aqueous or "free" Zn(II) ions*. This supports Outten and O'Halloran's conclusion that there is no "free" Zn(II) in the cell[35], but clarifies that there is a significant *labile zinc pool* nevertheless. The LMM labile Zn(II) species could potentially be involved in Zn(II) trafficking and regulation, and/or perhaps metallating the zinc proteome in *E. coli*. The situation is different when *E. coli* cells are grown in media that is supplemented with Zn(II). In this case, the cytosol contains high concentrations (10^{-5} M) of either *aqueous* Zn(II) ions or weaker-binding Zn(II) complexes that dissociate as they migrate down the column. Perhaps under zinc-stressed conditions, a secondary ligand of intermediate-binding strength sequesters excess Zn(II) ions in the cytosol. Based on the range of zinc concentrations observed upon media supplementation, cells containing high zinc may have been harvested in a transient state in which excess zinc was being actively trafficked and subsequently exported.

Bacillus subtilis and other Gram-positive bacteria use bacillithiol (BSH), a sugar-based LMM molecule with cysteine and malic acid groups attached, as a Zn(II) buffer. Zn(II) likely coordinates to the thiol, carboxylates, and/or amide functional groups. Helmann and coworkers[113]

have shown that the Zn(BSH) complex is strong-binding and present in the cell at sufficiently high (5 mM) concentrations such that the concentration of aqueous Zn(II) ions should be exceedingly low. They and others have suggested that GSH plays the same buffering role in *E. coli* and in other cells that contain GSH. Besides GSH, other potential ligands for the labile zinc pool includes ATP, citrate, and amino acids[12,114], all of which have been detected by ESI-MS of fractions from FTS eluate.

Hider and Kong have presented thermodynamic-based arguments that Fe(GSH) is the dominant LMM labile iron complex in the cytosol.[62,109] They simulated iron complex formation in the cytosol using known affinity constants, concentrations, pH, and redox properties. In support of this, we found that solutions of iron mixed with GSH at high concentrations afforded an LC peak that eluted ca. 22 mL suggesting complex formation. However, we were unable to demonstrate that any of the detected labile iron species in FTS was Fe(GSH), perhaps due to salt suppression in our samples.

Previous studies from our lab reported two LMM iron species in *E. coli* with similar apparent masses as observed here.[19] Mössbauer spectra of the LMM iron species in *E. coli* has parameters typical of complexes with 5 – 6 O/N ligands - and no sulfur.[19] However, previous batches used EDTA during cytosol isolation, and we are concerned that the Fe(EDTA) complex had formed and displaced the endogenous iron complexes. The concentration of LMM iron in *E. coli* was previous reported at ~ 200 µM, 2-3 times higher than observed here. However, growth conditions strongly affect the LIP concentration; for example, under aerobic conditions, the LIP concentration was only ~ 50 µM. Martin *et al.* determined a free intracellular iron concentration of 100 µM.[15] Daly and coworkers reported ultrafiltrate iron concentrations of just 1.2 µM.[115]

Like zinc, copper trafficking in both eukaryotic and prokaryotic cells does not involve aqueous copper ions.[43,46] Rather, copper is thought to be trafficked using copper-binding protein chaperones. Thus, the presence of non-proteinaceous LMM copper species in our FTSs was unexpected though we have recently detected similar LMM copper species in the cytosol of *S. cerevisiae*.[73] We have not chemically identified these copper species, but our results indicate that they are not simple aqueous Cu(II) ions; such ions adsorbed strongly to the column whereas the detected species eluted from the column at low V_e and sharp Gaussian lineshapes. Even more surprising is that the detected LMM copper species represent the majority of copper in the cell.

The labile Mn(II) species that we detected showed little interaction with the column, suggesting strong-binding ligands, but they also migrated in the same region as aqueous Mn(II) ions. Unstressed *E. coli* cells do not appear to use Mn(II), but under stressed conditions, Mn(II) replaces iron in superoxide dismutase and ribonucleotide reductase.[15] We suggest that the detected species metallates those enzymes. WT *E. coli* grown in LB medium reportedly contain ca. 5 μM Mn (similar to what we observed), most of which was associated with MnSOD.[15] Similar to our results, Martin et al. also observed a strong increase of Mn(II) concentration in *E coli* (to 35 μM) when media was supplemented with Mn(II), and they observed whole-cell EPR indicating that this was in the Mn(II) oxidation state. Daly and coworkers reported 13 μM manganese in *E. coli* cells and 0.3 μM manganese in FTSs.[115] Sharma et al. 2013 used electron spin-echo EPR and ENDOR spectroscopy to characterize the LMM Mn in *E. coli*.[116] They concluded that LMM Mn(II) ions were coordinated by orthophosphate or other phosphorus-containing ligands, some waters, but few, if any, nitrogen-containing ligands. While comigration between manganese and phosphorus traces was observed in our cytosolic FTS, further investigation is needed to determine if the LMM Mn(II) pool of *E. coli* is ligated by phosphorus-containing ligands.

Under anaerobic conditions, *E. coli* expresses the nickel permease system NikBCDE that imports Ni(II) ions which are then trafficked to Ni-containing [Ni-Fe] hydrogenases.[117,118] Trafficking involves a number of metallochaperone proteins as well as a Ni(L-His)$_2$ complex.[31] However, since our cells were grown aerobically, the Ni(II) species that we detected may not be associated with these processes. Under aerobic conditions, *E. coli* needs nickel for glyoxalase, with nickel imported (inefficiently) by magnesium transporters.[30,119] Further studies are required to establish the composition and cellular function of the detected nickel species.

In summary, the identification and characterization of labile metal pools in cells is extremely important in understanding metal ion trafficking, signalling, and regulation; however, this task is challenging due to the inherent lability of these complexes. In this study, we report major advances in overcoming problems and attaining this objective using LC-ICP-MS and ESI-MS. These advances position us closer than ever to identifying the sought-after endogenous LMM metal complexes that constitute labile metal pools in *E. coli* and other biological systems.

Acknowledgements

We thank Ryland Young (TAMU) for providing background strain MG1655 and plasmid pZa31mycR and Yohannes Rezenom of the Chemistry Mass Spectrometry Laboratory (TAMU) for ESI-MS data collection.

Supplementary Information

Zn (figure 1)		
Center (mL)	**Area (%)**	**FWHM (mL)**
(Ac) 20.3	26	1.4
(Ac) 21.9	15	1.0
(Ac) 24.1	30	3.3
(Ac) 26.1	4	1.4
(Ac) 31.3	25	4.5
(Ad) 20.2	2	1.8
(Ad) 23.9	1	3.3
(Ad) 25.7	0.4	2.0
(Ad) 30.5	2	4.5
Fe (figure 5)		
(Ab) 23.3	23	1.3
(Ac) 22.3	38	1.2
(Ac) 23.4	35	1.4
(Bb) 28.0	12	1.4
(Bc) 26.6	53	1.4
(Bc) 28.0	32	1.4
S (figure 6)		
Center (mL)	**Area (%)**	**FWHM (mL)**
20.1	28	1.6
21.1	51	1.2
21.3	14	0.8
22.1	7	1.4
P (figure 7)		
Center (mL)	**Area (%)**	**FWHM (mL)**
20.4	2	1.4
21.1	9	1.4
21.8	57	0.9
22.5	24	0.8
23.2	5	1.5
25.8	1	1.6
28.2	2	1.5
Fe (figure 9)		
Center (mL)	**Area (%)**	**FWHM (mL)**
(A) 20.4	51	2.0
(A) 21.8	18	1.2
(A) 23.6	24	3.3
(A) 26.1	2	1.4
(A) 28.3	5	4.6
(D) 20.4	6	1.6
(D) 21.9	3	1.1
(D) 23.6	4	2.8
(D) 25.9	1	1.4
Cu (figure 10)		
Center (mL)	**Area (%)**	**FWHM (mL)**
15.4	38	3.0
19.1	44	2.7
20.5	4	1.0
21.9	14	1.4
Mn (figure 11)		
Center (mL)	**Area (%)**	**FWHM (mL)**
20.2	32	0.9
21.2	68	0.9

Table III-S1. Parameters used to simulate chromatography peaks. FWHM, full width at half maximum. The areas listed for simulations of Figures 1Ad and 9D do not sum to 100% because the dominant peaks in those traces were not included.

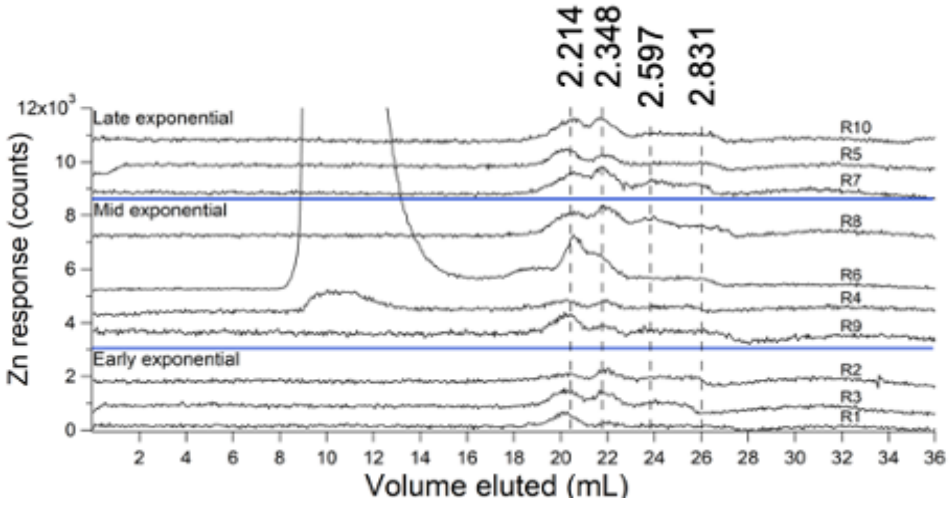

Figure III-S1. Zinc-detected chromatographic traces of individual batches of FTS. Replicates are listed in order from highest OD_{600} (top) at which cells were harvested to lowest (bottom). Blue horizontal lines separate the different exponential growth phases. Dashed vertical lines highlight LMM Zn species with V_e/V_o. R1-R10 are individual batches numbered chronologically.

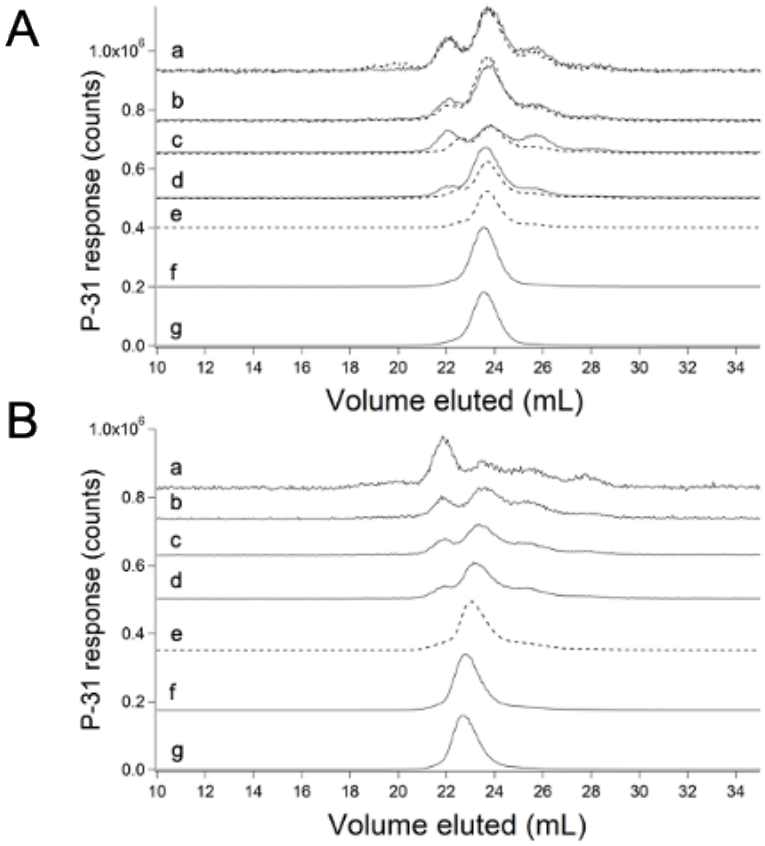

Figure III-S2. Phosphorus-detected chromatographic traces of Na_2ATP using 50 mM AA (A) or 20 mM AA (B) as the mobile phase. In A and B, the solid-line traces were from solutions containing 1 µM $FeSO_4$ + variable (final) concentrations of Na_2ATP, as follows in units of µM ATP. Panel A and B: (a), 5 ×200; (b), 10 ×100; (c), 25 ×40; (d), 50 ×20; (f), 500 ×2; (g), 1000. In A and B, the dashed-line traces were from solutions of Na_2ATP without added iron at the following concentrations (µM): Panel A and B: (a), 5 ×200; (b), 10 ×100; (c), 25 ×40; (d), 50 ×20; (e), 100 ×10; (f), 500 ×2; (g), 1000.

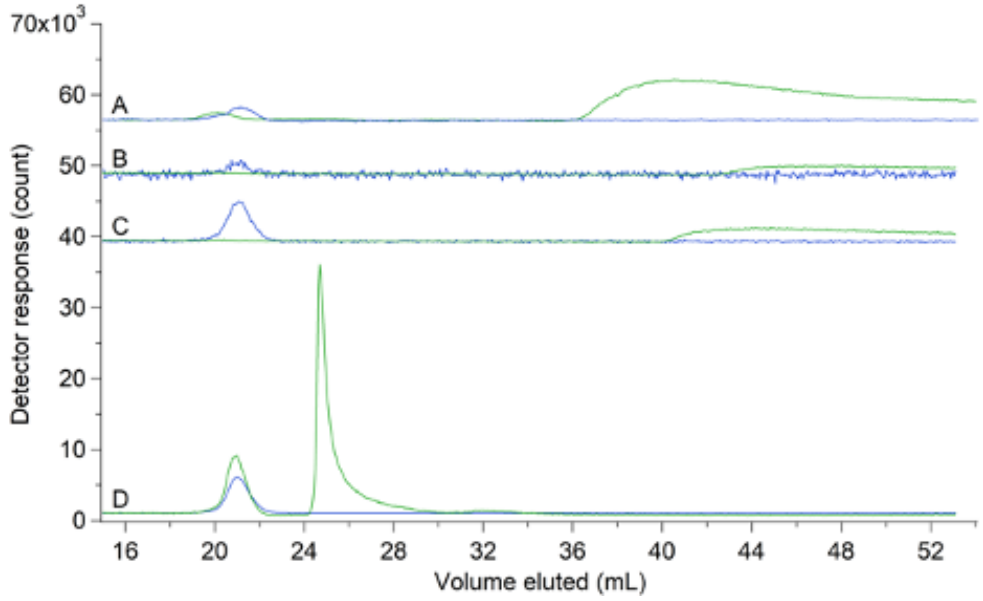

Figure III-S3. Zinc- and Sulfur-detected traces showing no Zn(GSH) complex in cytosolic FTS. (A), averaged FTS from cells supplemented with 100 µM Zn acetate (green line, Zn detected; blue line, S detected); (B), 100 µM GSH (blue) ×3 and 2 µM Zn acetate (green); (C), 2 µM Zn acetate (green) + 1 mM GSH (blue); (D), 2 µM Zn acetate (green) + 100 mM GSH (blue ÷100). Traces (B) – (D) were standards prepared in mobile phase buffer.

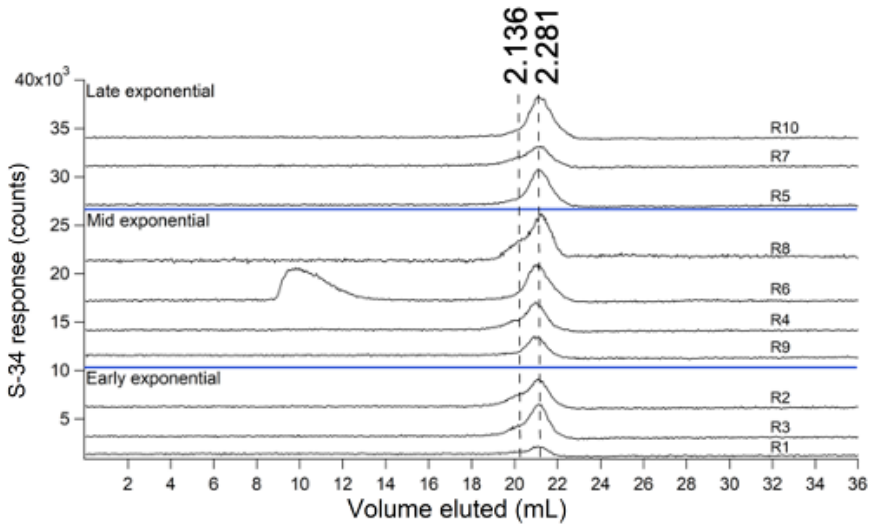

Figure III-S4. Sulfur-detected chromatographic traces of individual batches of FTS. Replicates in order from highest OD_{600} (top) at which cells were harvested to lowest (bottom). Blue horizontal lines separate the different exponential growth phases. Dashed vertical lines highlight LMM S species with V_e/V_o.

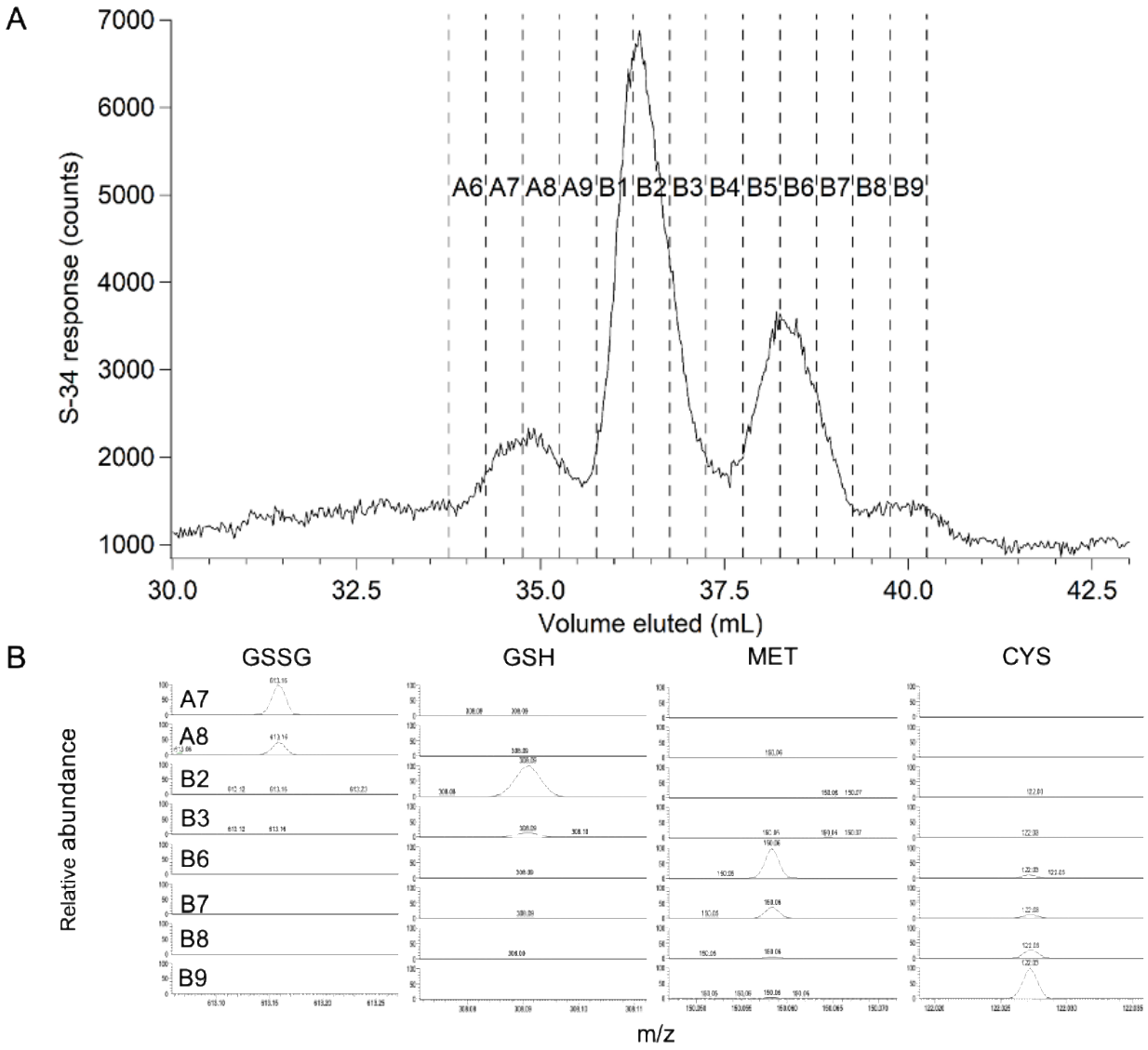

Figure III-S5. Positive mode ESI-MS spectra showing sulfur-containing metabolites in cytosolic FTS. (A), Sulfur-detected averaged FTS from cells collected on the double peptide column (dashed lines indicated fraction boundaries). (B), Positive mode ESI of selected fractions from (A). Peaks within each column have been normalized to the largest peak intensity.

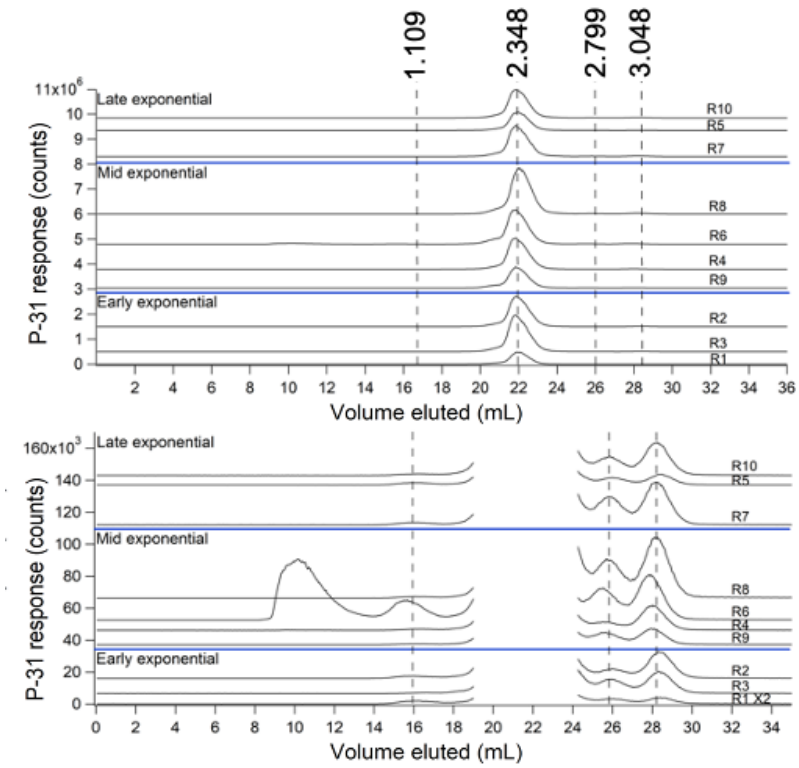

Figure III-S6. Phosphorus-detected chromatographic traces of individual batches of FTS. Panel A: replicates in order from highest OD_{600} (top) at which cells were harvested to lowest (bottom). Panel B: Same replicates as in Panel A with main peak removed. Blue horizontal lines separate the different exponential growth phases. Dashed vertical lines highlight LMM P species with V_e/V_o.

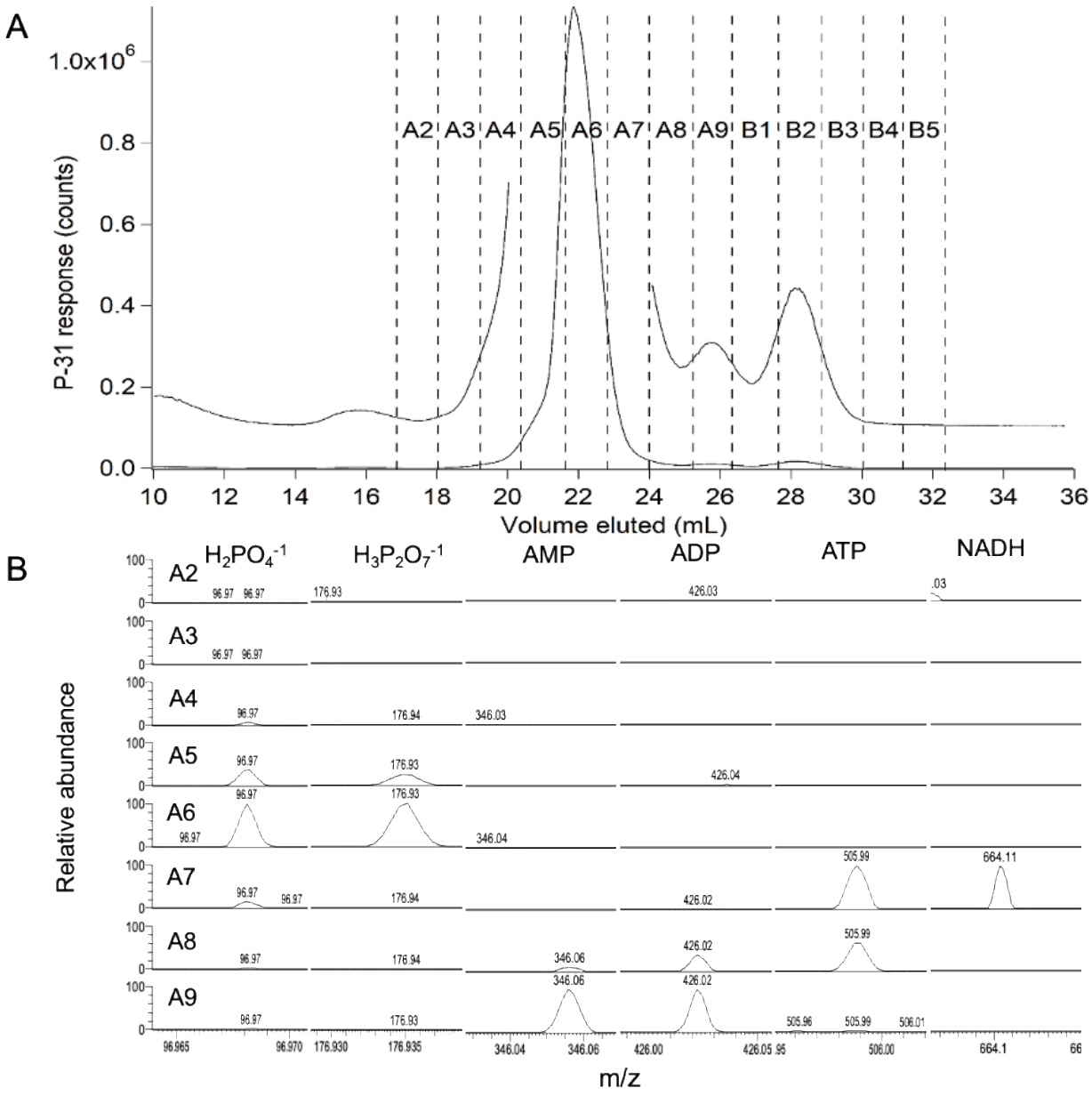

Figure III-S7. Negative mode ESI-MS spectra showing phosphorus-containing metabolites in cytosolic FTS. (A), Phosphorus-detected averaged FTS from cells collected on single peptide (dashed lines indicated fraction boundaries). The offset line is the ICP-MS data magnified ×20 excluding the dominating peak. (B), Negative mode ESI of selected fractions from (A). Peaks within each column have been normalized to the largest peak intensity.

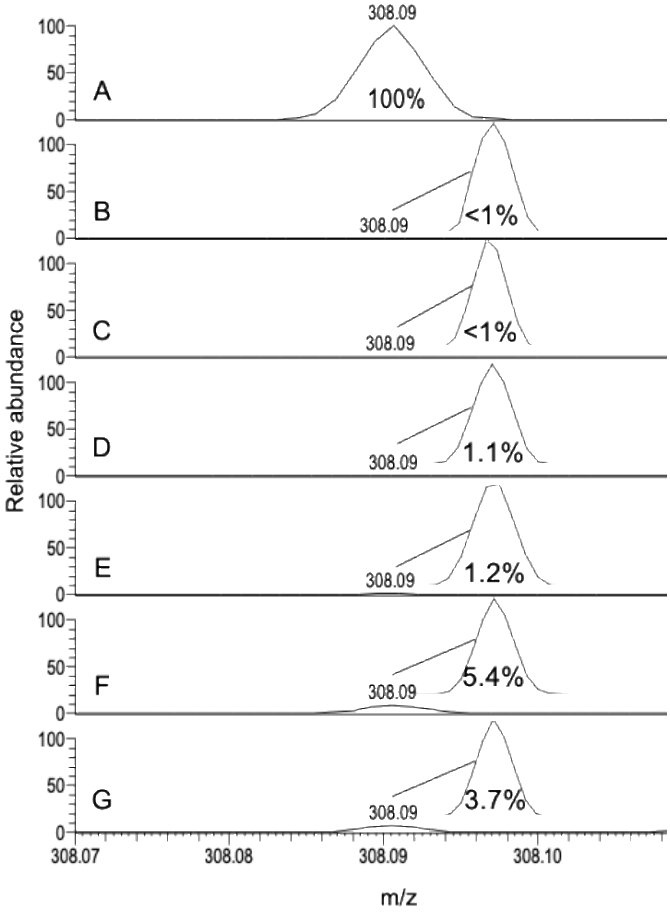

Figure III-S8. Positive mode ESI-MS spectra showing salt suppression of GSH. (A), 500 µM GSH; (B), a FTS replicate 8 (R8) (C), the sulfur-containing fraction collected from the FTS replicate in (B); (D), 500 µM GSH + 25 mM Na_2HPO_4; (E), 500 µM GSH + 25 mM KH_2PO_4; (F), 500 µM GSH + 25 mM NaCl; (G), 500 µM GSH + 25 mM $MgSO_4$. Spectra were normalized to the peak intensity of the GSH standard in (A). Relative percentage intensities for (B) – (G) are indicated.

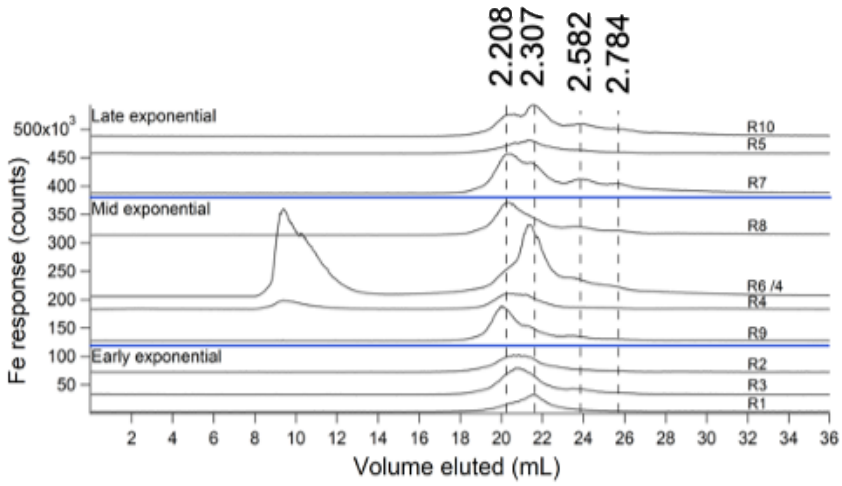

Figure III-S9. Iron-detected chromatographic traces of individual batches of FTS. Replicates in order from highest OD_{600} (top) at which cells were harvested to lowest (bottom). Blue horizontal lines separate the different exponential growth phases. Dashed vertical lines highlight LMM Fe species with V_e/V_o.

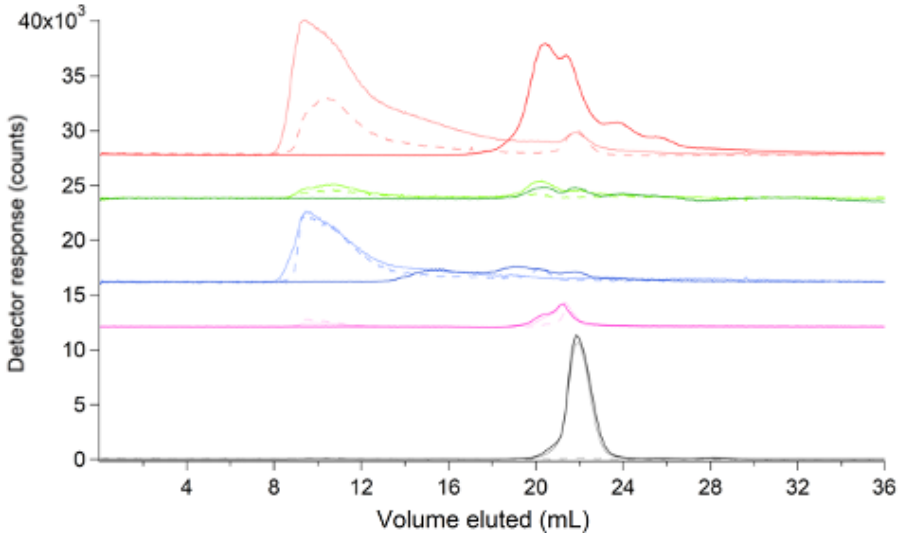

Figure III-S10. Acid phosphatase chelates metals from LMM metal complexes. Solid, dark-colored traces are the average of 8-10 FTSs for Fe (red, ÷4), Zn (green), Cu (blue), Mn (pink), and P (black, ÷100). Solid, light-colored traces are FTS + 2 mg/mL acid phosphatase for (same scaling for average FTSs). Dashed traces are metal content of standard 2 mg/mL acid phosphatase.

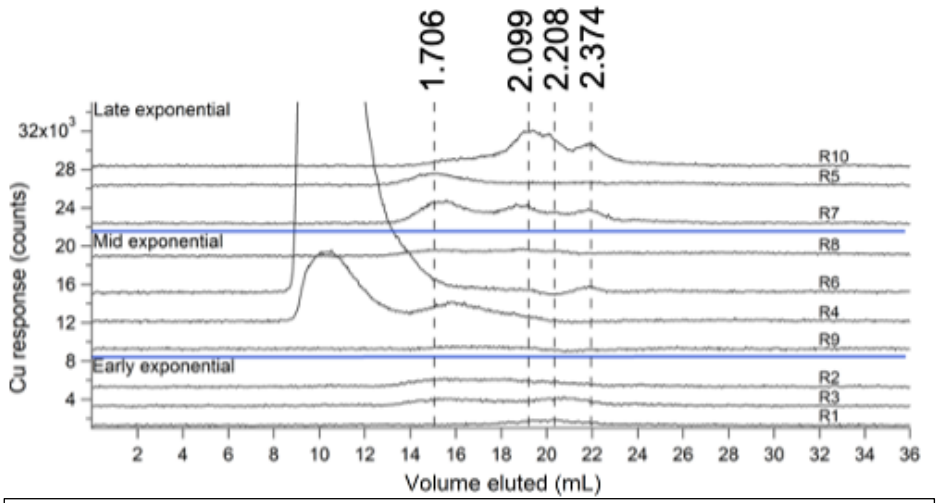

Figure III-S11. Copper-detected chromatographic traces of individual batches of FTS. Replicates in order from highest OD_{600} (top) at which cells were harvested to lowest (bottom). Blue horizontal lines separate the different exponential growth phases. Dashed vertical lines highlight LMM Cu species with V_e/V_o.

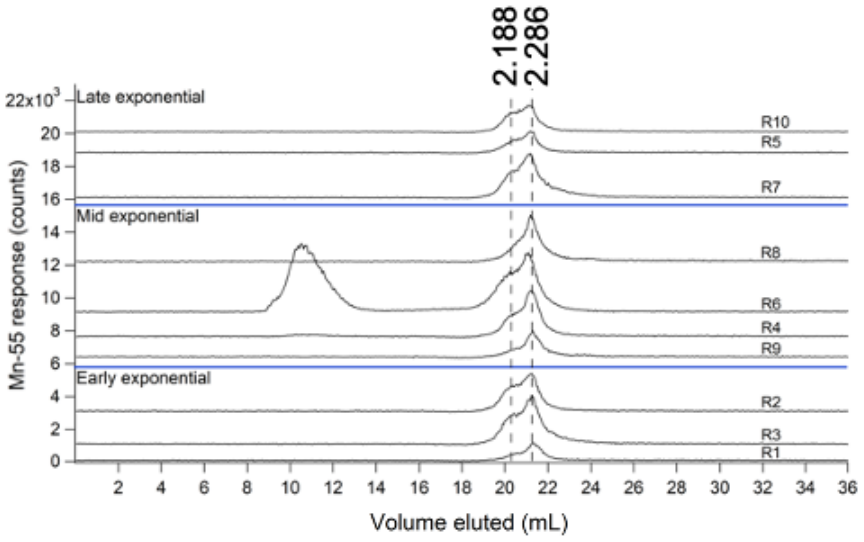

Figure III-S12. Manganese-detected chromatographic traces of individual batches of FTS. Replicates in order from highest OD_{600} (top) at which cells were harvested to lowest (bottom). Blue horizontal lines separate the different exponential growth phases. Dashed vertical lines highlight LMM Mn species with V_e/V_o.

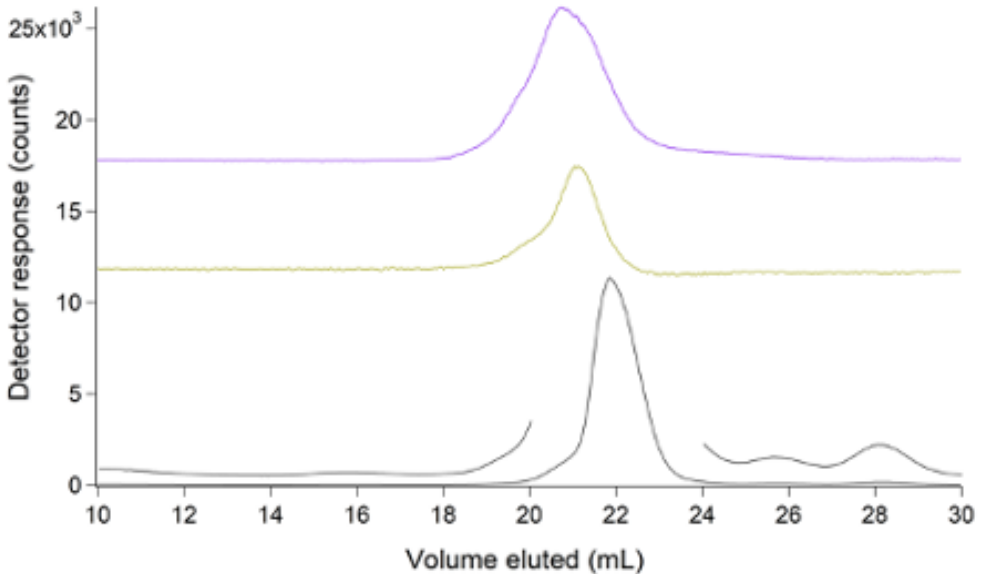

Figure III-S13. Average of 9 – 10 FTS traces of Ni (purple), S (yellow), and P (black) ÷100. The offset line in the bottom trace has been magnified ×10 with the dominating peak excluded.

CHAPTER 4

DIRECT DETECTION AND CHARACTERIZATION OF THE LABILE NICKEL POOL IN *ESCHERICHIA COLI*

Introduction

Nickel has novel redox and catalytic properties that allow certain bacteria and archaea to grow in unusual environments that are inaccessible to humans and other eukaryotes. For example, *E. coli* contains four [Ni-Fe] hydrogenases which allow them to grow anaerobically. The enzymes are membrane-bound and serve various metabolic functions typically involving energetics e.g. generating a redox-dependent proton gradient as part of a chemiosmotic mechanism for generating ATP.[120] Anaerobic respiration uses protons rather than O_2 as the terminal electron acceptor, forming H_2 as the product. The [Ni-Fe] active sites of hydrogenases are assembled by a multistep mechanism in which nickel is imported from the environment and trafficked to the assembly site on the HypA chaperone in complex with the HypB GTPase. Under *in vitro* conditions, aqueous Ni(II) binds this complex with nM affinity.[121] Then through a mechanism involving GTP hydrolysis and conformational changes, the bound Ni(II) is transferred into the large subunit of hydrogenase.[118]

Under anaerobic conditions, *E. coli* expresses *NikABCDE*, an ABC transporter system that specifically imports environmental nickel in an ATP-dependent manner. NikA, which is located in the periplasmic membrane, binds a Ni(L-histidine)$_2$ complex.[27,31] The details of how nickel is trafficked from NikA at the cell membrane to HypAB in the cell's interior remains a mystery. Krężel and Bal suggested that nickel might bind glutathione as a labile trafficking complex in cells due to the high concentration of this sulfur-containing tripeptide in the cytosol as well as its strong

binding constant with nickel (logβ values between 11 – 20).[122] The Ni(II) ion in GSH-containing complexes was considered to be square-planar with an $S_2N_1O_1$ ligand environment. However, these authors ultimately concluded that "GSH may play only a minor role in Ni(II) speciation, in favor of histidine, ATP, and histone proteins".

Nickel homeostasis in *E. coli* involves two DNA-binding metalloregulatory proteins, NikR and RcnR. NikR is a transcription factor that controls nickel import by stimulating expression of the *NikABCDE* operon under nickel-deficient conditions. Ni(II) binds NikR using three His and 1 Cys residues in a square-planar geometry.[123] The K_d for binding, determined under *in vitro* conditions is again in the nM range.[124] RcnR controls nickel export from the cell by controlling expression of RcnA (a membrane permease) and RcnB (periplasmic protein) on the outer membrane; expression levels are high when the Ni(II) ion concentration is excessive. RcnR binds Ni(II) in six-coordinate sites, and again in the nM range.[125] Both transcription factors bind aqueous nickel[126], but the trafficking species that serve(s) as nickel donor is(are) unknown.

A long-term goal of our research is to detect, identify, and characterize labile metal pools (LMPs) in biological cells. Such pools play critical roles in metal ion trafficking and regulation, but many specifics remain unestablished. LMPs are commonly studied using custom-designed fluorescence-based chelator probes that are selective for the metal of interest.[127] For example, Dodani *et al.* used a Ni-specific probe to detect nickel in human lung carcinoma cells that had been exposed to 1 mM $NiCl_2$.[128] The advantage of the chelator-based approach is that membrane-permeable probes penetrate in-tact and undisrupted cells; their major disadvantage is that the metal complexes of interest are destroyed during detection (by binding to the chelator).

We are developing a complementary chromatography-based approach which has the potential for allowing the metal complexes of interest to be isolated, detected, and characterized. Towards this end, we have assembled an LC-ICP-MS system in which the LC portion is located in a refrigerated anaerobic glove box. The disadvantage of the chromatography-based approach is that the cell must be disrupted to access the LMPs. Cell lysates are typically filtered using a 3 kDa cutoff membrane. The flow-through-solution (FTS), which ought to contain the LMPs, is collected and subjected to LC for metal-based detection by ICP-MS or for molecular characterization by downstream ESI-MS.

Although we have not had a long-term historical interest specifically in the LNP of *E coli*, we strategically targeted it in this study because *E. coli* is easily grown and large quantities of cytosolic FTS could be obtained. Moreover, Ni(II) complexes appear to be less labile than comparable complexes of other biologically relevant transition metals, based on rates of exchanging water with sulfate ions coordinated to aqueous d-block transition metal complexes; waters coordinated to Ni(II) ions exchange slower than those coordinated to Co(II), Fe(II), Mn(II), Zn(II), and Cu(II).[129] Moreover, we previously found that Ni(II) adsorbs less tightly to the SEC column employed here than Zn(II) or Cu(II).[130] These properties suggested a greater chance of detecting and identifying the Ni(II) complex(es) that compose(s) a LMPs in cells. Herein we report the detection and ESI-MS-based identification of four species that are members of the LNP in *E. coli*. This appears to be the first molecular-level identification of a LMP in a non-plant biological system.

Results

We grew 8 batches *E. coli* aerobically and isolated the cytosol which was then passed through a 3 kDa cutoff membrane. The FTS contained an average of 11 ± 2 μM Ni (Table IV-S1), which corresponds to nearly 100% of the total Ni(II) in the cell. These FTSs were subjected to SEC chromatography and ICP-MS detection. SEC chromatograms included four LMM Ni(II) complexes (Figure IV-1A offset), with apparent molecular masses between 950 – 2200 Da (all quoted masses in this chapter are apparent). Small metal complexes do not migrate down the column exclusively as a function of molecular mass; there are significant non-specific interactions between analytes and the column that also contribute. Thus, we simply labeled these peaks (from left-to-right) Ni-A, Ni-B, Ni-C, and Ni-D rather than according to their apparent masses. Respective percent intensities for the average of all 8 traces were 10:78:9:3.

The simplest interpretation of these chromatograms was that the LNP in *E. coli* consists of 4 endogenous LMM (presumably non-proteinaceous) complexes (Ni-A, -B, -C, and –D) with approximate concentrations of 1.1, 8.6, 1, and 0.3 μM of Ni(II), respectively. Alternatively, the LNP may consist of fewer (1 – 3) Ni(II) complexes, with some or all of the detected peaks arising from Ni-containing products of ligand-exchange processes. Such processes could have occurred when cells were disrupted or when FTS migrated through the SEC column. Distinguishing between these two interpretations remains a challenge, though results presented below help resolve this issue.

For one replicate, we added $NiSO_4$ at increasing concentrations to the cytosolic FTS and subjected the resulting solutions to SEC. A similar set of Ni-detected peaks were observed, albeit with higher overall intensities and some changes in relative intensities (Figure IV-1B-E). We concluded that the ligands in the cytosol that coordinate Ni(II) ions, whatever they may be, are present in excess. We further concluded that the distribution of Ni(II) bound to the various detected species is established quickly (less than a few minutes) after exposing FTS to $NiSO_4$.

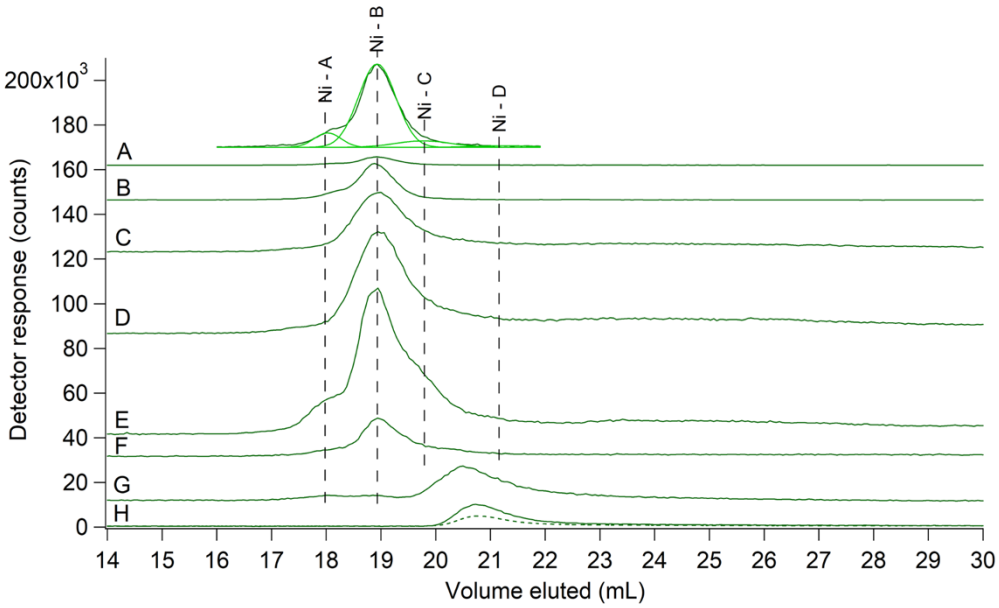

Figure IV-1. SEC-ICP-MS (single column) detection of the labile nickel pool in *E. coli*. Ni (green) traces for (A), Representative FTS. Offset is (A) (×10) with 4 simulations overlaid in light green; (B), (C), (D), FTS plus 1, 2, and 5 µM $NiSO_4$, respectively (×3); (E), same as (D) but with 150 µM $Na_2S_2O_4$ in the mobile phase; (F), FTS from cells grown in media supplemented with 1 µM $NiSO_4$ (×3); (G), same as (A) but with 100 µM 1,10-phenanthroline (final concentration) added to the FTS; (H), standard solution of 2 µM $NiSO_4$ + 20 µM 1,10-phenanthroline. Dashed line in (H) is Abs at 260 nm ×1000. Vertical dashed black lines represent position of nickel species according to simulations.

We were generally concerned about inadvertently generating artifacts when LMPs were exposed to O_2, so experiments were performed in a refrigerated anaerobic glove box using degassed mobile phase buffers. Oxidation was not a concern for the Ni(II) ions in the sought-after complexes, but it was a concern for potential redox-active ligands such as glutathione (GSH) and other reduced sulfur-containing species. Degassed buffers contain trace concentrations of O_2, so we equilibrated the column with degassed mobile phase buffer to which dithionite, a powerful reductant, was added. The resulting traces were not majorly affected, but the peaks sharpened noticeably (Figure IV-1E). This may have resulted from the higher ionic strength of the mobile phase, which diminished column interactions with the Ni(II) complexes; small changes in pH and ionic strength can significantly affect the separation factor.[131]

We next investigated whether growing cells aerobically vs. anaerobically or supplementing the growth medium with Ni(II) ions or with a potential ligand (L-histidine) had any effect on the LNP. The intensities of the Ni(II) peaks were stronger in the FTS from the cells grown on medium supplemented with 1 μM $NiSO_4$ (Figure IV-1A vs. IV-1F) and were of comparable intensity to that of FTS spiked with 1 μM $NiSO_4$. In anaerobically-grown cells, the number of species composing the LNP was unchanged relative to that in aerobically-grown cells (Figure IV-2A). Under anaerobic conditions, the LNP was sensitive to Ni(II) and L-His supplementation in the growth media (Figure IV-2B), consistent with previous results.[31]

The lability of the Ni(II) complexes in the FTS was investigated by treating it with 1,10-phenanthroline, a strong Ni(II) chelator, and then passing the resulting solution down the SEC column. In the resulting trace, the 4 original Ni(II) peaks were replaced by an intense peak at 20.8 mL which we assigned to $[Ni(phen)_3]^{2+}$ (Figure IV-1G). This experiment demonstratedsthe lability of the 4 LMM Ni(II) species observed in unperturbed FTS. By passing the FTS through a “ghost

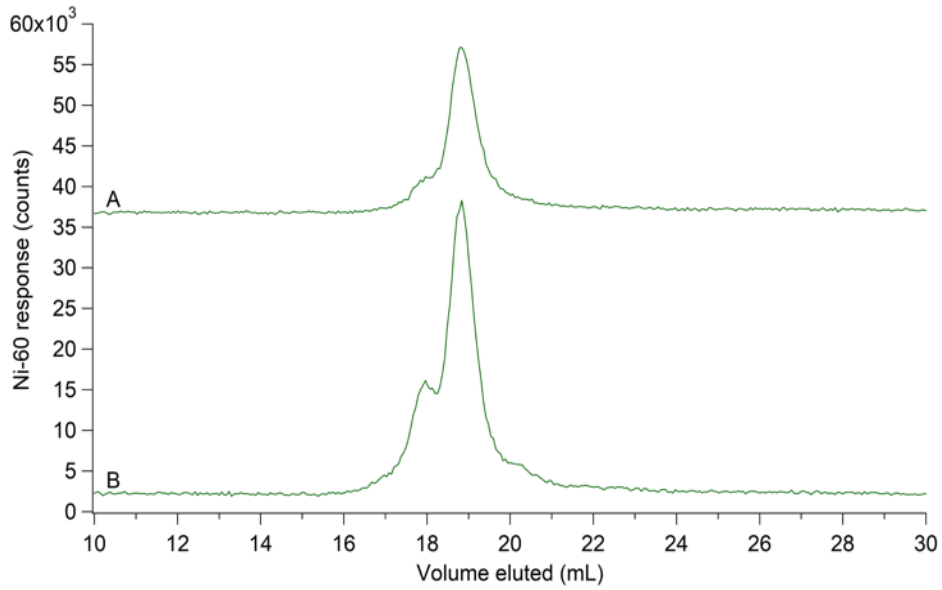

Figure IV-2. Nickel chromatographic traces showing the effect of anaerobic growth conditions on the LNP. Ni (green) traces for (A), FTS from cells grown anaerobically; (B) same as (A) but with 1 µM $NiSO_4$ and 400 µM L-histidine supplemented in the growth media.

column" (replacing the column with PEEK tubing), we also determined that, on average, 20% of the Ni(II) in the FTS adsorbed to the zinc-loaded column.

Corresponding S-detected and P-detected peaks comigrated with the Ni-detected peaks (Figure IV-S1). Previously, we reported that the labile sulfur pool was composed of glutathione (reduced and oxidized), methionine, and cysteine with approximate concentrations of 3, 0.4, 0.8, and 0.2 mM, respectively.[130] Likewise, the total phosphorus content of FTS was determined to be 140 ± 40 mM with many phosphorus-containing metabolites detected via ESI-MS.[130] The observed comigration can again be interpreted in two ways. One possibility was that 1 or 2 of the detected Ni(II) complexes was coordinated by sulfur-containing ligands. Another possibility was that either or both LMM sulfur species *fortuitously* comigrated with the Ni(II) complexes. The same interpretations hold for the comigrating phosphorus species. Distinguishing these possibilities proved difficult, but again, data presented below helps to resolve this issue.

We next investigated the chromatographic properties of prepared Ni(II) standards that we regarded as potential candidates for the species detected in *E. coli* FTS. Aqueous Ni(II) ions, obtained by dissolving $NiSO_4$ in the mobile phase buffer, eluted as a broad peak between 25 – 33 mL (Figure IV-3A). Aqueous Ni(II) ions interact with the column which retards its migration and causes broadening. When L-histidine was added to a solution of $NiSO_4$, a much sharper peak was observed at ~ 19.5 mL elution volume (Figure IV-3B). The absence of absorption in the region between 26 – 32 mL in these traces suggests that L-histidine coordinated tightly to aqueous Ni(II) ions, forming a Ni-L-His complex. Both Ni(L-His)$_1$ and Ni(L-His)$_2$ complexes are known, but the former is more stable.[132] In general, more stable complexes eluted as shaper peaks and at lesser elution volumes as compared to aqueous Ni(II) ions. Another signature of high stability is the

absence of a ligand-dependent shift in the elution volume of the nickel; such shifts are typical of metal-ligand complexes of intermediate stability.[130]

The complex that resulted when 2 μM $NiSO_4$ was mixed with oxidized glutathione (GSSG) eluted as a sharp peak at ~17.5 mL (Figure IV-3C). Some Ni(II) also eluted as a broad peak with elution volumes typical of aqueous Ni(II). The intensity of the peak at 17.5 mL increased with increasing concentrations of GSSG while that associated with aqueous Ni(II) decreased. We conclude that Ni(II) forms a complex with GSSG, but one that is less stable than Ni-L-His. The chromatographic behavior of $NiSO_4$ mixed with reduced glutathione (GSH) suggested formation of an even weaker complex. A low-intensity Ni(II) peak was evident only in the trace in which the highest concentration of GSH was used (Figure IV-3D). Supporting this conclusion was strong Ni(II) adsorption in the region where aqueous Ni(II) migrates. The solution in which $NiSO_4$ was mixed with cysteine exhibited similar weak-binding chromatographic properties (Figure IV-3E). A low-intensity sharp Ni(II) peak was observed in the region where complexes migrate; the vast majority of the Ni(II) migrated in the region typical of aqueous Ni(II).

With ATP as the added ligand, a more intense Ni(II) peak was observed at ~ 21 mL, which comigrated with P. The remaining eluted Ni(II) was aqueous with perhaps some shifting to lesser elution volumes at higher ATP concentrations, which suggested less column interactions. The vast majority migrated as aqueous Ni(II) (Figure IV-3F). There was no evidence for an interaction between Ni(II) and phosphate ions (Figure IV-3G). In contrast, the addition of citrate appears to have resulted in strong complex formation, as an intense Ni(II) peak was observed at ~ 18.5 mL elution volume; aqueous Ni(II) was evident at citrate concentrations $\leq$ 1mM (Figure IV-3H).

The traces obtained when aspartic acid and glutamic acid were added to solutions of $NiSO_4$ exhibited a remarkable contrast; aspartic acid formed a relatively strong complex with Ni(II)

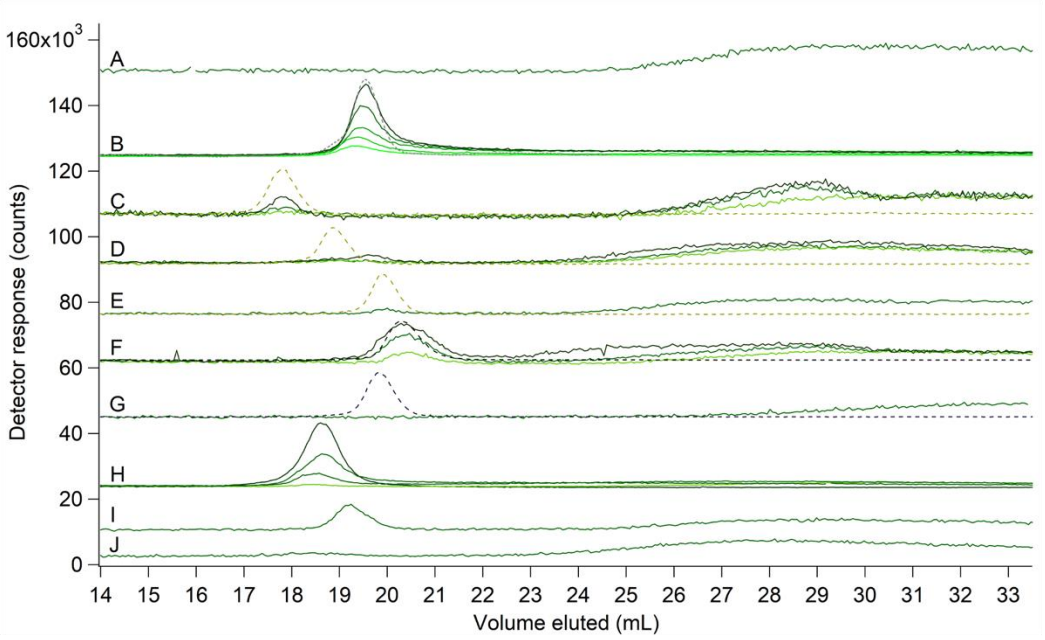

Figure IV-3. Chromatographic behavior of nickel standards. Ni-, S-, and P-detected traces are green, yellow, and black lines, respectively, for solutions of 2 µM $NiSO_4$ and the following ligands in mobile phase buffer (all final concentrations): (A), **nothing** (×10); (B), **L-histidine** (from lightest to darkest) at 25, 50, 100, 500, and 1000 µM (×2); the grey dashed line is Abs at 210 nm (×600); (C), **GSSG** at 1 mM (light), 5mM (darker) with S trace (dashed, ×0.25), and 10 mM (darkest) (×5); (D), **GSH** at 1 mM (light), 5 mM (darker) with S trace (dashed, ×0.5), and 20 mM (darkest) (×5); (E), **cysteine** at 5 mM with S trace (dashed, ×0.5) (×5); (F), **ATP** at 1 mM (light), 5 mM (darker) with P trace (dashed, ×0.015), and 10 mM (darkest) (×5); (G), **KH_2PO_4** at 500 µM with P trace (dashed, ×0.025) (×5); (H), **citrate** (from lightest to darkest) at 100, 500, 1000, and 5000 µM; (I), **aspartic acid** at 5 mM (×5); (J), **glutamic acid** at 5 mM (×5).

whereas glutamic acid did not (Figure IV-3I vs. IV-3J). This would not be the behavior expected if Ni-L coordination exclusively involved the amino group and the C_α-carboxylic acid; rather it suggests that coordination involves the $–CH_2\text{-}COO^-$ group on Asp and that the corresponding $–CH_2\text{-}CH_2\text{-}COO^-$ group on Glu is unable to form a stable complex.

In the absence of Ni(II), potential ligands GSH, GSSG, L-His, ATP, NaH_2PO_4 and K_2HPO_4 were subjected to SEC and detected by UV-Vis or ICP-MS. These species migrated with the same elution volume as when they were coordinated by Ni(II), indicating that the SEC could not resolve Ni-bound complexes from the corresponding Ni-unbound ligands. Based on the chromatographic behavior or the Ni-L standards, we qualitatively rank-ordered the apparent binding interactions between aqueous Ni(II) and these ligands as follows:

L-His > Citrate > Asp > GSSG > ATP > GSH > Cys > Glu > NaH_2PO_4/K_2HPO_4

Since the detected Ni(II) species in the FTS migrated as sharp peaks and at lesser elution volumes relative to aqueous Ni(II), and there was no evidence of aqueous Ni(II) in those traces, we conclude that *the endogenous LMM labile Ni(II) complexes in the E. coli cytosol are relatively strong binding complexes; none of them are aqueous (sometimes informally called "free") Ni(II).* The detected Ni(II) complexes in FTS are comparable, in terms of binding strength, to complexes formed with, L-His, citrate, Asp, GSSG, and ATP. Given that the elution volumes of these Ni(II) standards were comparable to those of Ni-A, Ni-B, Ni-C, and Ni-D (between 17.3 – 21.3 mL), we considered that there might be some correspondence between the FTS Ni(II) complexes and the Ni(II) standards.

We investigated the effect of these top five ligand candidates on the labile Ni(II) pool by spiking 1 mM of each ligand into a replicate of FTS and then subjecting the solution to SEC. The Ni-A peak intensity increased when additional GSSG was added to the FTS (Figure IV-4B). The

intensity of Ni-B increased when additional Asp was added to the FTS (Figure IV-4C). The addition of L-His resulted in an increase in the Ni-C peak intensity (Figure IV-4D), and the Ni-D peak increased with 1mM ATP (Figure IV-4E). Interestingly, when 1mM citrate was added to the FTS, a peak at ~18.5 mL was observed, which did not correspond to a previously observed Ni-containing peak (Figure IV-4F). These results suggest that GSSG, Asp, L-His, and ATP are ligands to the LMM Ni(II) complexes and that citrate is not. However, it is also possible that these ligands coordinated Ni(II) from the LNP due to ligand-exchange reactions during isolation of the FTS. The fact that these complexes "hold together" down the SEC column discounts the latter possibility.

The resolution obtained using the single SEC column was acceptable but not ideal. To improve this, FTS was passed through two SEC columns placed in series (the double column). Run-times on the double column were slower (3.5 hrs vs. 1 hr for the single column), but it also served to resolve salts, which had been previously found to suppress FTS signals in ESI-MS.[130] The results for the average of 6 replicates collected using the double column (Figure IV-5A) revealed 4 major Ni(II) peaks (and perhaps ~ 2 additional Ni(II) peaks just barely distinguishable from baseline). The elution of Ni-L standards on the single vs. double SEC did not follow the same elution profile, therefore, we could not assign that the FTS peaks, from left-to-right, corresponded to the Ni(II) peaks named in the single column traces. While the relative area of the Ni(II) peaks from the double column (7:6:72:15) were similar to those of Ni-C, Ni-D, Ni-B, and Ni-A of the single column, respectively, we hypothesized that slight differences in column material and/or zinc-loading between the single and double column may have resulted in variation in both peak position and intensity. Ligand exchanges processes on the double column cannot be dismissed

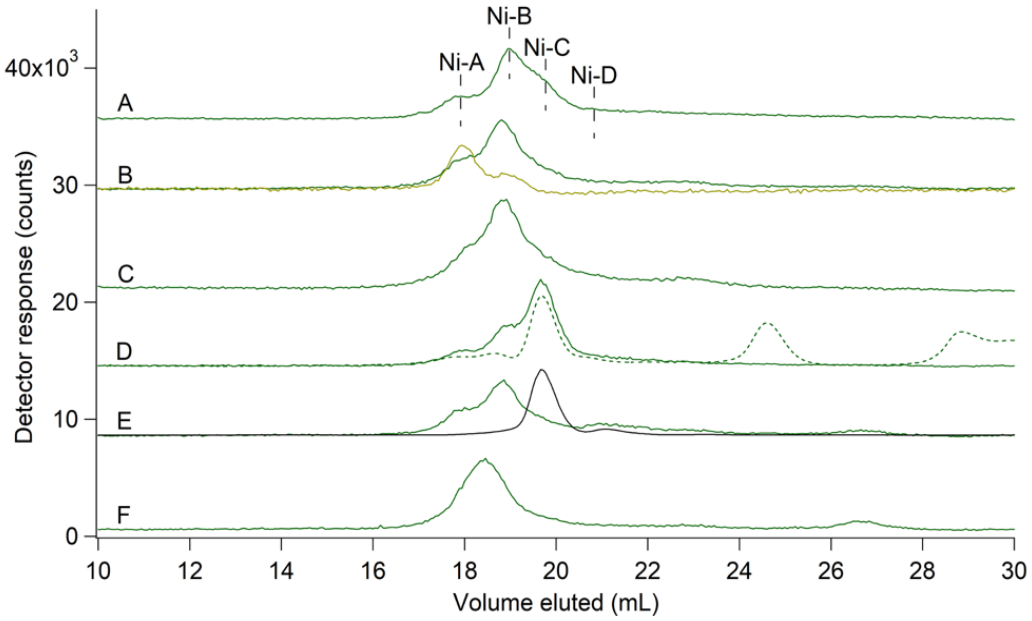

Figure IV-4. Sensitivity of LNP to exogenous low-molecular-mass ligands via SEC-ICP-MS (single column). Ni (green) traces for (A), Representative FTS with Ni-ABCD peaks indicated with vertical dashed black lines; (A) plus: (B), 1 mM **GSSG** with S trace (yellow); (C), 1 mM **Aspartate**; (D), 1 mM **L-histidine**. Dashed green line is Abs at 210 nm (×15); (E), 1 mM **ATP** with P trace (black, ×0.05); (F), 1 mM **Citrate**.

either. Other replicates exhibited some variation in terms of peak intensities and elution volumes, but 4 peaks were always observed, and, in most cases, Ni-B was the most intense (Figure IV-S2).

A pseudo-flow-through-solution (pFTS) was prepared to mimic the FTS; it consisted of 2 µM $NiSO_4$, 100 µM cysteine, 70 µM L-histidine, 500 µM GSSG, 5 mM GSH, 2 mM citrate, 5 mM aspartate, 5 mM ATP, 50 mM glutamate, 5 mM $H_2PO_4^-/HPO_4^{2-}$, and 0.5% (v/v) sodium polyphosphates prepared in 20mM AA (pH 6.5) that had been passed through a 3 kDa filter. Unexpectedly, the chromatography trace of pFTS exhibited 4 Ni(II) peaks that comigrated with the 4 Ni-containing peaks in the FTS (Figure IV-5B). The simplest explanation is that comigrating peaks indicate a common species, but we must also consider that two independent Ni(II) species may comigrate coincidentally. By analyzing individual Ni-L and L standards on the double column (Figure IV_5C-I), we *tentatively* assigned the first Ni-containing peak to Ni(GSSG), the second peak to Ni(ATP), and the third peak to Ni(Asp). Thus, in accordance with the single column, we labeled these peaks Ni-A, Ni-D, and Ni-B, respectively. Surprisingly, a Ni(L-His) standard eluted *beyond* the Ni-containing region of interest for the cytosolic FTS and pFTS. The chromatographic behavior of the Ni(L-His) standard warrants further investigation.

FTS and pFTS were each chromatographed on the double-length column and fractions were collected (Figure IV-5 brackets) and analyzed by ESI-MS. In FTS fractions containing Ni-A, a peak corresponding to Ni-GSSG was observed albeit with low intensity (Figure IV-6A, asterisks). When the FTS was spiked with 5 µM of $NiSO_4$ prior to separation on the double column (with subsequent fraction collection), the Ni-GSSG peak signal intensity increased in the Ni-A fractions (Figure IV-6B). When 2 µM of $NiSO_4$ was added to the Ni-A fraction, the full Ni isotopologue signature was observed in the mass spectrum (Figure IV-6C, asterisks). While other

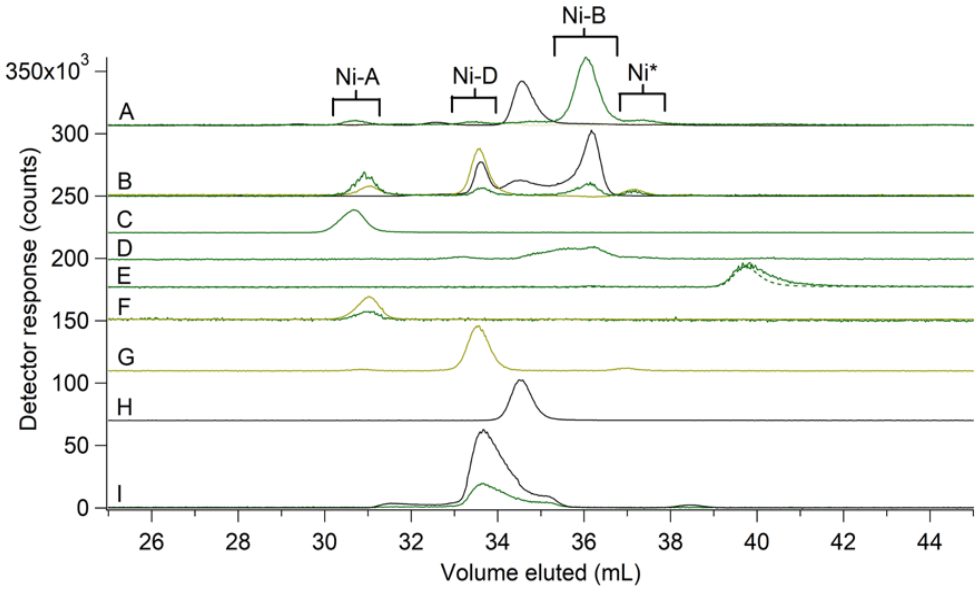

Figure IV-5. SEC-ICP-MS (double column) chromatograms of FTS (A), "Pseudo-FTS" (B), and standards (C – I). (A), Ni (green, ×3), S (yellow, ×3), and P (black, ×0.25) traces of a representative FTS replicate. Brackets indicate Ni-containing fractions collected for ESI-MS analysis. Ni* represents an unassigned Ni-containing peak. (B), Ni (×3), S (yellow), and P (×0.05) traces for 2 µM $NiSO_4$ added to the ligand cocktail; 2 µM $NiSO_4$ plus: (C), 2 mM **Citrate**; (D), 5 mM **Aspartate** (×5); (E), 1 mM **L-histidine** (×3). Green dashed line is Abs at 210 nm (×25); (F), 5 mM **GSSG** (×10) with S trace (×0.25); (I), 5 mM **ATP** (×5) with P trace (×0.05); (G), S trace of 5 mM **GSH**; (H), P trace of 500 µM **NaH_2PO_4** (×0.5).

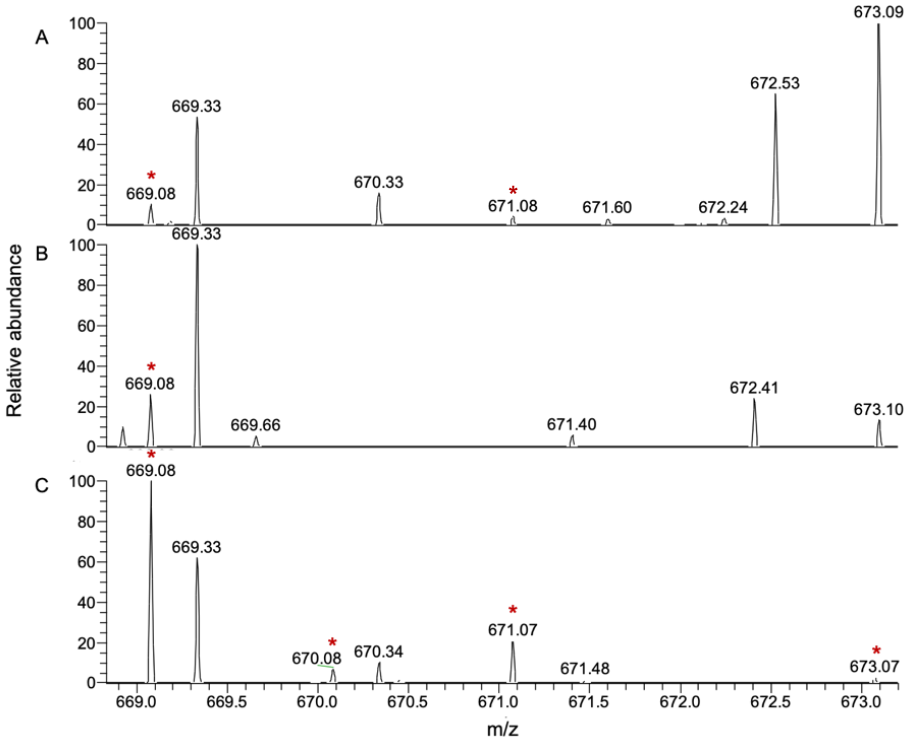

Figure IV-6. ESI-MS of fractions (double column) from FTS. (A), FTS + 0 µM $NiSO_4$; (B), FTS + 5 µM $NiSO_4$; (C), FTS + 5 µM $NiSO_4$ + 2 µM $NiSO_4$ added post fraction collection. All spectra were acquired in positive mode. Red asterisks indicate the isotopologue peaks predicted by simulation of Ni-GSSG (Xcalibur 4.1).

ligands were present, no other Ni(II) complexes were observed in the remaining fractions likely due to dilution down the double column. These ESI-MS results *establish* the presence of Ni-GSSG in the FTS and allow for the accurate assignment of Ni-A as such.

In another experiment, an aliquot of a FTS replicate was lyophilized and subjected to SEC (double column) (Figure IV-S2B). While a few new peaks were evident, the predominant Ni-containing peak was Ni-A.

In the pFTS fractions, Ni-GSSG, $Ni(Asp)_2$, and Ni-ATP were observed in the Ni-A, Ni-B, and Ni-D-containing fractions, respectively (Figure IV-7), *thereby confirming the assignments of these peaks*. Moreover, the abundance of each of these species in the pFTS corresponded to their intensity in the SEC (double column) chromatogram (Ni-GSSG > $Ni(Asp)_2$ > Ni-ATP).

Hydrophilic Interaction Chromatography (HILIC) separates molecular species according to different properties than SEC, and so we used HILIC as a complementary approach to SEC to probe the LNP of *E. coli*. FTS was diluted 5-fold in ACN and injected onto a HILIC column with ESI-MS detection. Ni(II) complexes were expected to adhere to the polar aqueous surface on the stationary phase and elute as function of increasing aqueous content in the mobile phase (10 mM AA pH 6.5). Ni-GSSG (m/z = 669.07732 (detected) vs. m/z = 669.07894 (simulated)) was detected in 7 out of 8 FTS replicates from aerobically-grown cells. $Ni(L\text{-}His)_2$ (m/z = 367.06527 (detected) vs. m/z = 367.06593 (simulated)) was observed in 6 of the 8 replicates at a lower intensity compared to the Ni-GSSG complex. $Ni(Asp)_2$ (n=2) (m/z = 323.00124 (detected) vs. m/z = 323.00199 (simulated)) and Ni-ATP (n=1) (m/z = 563.92991 (detected) vs. m/z = 563.92272 (simulated)) complexes were also observed. When the FTS replicates were spiked with 2 µM of $NiSO_4$, the signal intensities for the complexes increased and/or appeared in the following order:

$$\text{Ni-GSSG} > Ni(L\text{-}His)_2 > \text{Ni(ATP)} \sim Ni(Asp)_2$$

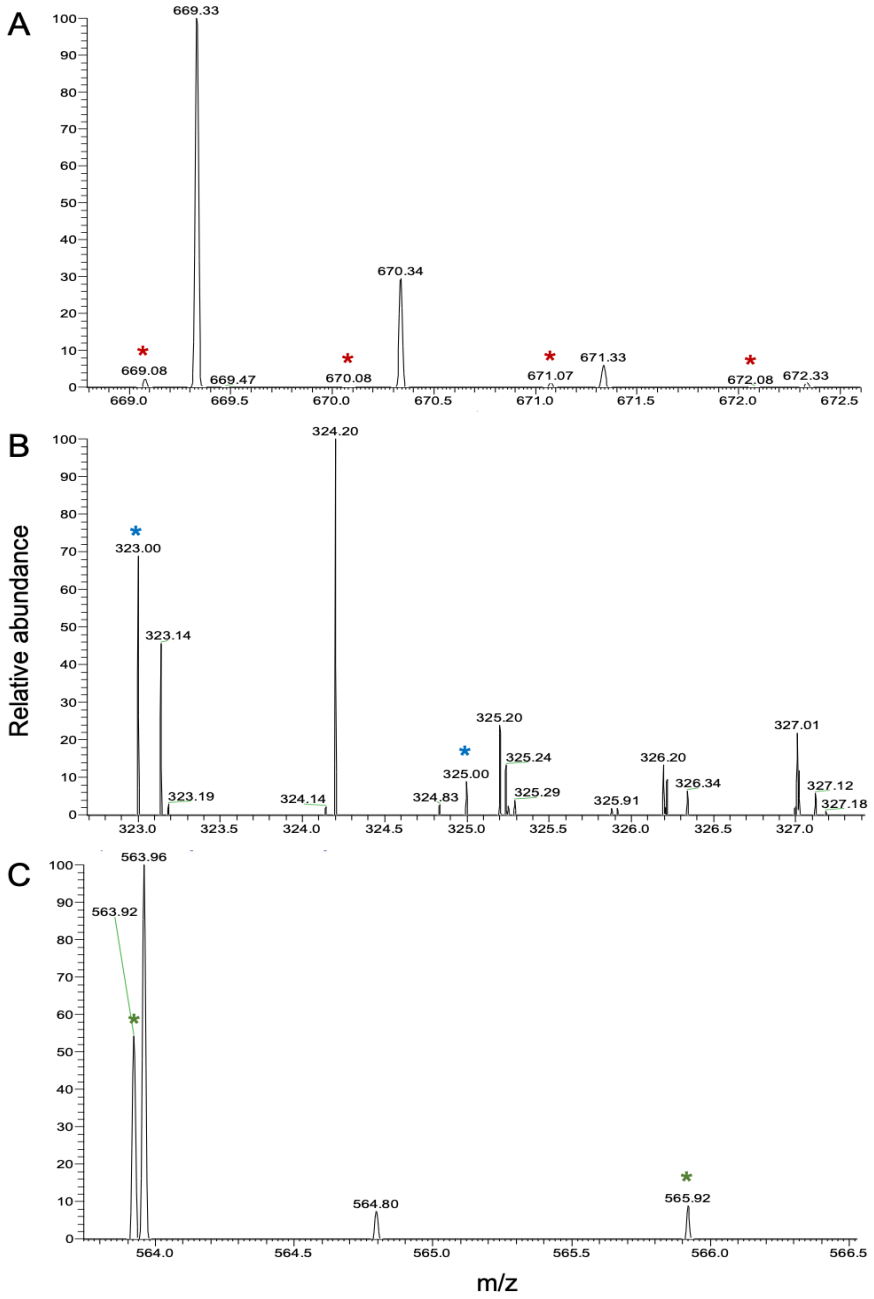

Figure IV-7. ESI-MS of fractions (double column) from pFTS for (A), Ni-A-containing fraction; (B), Ni-B-containing fraction; (C), Ni-D-containing fraction. All spectra were collected in positive mode. Red, blue, and green asterisks indicate the isotopologue peaks (in accordance with simulations) for Ni-GSSG, $Ni(Asp)_2$, and Ni-ATP, respectively.

For FTS isolated from anaerobically-grown *E. coli* (n=1), only the Ni-GSSG complex was detected by ESI-MS. To determine whether dilution of FTS with ACN altered Ni(II) speciation, FTS was diluted 10-fold in ACN (i.e., the solution loaded onto HILIC) was subjected to SEC (single column). Minor differences in the LMM Ni(II) pool was observed (Figure IV-S3). Future investigations are necessary to determine if this the result of ACN or dilution.

FTS was also subjected to HILIC-ICP-MS (Figure IV-8). On average, the predominant Ni-containing peak was Ni-GSSG (confirmed based on comigration with a Ni-GSSG standard). This contrasts the SEC results but is in accordance with HILIC-ESI-MS results, which demonstrated that Ni-GSSG was the most intense and reproducible Ni-containing species in the FTS. These results suggest that ligand exchange processes are occurring on the SEC columns utilized in this study. Additionally, although poorly resolved, there was evidence of Ni-L-His, Ni-Asp, and Ni-ATP in the averaged FTS (for aerobically-grown cells).

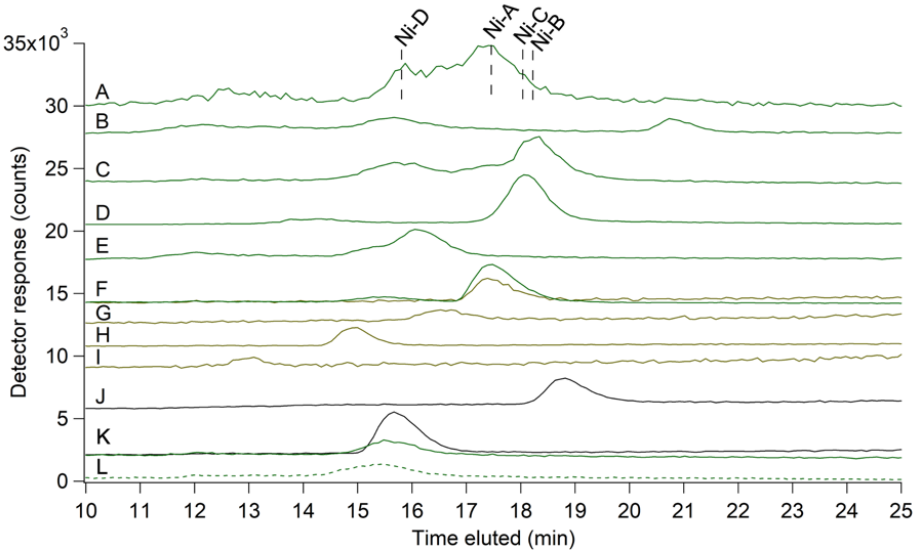

Figure IV-8. HILIC-ICPMS chromatograms of FTS (A) and standards (B – L). Ni (green) traces for (A), Averaged (n = 8) FTS isolated from aerobically-grown cells (×3); 5 µM $NiSO_4$ plus: (B), 10 mM **glutamate**; (C), 5 mM **aspartate**; (D), 500 µM **L-histidine** (×0.5); (E), 2 mM **citrate**; (F), 5 mM **GSSG** with S (yellow, ×3) trace; (K), 5 mM **ATP** with P (black, ×0.075) trace; 0 µM $NiSO_4$ plus: (G), S trace for 5 mM **GSH** (×3); (H), S trace for 50 mM **cysteine**; (I), S trace for 1 mM **methionine** (×5); (J), P trace for 10 mM **KH_2PO_4**; and (L), blank of 90% ACN/10% 10 mM AA pH 6.5 (dashed). Vertical dashed black lines represent position of nickel species according to standard comigration.

Discussion

The total nickel quota for aerobically-grown *E. coli* has been reported to be between 3 and 10 μM.[1,133] This quota corresponds to the total concentration of Ni(II) we measured by ICP-MS for both the lysate (11 ± 7 μM) and cytosolic FTS (11 ± 2 μM). Thus, we conclude that in aerobically-grown *E. coli*, nearly all of the Ni(II) in the cell is in the LNP. Anaerobically-grown *E. coli* demonstrated no significant increase in the LNP although a slight increase in the LNP was observed when anaerobically-grown cells were supplemented with $NiSO_4$ and L-histidine in the growth medium. Chivers *et al* found that nickel uptake in anaerobically-grown *E. coli* and nickel binding to purified NikA of the Ni-ABCDE import system depended on the L-His concentration, suggesting that the protein recognizes a Ni(L-His)$_2$ complex.[31] Additional anaerobic growth replicates are necessary to confirm that the size of the LNP increases under anaerobic conditions and with L-histidine added to the growth medium and to determine whether the composition of the LNP is altered.

Currently, all affinity constant for Ni(II) binding to various proteins have been determined by a titration of the apo-protein with an aqueous nickel salt (e.g. $NiCl_2$, $NiSO_4$, or Ni(acetate)$_2$). The results are likely to be overestimate the actual binding affinities because the actual reaction occurring *in vivo* probably involves a direct transfer of Ni(II) from one of these LNP complexes, not from aqueous Ni(II). The overestimate may be as large as several orders-of-magnitude, comparable to the K_d of aqueous Ni(II) binding to the LNP complexes themselves. These errors have likely distorted the estimate of the concentration of the LNP in the cytosol. For example, based on the reported Ni(II) dissociation constants, Musiani *et al.* speculated that the physiological cytosolic concentration of Ni(II) in *E. coli* is between 10 – 500 nM. In contrast, we measured ~ 11 μM for the LNP. The 20-1000 fold discrepancy may be due to use of aqueous ("free") Ni(II) in titrations against various Ni(II)-binding proteins in *E. coli*. Thus, the actual concentration of these

pools will be significantly higher than is generally assumed. The same situation might hold for other LMPs since such titrations are typically performed using aqueous metal salts.[12]

The evidence presented above suggests that Ni(GSSG) is the dominant component of the LNP in aerobically-grown *E. coli*, followed by Ni(L-His)$_2$, then Ni(Asp)$_2$ and Ni(ATP). First, we detected Ni(GSSG) by HILIC-ESI-MS in virtually every replicate of FTS that we examined. HILIC-ICP-MS supported Ni(GSSG) as the predominant Ni(II) complex in FTS as it was most the intense Ni(II) species observed. While SEC-ICP-MS demonstrated the presence of Ni(GSSG) in FTS, this species was not the most intense complex observed. We attribute this to ligand exchange processes taking place as the FTS migrated through the SEC columns, resulting in new and/or artefactually-high Ni(II) complexes being detected. When FTS was concentrated via lyophilization, the main Ni(II) species observed was Ni(GSSG); however, this experiment has only been performed once. As the concentration of the labile Ni(II) pool increases, the degree of dissociation down the SEC columns is lessened.

When FTSs were spiked with an additional 2 μM of $NiSO_4$ and subjected to HILIC-ESI-MS, the intensity of Ni(GSSG) increased slightly, the intensity of Ni(-L-His)$_2$ increased more modestly, and the Ni(Asp)$_2$ and Ni(ATP) complexes appeared (in FTS replicates with no previous observation of these complexes). This suggests that amount of GSSG, and subsequently L-His, available to coordinate Ni(II) in the cytosol is limiting. The composition of the LNP could change as metabolism changes. Since GSSG, L-His, Asp, and ATP are metabolites in the cell, the concentrations of these species might change depending on metabolism and the growth rate of the cell. Understanding these changes in detail will require further studies, but the possibility of this should be considered. Additionally, cells are disrupted (by freeze-thaw) in order to isolate the FTS.

Despite minimal dilution in buffer, we would like to caution that these Ni(II) complexes could result from ligand exchange processes during isolation.

Fractions collected by SEC of a "pseudo-FTS" and analyzed by ESI-MS revealed the presence of Ni(GSSG), $Ni(Asp)_2$, and Ni(ATP), but not $Ni(L\text{-}His)_2$. We attribute the lack of $Ni(L\text{-}His)_2$ to ligand exchange processes on the SEC columns employed herein. Such processes do not seem to be as problematic for the HILIC column. In this case, analysis of the pFTS was analyzed by HILIC-ESI-MS and revealed the presence of both $Ni(L\text{-}His)_2$ and Ni(GSSG), with the latter complex present at a higher intensity.

Surprisingly, $Ni(GSH)_n$ and $Ni(citrate)_n$ do not appear to be components of the LNP. Previous studies have speculated that glutathione- and citrate-based metal complexes are dominant components of LMPs.[61] These studies, which mainly focus on the labile iron pool, were based on theoretical calculations involving the concentrations of candidate ligands and metal ions and corresponding thermodynamic binding affinities. The affinities of nickel (and iron) for binding GSH are reportedly quite strong[122], and the cytosolic concentration of GSH in *E. coli* is quite high (~ 3 mM).[130] For these reasons, we initially expected $Ni(GSH)_n$ to be an important member of the LNP. However, the results presented here suggest otherwise. First, standards of $Ni(GSH)_n$ analyzed via SEC-ICP-MS demonstrated weak binding, which was not observed in the FTS. These same standards when subjected to ESI-MS (direct injection), however, did reveal Ni(GSH) and $Ni(GSH)_2$ complexes. When FTS was spiked with 1 mM GSH, the chromatographic profile of the LNP was unchanged (data not shown) unlike what was observed upon the addition of GSSG, L-His, and other LMM ligands. Despite the sulfur peak of GSH comigrating in the area of interest on the HILIC column (as detected by ICP-MS), neither Ni(GSH) or $Ni(GSH)_2$ was detected via

HILIC-ESI-MS. Thus, while Ni and GSH are capable of complexation, we do not suspect that such complexes occur endogenously in the *E. coli* cytosol.

Likewise, we had expected that $Ni(citrate)_n$ would be an important member of the LNP, but this also does not seem to be the case. $Ni(citrate)_n$ standards subjected to SEC-ICP-MS showed intermediate binding, similar to L-His, GSSG, ATP, and Asp, and $Ni(citrate)_1$ and $Ni(citrate)_2$ complexes were observed via ESI-MS. When we added 1 mM citrate to the FTS, a new Ni-containing peak was observed in SEC-ICP-MS. While this new peak did not comigrate with the previously observed Ni-ABCD peaks, the position of this peak was within the region of interest. Chromatograms of FTS may have included a $Ni(citrate)_n$ peak at low intensity such that its presence was unresolved and undetected on the single SEC column, and the complex may have been too dilute for detection with the double SEC column (as we noticed some low intensity Ni-containing peaks slightly above the baseline for multiple replicates of FTS). The same observation was made for HILIC-ICP-MS in which a $Ni(citrate)_n$ standard comigrated in the region of interest of Ni-containing peaks; however, no $Ni(citrate)_1$ or $Ni(citrate)_2$ complex was observed via HILIC-ESI-MS. If this species is of low abundance in the FTS, further dilution of the sample (via double column separation or in ACN for HILIC analysis) could lead to these complexes being undetected by ESI-MS. Future investigations are needed to establish whether $Ni(citrate)_n$ is a constituent of the LNP of *E. coli*.

In summary, the presence and importance of LMPs in cells has been recognized for the past 50 years, yet due to their fundamental lability, little progress has been made in their identity and characterization. The methods developed herein, and results obtained using those methods, provide a demonstrably successful pathway for future advances in this field. In this project, we report the first molecular characterization of a labile metal pool, specifically that of Ni(II), in *E.*

coli. Using SEC and HILIC separation techniques in conjunction with ICP-MS and ESI-MS detection systems, we identified Ni(GSSG) and Ni(L-His)$_2$ as the major constituents of the LNP while Ni(Asp)$_2$ and Ni(ATP) likely play minor roles. We envision that the four species are in equilibrium, as show in Figure IV-9. The cellular function of each of these complexes within this pool remain to be elucidated.

Acknowledgements

We acknowledge Yohannes Rezenom of the Chemistry Mass Spectrometry Laboratory (TAMU) for ESI-MS data collection and assistance in HILIC method development.

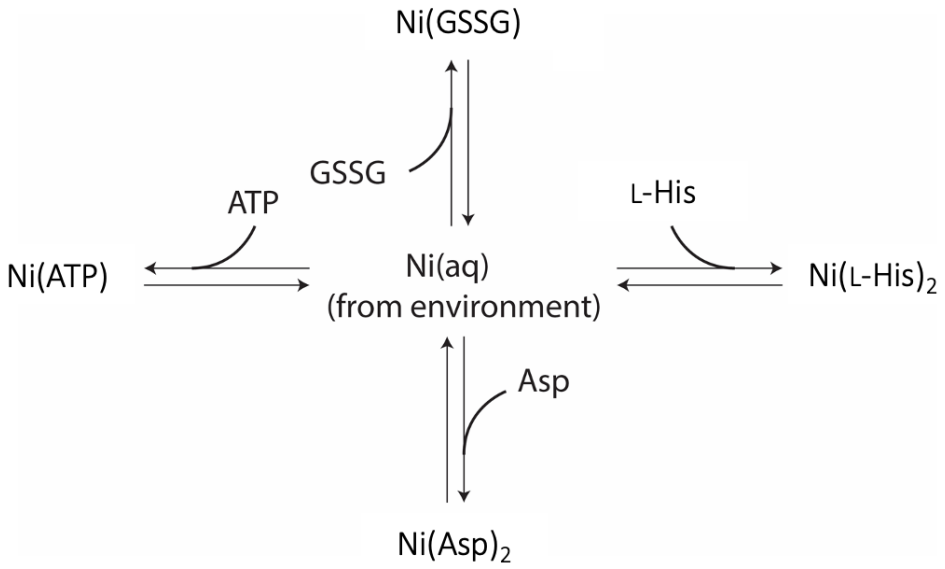

Figure IV-9. Proposed Ni(II) flux into the LNP of the *E. coli* cytosol. Nickel imported into the cytosol from the environment is sequestered into a LNP composed of the LMM Ni(II) complexes: Ni(GSSG), Ni(L-His)$_2$, Ni(Asp)$_2$, and Ni(ATP).

Supplementary information

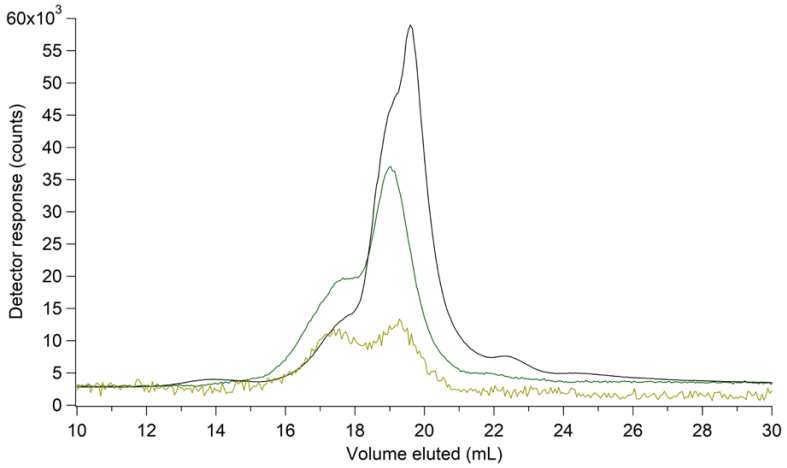

Figure IV-S1. SEC-ICP-MS (single column) chromatogram of averaged FTS. (A), Averaged Ni (green, ×3), S (yellow, ×10), and P (black, ×0.25) traces for 8 replicates of FTS isolated from aerobically-grown *E. coli*.

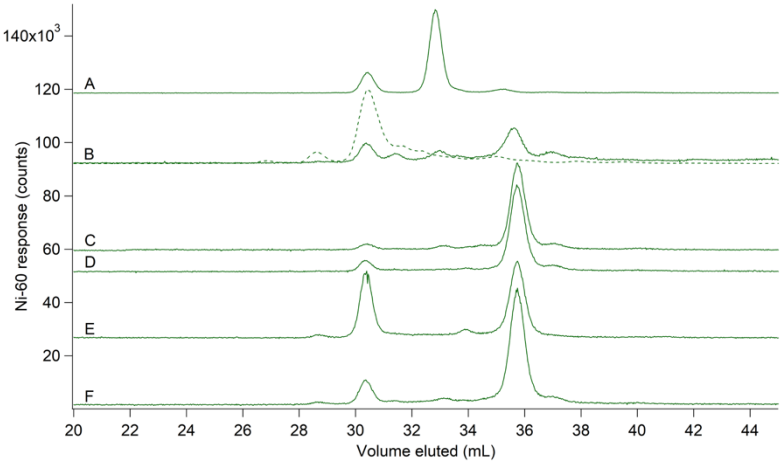

Figure IV-S2. SEC-ICP-MS (double column) chromatograms of FTS replicates (n = 7). Ni (green) traces for (A), FTS replicate 1 isolated from aerobically-grown cells; (B), FTS replicate 2 isolated from aerobically-grown cells (×3) with overlaid lyophilized FTS of replicate (×0.2); (C), FTS isolated from aerobically-grown cells grown in media supplemented with 1 µM $NiSO_4$ (×3); (D), FTS isolated from anaerobically-grown cells (×3); (E), FTS isolated from anaerobically-grown cells grown in media supplemented with 1 µM $NiSO_4$ (×3); (F), FTS isolated from aerobically-grown cells grown in media supplemented with 1 µM $NiSO_4$ and 400 µM L-histidine (×3).

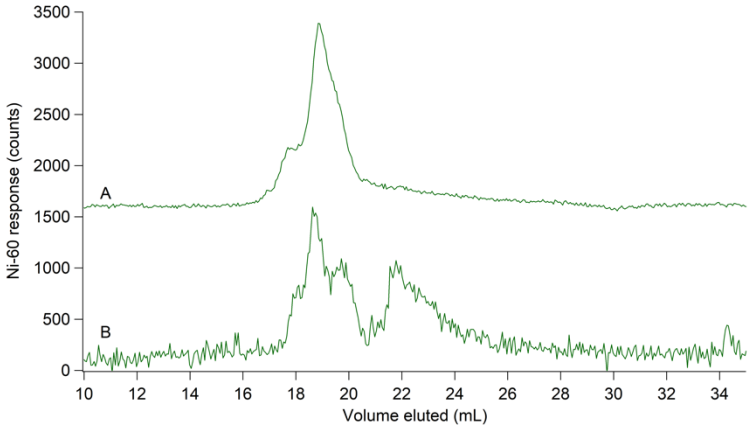

Figure IV-S3. Effect of ACN on labile Ni(II) pool (single column). Ni (green) traces for (A), representative FTS replicate (×0.1); (B), (A) diluted 10-fold in ACN.

Table IV-S1. Nickel analysis for *E. coli* whole cell (WC) lysate and cytosolic FTS replicates as determined by ICP-MS.

Sample	WC [Ni], µM	SD, µM	FTS [Ni], µM	SD, µM
Aerobic (n = 5)	11	7	11	2
Anaerobic (n = 1)	12	1*	12.0	0.7*
Anaerobic + 1 µM $NiSO_4$ (n = 1)	23	5*	32.2	0.1*
Anaerobic + 1 µM $NiSO_4$ + 400 µM L-His (n = 1)	36	1*	16.4	0.9*

*Error in triplicate measurement of sample

Table IV-S2. Parameters used to simulate chromatography peaks. FWHM, full width at half maximum.

Center (mL)	Relative Area (%)	FWHM (mL)
18.0	9.7	0.573
18.9	78	0.802
19.8	9	1.22
21.2	0.3	1.31

CHAPTER V

CONCLUSIONS

Conclusions

The principal objective of this dissertation was to develop analytical methods for isolating, separating, detecting, and identifying labile metal pools (LMPs) in the *E. coli* cytosol. The primary approach employed a novel LC-ICP-MS system in conjunction with downstream ESI-MS analysis. For the last four decades, chelator-based probes have served as the dominating technique for characterizing LMPs. The key advantage of these probes is their ability to penetrate cells and organelles without disrupting them. This allows for the detection of the endogenous LMPs within such biological milieu. However, this strategy is limited in its ability to chemically characterize LMPs since the endogenous metal complexes of interest are destroyed during their detection.

There have been few investigations utilizing chelator probes to characterize LMPs of the *E. coli* cytosol. This is likely due to the notion that no "free," or aqueous, metal ions exist in the cytosol. Since there are no "free" metal ions, how metalloproteins obtain, or metalloregulators sense, their metal cofactors has largely remained elusive. LMPs are metal complexes in which the metal ion is weakly coordinated to LMM ligands, and hence, are not "free" metal. To overcome the lack of "free" metal in the face of metal demand, the role of LMPs arise as a potential mechanism by which the metal cofactor could be supplied to metalloproteins. Thus, it is necessary to not only detect but to chemically characterize the LMPs of the *E. coli* cytosol to elucidate their cellular function and better understand the mechanism of metalloprotein metallation.

To identify LMPs in the *E. coli* cytosol, we advanced the chromatography-based approach of separating the labile metal complexes that constitute these pools and of detecting/identifying these complexes via ICP-MS and ESI-MS. The major disadvantage of this approach is that cells

must be disrupted and cytosol isolated, as this affords the potential to generate artefactual metal complexes in which ligands have exchanged relative to the endogenous complexes of interest. Ultimately, both the chelator probe and chromatography-based approaches, perhaps along with the development of new methods, will be required to identify and characterize the LMPs that are almost certainly involved in metal ion trafficking, regulation, and signalling.

The study in Chapter III highlighted the challenges associated with attempting to identify LMPs in the cytosol of *E. coli* and how these problems were overcome, thereby allowing for the examination of LMPs via LC-ICP-MS and identification of the labile sulfur and phosphorus pools by ESI-MS. First, a strain of *E. coli* was employed, which allowed cellular lysates to be prepared without using EDTA. *E. coli* was originally select as the organism of choice due to their quick doubling times and lack of organelles. With this specific strain, growing cells and subsequently isolating cytosolic components of interest allowed us to generate multiple replicates for analyses. In addition, this move towards an EDTA-free preparation sparked a laboratory-wide move to remove or reduce EDTA in organelle isolation for higher-order biological systems.

Pre-loading a SEC column with $^{67}ZnSO_4$ occupied sites on the column matrix that would have otherwise reacted with metal ions that migrated through the column. Even when using a zinc-loaded column, aqueous metal ions still interacted with the column, retarding their elution but to a lesser extent than when the column was not zinc-loaded. A "ghost column" consisting of PEEK tubing that replaced the SEC column was used to evaluate the proportion of metal ions in a sample that adhered to the column. The degree of column interaction varied approximately with the Irving-Williams series: Mn(II) (least) < Fe(II) < Ni(II) < Zn(II) < Cu(II) (most). Zinc-loading the SEC (single and double) columns afforded more reproducibility between not only batches of *E. coli* cytosol but also cytosol of *Saccharomyces cerevisiae*[73] and other extracts from biological milieu.

The mobile phase buffer impacted chromatographic behavior; lower ionic strengths encouraged metal complexes to remain intact as they passed through the column, but they also promoted greater column interactions. The chromatographic behavior of iron and zinc standards reflected the M-L binding strength of the complexes; thermodynamically stable complexes (e.g. those bound to 1,10-phenanthroline and 2,2'-bipyridyl) held together as they migrated down the column whereas less stable complexes (e.g. Fe(II)-ATP and Fe(II)-GSH) showed evidence of partial dissociation (shifting elution volumes with changing M-L ratios and mobile phase buffer composition). With LMM standards (less than ~ 1000 Da), elution volumes did not follow the classic steric-exclusion mechanism dictated by SEC theory. Thus, all masses obtained using such calibration curves in which Log(MM) is correlated to V_e/V_0 were considered apparent. This finding highlighted the fact that we are at the limit of utility for the SEC columns employed within studies of Chapter III and IV such that the primary physical properties dictating migration through these columns are hydrophobicity, charge, and affinity. Additionally, this finding was one of the motivations for seeking out a complementary LC column, such as the HILIC column utilized in Chapter IV.

The LMM sulfur pool in cytosol consisted of GSH, GSSG, methionine, and cysteine, as confirmed by ESI-MS. Approximate cytosolic concentrations were 3000, 400, 800, and 200 µM, respectively. The LMM phosphorus pool consisted of 1 intense LC peak and ca. 6 minor peaks. ESI-MS established the presence of phosphates, pyrophosphate, AMP, ADP, ATP, and NADH. The dominant LC peak probably arose from phosphate ions. The total concentration of the LMM phosphorus pool in *E. coli* was ~ 140 mM. Estimated ATP, ADP, and AMP concentrations were 1000, 200, and 1000 µM, respectively.

No endogenous manganese, iron, nickel, zinc, or copper complexes in cytosol were detected by ESI-MS, plausibly due to salt suppression and low concentrations. Salt suppression was identified as a major challenge because cytosol and other cell compartments contain high concentrations of salts. Using a longer column (double SEC column) diminished this problem but also further diluted samples.

The chromatographic profile of cytosolic FTS from *E. coli* cells contained 2 – 5 labile LMM zinc complexes with a collective concentration of ~ 13 µM. Supplementing the growth medium with 100 µM $Zn(acetate)_2$ increased the zinc pool concentration to ~ 200 µM. The *E. coli* cytosol chromatographically consisted of 2 – 5 LMM iron species with a collective concentration of ~ 80 µM. For the growth conditions used, this represented 8% of the iron in the cell and 20% of the iron in the cytosol. When cells were grown on high iron, the concentration of iron in the FTS increased to ~ 200 µM. After the FTS was treated with BPY, iron LC peak intensities declined ~ 70%, indicating that the detected peaks were labile as commonly defined. FTS chromatographically contained 2 – 4 LMM copper complexes with a collective concentration of ~ 10 µM. These complexes are not aqueous copper as such ions adhere tightly to the column. Increasing the copper concentration in the growth medium had little effect on the copper concentration in the FTS, but the relative intensities of the peaks changed. Surprisingly, *E. coli* contain a LMM labile copper pool that represents the vast majority (~ 80%) of the copper in the cell. FTS chromatographically contained 2 LMM manganese species with a collective concentration of ~ 1.4 µM. These species represented ~ 20% of the manganese in the cell. Supplementing manganese in the growth increased the manganese concentration in the FTS hugely. Lastly, the chromatographic profile of FTS contained ~ 2 LMM nickel species with a collective

concentration of ~ 15 μM. These peaks comigrated with sulfur suggesting a LMM Ni-S complex(es) in *E. coli*.

Building on the foundation established in Chapter III, in Chapter IV, we sought out to identify the labile Ni(II) pool (LNP) in the *E. coli* cytosol as Ni(II) complexes appear to be less labile than comparable (biologically-relevant) transition metal complexes[129] and aqueous Ni(II) interacts less with the SEC columns employed herein than Zn(II) or Cu(II).[130] Towards this end, we (aerobically) grew 8 batches *E. coli*, isolated the cytosol, and observed 4 Ni-containing peaks via SEC-ICP-MS (single column). By adding either exogenous $NiSO_4$ or ligand (GSSG, L-histidine, citrate, etc.) to the FTS, we evaluated the sensitivity of the LNP towards such and determined that the ligands of the LMM Ni(II) complexes were likely GSSG, L-histidine, aspartate, and ATP and that these ligands, in total, were in excess of the metal ion.

In accordance with Chapter III, the chromatographic behavior of nickel standards reflected the M-L binding strength of the complexes and allowed us to qualitatively rank-order the apparent binding interactions between aqueous Ni(II) and potential ligands in the following order:

L-His (strong) > Citrate > Asp > GSSG > ATP > GSH > Cys > Glu > NaH_2PO_4/K_2HPO_4 (weak)

We concluded that the endogenous LNP was composed of relatively strong-binding complexes as no "free" nickel was detected in FTS via SEC-ICP-MS. Based on the elution of these nickel standards, the notion of GSSG, L-histidine, aspartate, and ATP as ligands of the LMM Ni(II) complex(es) in the LNP was further supported.

The chromatographic profile of the LNP on the double SEC also revealed four, better resolved Ni-containing peaks. A pseudo-flow-through-solution (pFTS) prepared by mixing $NiSO_4$ with a ligand cocktail to mimic the FTS chromatographically exhibited 4 Ni(II) peaks that

comigrated with the 4 Ni-containing peaks in the FTS. When fractions collected from FTS and pFTS double column eluate were analyzed by ESI-MS, Ni(GSSG) was observed in both solutions. Additionally, $Ni(Asp)_2$ and Ni(ATP) was observed in pFTS albeit at lower intensities than Ni(GSSG).

We employed HILIC as a complementary approach to SEC to probe the LNP of *E. coli*. We detected Ni(GSSG) by HILIC-ESI-MS in almost all replicates of FTS that we examined, and Ni(GSSG) was the dominant Ni(II) complex in FTS when analyzed by HILIC-ICP-MS. While SEC-ICP-MS demonstrated the presence of Ni(GSSG) in FTS, this species was not the most intense complex observed, which we attributed to ligand exchange processes taking place as the FTS migrated through the SEC columns thereby resulting in new and/or artefactually-high Ni(II) complexes being detected. While HILIC-ESI-MS HILIC-ICP-MS indicated that Ni(GSSG) is the dominant component of the LNP in aerobically-grown *E. coli*, $Ni(L\text{-}His)_2$, $Ni(Asp)_2$ and Ni(ATP) were also observed and in the following abundance: $Ni(L\text{-}His)_2 > Ni(Asp)_2 \sim Ni(ATP)$. These findings provided the first identification of a LMP in *E. coli.*

Future Work

Although the existence of LMPs has been recognized for decades, the number of species involved, their chemical composition, and their specific roles in cellular physiology remained enigmatic. This dissertation presented the first molecular description of a non-plant LMP, revealing both the number of species involved and the chemical composition for the LNP within the *E. coli* cytosol. As the chromatography-based approach must disrupt cells in order to isolate the LNP, a future study involving WC analysis via extended x-ray absorption fine structure (EXAFS) spectroscopy could be utilized to determine the coordination number and assess the

ligand environment as we demonstrated that nearly all of the nickel present in the WC of *E. coli* is found within the cytosolic LNP. Although this technique is unable to differentiate between N- and O-ligation, it could confirm the lack of S-ligation and provide Ni-L bond distances for creating an accurate intracellular structure of Ni-GSSG, which has yet to be produced in literature.

The specific function of the four Ni(II) species (Ni(GSSG), Ni(L-His)$_2$, Ni(Asp)$_2$, and Ni(ATP)) remains to be elucidated and/or differentiated between aerobically- and anaerobically-grown *E. coli*. Additional anaerobic growth replicates are necessary to determine if the LNP in *E. coli* is different, composition-wise, than the pool present under aerobic conditions. Once this is clarified, functional assays could be established using the apo-enzymes, glyoxalase and hydrogenase for LNPs isolated from aerobically- or anaerobically-grown *E. coli*, respectively, in an ESI-MS (mass difference) or spectrophotometric (enzyme activity) experiment to determine if and which LMM Ni(II) complex supplies the metal cofactor to these metalloenzymes. Furthermore, various genetic mutants in which the distribution or quantity of the LNP is altered could assist in elucidating the role of the LNP. For example, a genetic variant in which the nickel export system, RncAB, is deleted would lead to an accumulation of Ni(II) in the cell. We've demonstrated with the addition of exogenous $NiSO_4$ to the FTS that the LNP accumulates in the following manner: Ni(GSSG) > Ni(L-His)$_2$ > Ni(Asp)$_2$ ~ Ni(ATP). It would be interesting to observe if this trend continues and to determine a preference for Ni(II) to bind Asp or ATP under cellular conditions. This trend could also be examined in genetic mutants in which the cell cannot synthesize particular ligands (GSSG, L-His, etc).

Chapter IV demonstrated the use of HILIC for the first time in the Lindahl lab. The conditions of the HILIC column were minimally optimized for Ni-L standard detection by ESI-MS. Thus, although the utility of the HILIC was demonstrated, operational conditions could be

further refined by adjusting parameters such as the gradient, aqueous mobile phase component, and injection volume to yield more resolved Ni-L peaks. For example, a 90 to 40% ACN gradient was applied over a 20-minute period. As the separation in HILIC is driven by the thickness of the water layer on the surface of the stationary phase, a gradient elution should be performed in which the water content is increased slowly (typically 40% water in 20 minutes). The gradient employed herein is slightly steeper than typically applied, likely resulting is more peak overlap.

As previously alluded to, the conditions of the HILIC experiment yielded sufficient separation to allow for detection of Ni-L standards and cytosolic LMM Ni(II) complexes by ICP-MS and ESI-MS. However, particular conditions, specifically the pH of the aqueous component of the mobile phase gradient and the temperature, associated with the LC system were different between the two setups that resulted in differing migration patterns and peak shape for Ni-L standards. While we were able to overcome such and achieve identification by re-analyzing all standards and cytosolic FTSs under both systems, ideally, the conditions would be reproducible to permit direct comparison between the systems.

Our journey into identification of LMPs in the *E. coli* cytosol began with a metal focus that excluded nickel. There are currently no known nickel-requiring enzymes in the mammalian proteome. Thus, while we deem nickel an essential element for bacteria and consider the LNP of great homeostatic importance for such organisms, the aim moving forward should be to utilize this foundation of methodology present herein this dissertation to isolate, separate, detect, and identify other LMPs in *E. coli* that perhaps have an evolutionary connection to eukaryotes. In terms of other LMPs, such as those of iron, zinc, copper, and manganese, the increased lability of these complexes presents a greater chemical characterization challenge than nickel. However, while challenging, it will not be impossible! Other techniques such as Mössbauer spectroscopy, electron

paramagnetic resonance, and NMR could assist in identification efforts for iron, manganese, and zinc respectively.

From a concentration standpoint, the *E. coli* cytosolic labile iron pool (LIP) presents the most attractive next target for identification. Ligand exchange processes were evident in SEC-ICP-MS nickel analyses and will undoubtedly be apparent and perhaps more problematic for iron analyses. Thus, the HILIC column positions itself as valuable tool towards characterization of the LIP. Additionally, a reductant can be utilized in the aqueous component of the HILIC mobile phase to ensure the iron in the standards or samples analyzed is reduced as it in cytosol of *E. coli*.

It has been hypothesized that copper is trafficked within *E. coli* by metallochaperones as opposed to a labile pool. A labile pool of copper was detected within the cytosol of *E. coli* but only when the cells were grown in a medium supplemented with iron (10 μM). In cells grown with no metal supplementation in the growth media, a copper species was detected the V_0 region of the SEC column suggesting a high mass copper complex. Further investigations, including periplasm isolation, are necessary to elucidate if the high mass copper complex is a copper-bound metallochaperone in the cytosol and why under conditions of increased iron does a labile copper pool form.

REFERENCES

(1) Finney, L. A.; O'Halloran, T. V. Transition Metal Speciation in the Cell: Insights from the Chemistry of Metal Ion Receptors. *Science* **2003**, *300* (5621), 931–936.

(2) Zhang, Y.; Zheng, J. Bioinformatics of Metalloproteins and Metalloproteomes. *Molecules* **2020**, *25* (15).

(3) Capdevila, D. A.; Edmonds, K. A.; Giedroc, D. P. Metallochaperones and Metalloregulation in Bacteria. *Essays Biochem* **2017**, *61* (2), 177–200.

(4) Imlay, J. A. Pathways of Oxidative Damage. *Annu Rev Microbiol* **2003**, *57*, 395–418.

(5) Macomber, L.; Imlay, J. A. The Iron-Sulfur Clusters of Dehydratases Are Primary Intracellular Targets of Copper Toxicity. *PNAS* **2009**, *106* (20), 8344–8349.

(6) Chandrangsu, P.; Rensing, C.; Helmann, J. D. Metal Homeostasis and Resistance in Bacteria. *Nature Reviews Microbiology* **2017**, *15* (6), 338–350.

(7) Lindahl, P. A.; Moore, M. J. Labile Low-Molecular-Mass Metal Complexes in Mitochondria: Trials and Tribulations of a Burgeoning Field. *Biochemistry* **2016**, *55* (30), 4140–4153.

(8) Irving, H.; Williams, R. J. P. 637. The Stability of Transition-Metal Complexes. *J. Chem. Soc.* **1953**, No. 0, 3192–3210.

(9) Foster, A. W.; Osman, D.; Robinson, N. J. Metal Preferences and Metallation. *J Biol Chem* **2014**, *289* (41), 28095–28103.

(10) Hadacek, F.; Bachmann, G. Low-Molecular-Weight Metabolite Systems Chemistry. *Front. Environ. Sci.* **2015**, *3*.

(11) Singh, J.; Srivastav, A. N.; Singh, N.; Singh, A. Stability Constants of Metal Complexes in Solution. *Stability and Applications of Coordination Compounds* **2019**.

(12) Krężel, A.; Maret, W. The Biological Inorganic Chemistry of Zinc Ions. *Arch Biochem Biophys* **2016**, *611*, 3–19.

(13) Ahrland, S.; Chatt, J.; Davies, N. R. The Relative Affinities of Ligand Atoms for Acceptor Molecules and Ions. *Q. Rev. Chem. Soc.* **1958**, *12* (3), 265–276.

(14) Pearson, R. G. Hard and Soft Acids and Bases. *J. Am. Chem. Soc.* **1963**, *85* (22), 3533–3539.

(15) Martin, J. E.; Waters, L. S.; Storz, G.; Imlay, J. A. The Escherichia Coli Small Protein MntS and Exporter MntP Optimize the Intracellular Concentration of Manganese. *PLOS Genetics* **2015**, *11* (3), e1004977.

(16) Lisher, J. P.; Giedroc, D. P. Manganese Acquisition and Homeostasis at the Host-Pathogen Interface. *Front. Cell. Infect. Microbiol.* **2013**, *3*.

(17) Barnese, K.; Gralla, E. B.; Valentine, J. S.; Cabelli, D. E. Biologically Relevant Mechanism for Catalytic Superoxide Removal by Simple Manganese Compounds. *PNAS* **2012**, *109* (18), 6892–6897.

(18) Ayala-Castro, C.; Saini, A.; Outten, F. W. Fe-S Cluster Assembly Pathways in Bacteria. *Microbiol Mol Biol Rev* **2008**, *72* (1), 110–125.

(19) Wofford, J. D.; Bolaji, N.; Dziuba, N.; Outten, F. W.; Lindahl, P. A. Evidence That a Respiratory Shield in Escherichia Coli Protects a Low-Molecular-Mass FeII Pool from O2–Dependent Oxidation. *J. Biol. Chem.* **2018**, jbc.RA118.005233.

(20) Fontenot, C. R.; Tasnim, H.; Valdes, K. A.; Popescu, C. V.; Ding, H. Ferric Uptake Regulator (Fur) Reversibly Binds a [2Fe-2S] Cluster to Sense Intracellular Iron Homeostasis in Escherichia Coli. *J Biol Chem* **2020**, *295* (46), 15454–15463.

(21) Pi, H.; Helmann, J. D. Ferrous Iron Efflux Systems in Bacteria. *Metallomics* **2017**, *9* (7), 840–851.

(22) Lau, C. K. Y.; Krewulak, K. D.; Vogel, H. J. Bacterial Ferrous Iron Transport: The Feo System. *FEMS Microbiology Reviews* **2016**, *40* (2), 273–298.

(23) Beauchene, N. A.; Mettert, E. L.; Moore, L. J.; Keleş, S.; Willey, E. R.; Kiley, P. J. O2 Availability Impacts Iron Homeostasis in Escherichia Coli. *Proc Natl Acad Sci U S A* **2017**, *114* (46), 12261–12266.

(24) Yang, J.; Tan, G.; Zhang, T.; White, R. H.; Lu, J.; Ding, H. Deletion of the Proposed Iron Chaperones IscA/SufA Results in Accumulation of a Red Intermediate Cysteine Desulfurase IscS in Escherichia Coli*. *Journal of Biological Chemistry* **2015**, *290* (22), 14226–14234.

(25) Kaluarachchi, H.; Chung, K. C. C.; Zamble, D. B. Microbial Nickel Proteins. *Nat. Prod. Rep.* **2010**, *27* (5), 681–694.

(26) Iwig, J. S.; Rowe, J. L.; Chivers, P. T. Nickel Homeostasis in Escherichia Coli – the RcnR-RcnA Efflux Pathway and Its Linkage to NikR Function. *Molecular Microbiology* **2006**, *62* (1), 252–262.

(27) Lebrette, H.; Iannello, M.; Fontecilla-Camps, J. C.; Cavazza, C. The Binding Mode of Ni-(L-His)2 in NikA Revealed by X-Ray Crystallography. *J Inorg Biochem* **2013**, *121*, 16–18.

(28) Higgins, K. Nickel Metalloregulators and Chaperones. *Inorganics (Basel)* **2019**, *7* (8).

(29) Rowe, J. L.; Starnes, G. L.; Chivers, P. T. Complex Transcriptional Control Links NikABCDE-Dependent Nickel Transport with Hydrogenase Expression in Escherichia Coli. *JB* **2005**, *187* (18), 6317–6323.

(30) Boer, J. L.; Mulrooney, S. B.; Hausinger, R. P. Nickel-Dependent Metalloenzymes. *Archives of Biochemistry and Biophysics* **2014**, *544*, 142–152.

(31) Chivers, P. T.; Benanti, E. L.; Heil-Chapdelaine, V.; Iwig, J. S.; Rowe, J. L. Identification of Ni-(L-His)2 as a Substrate for NikABCDE-Dependent Nickel Uptake in Escherichia Coli. *Metallomics* **2012**, *4* (10), 1043–1050.

(32) Takahashi, H.; Oshima, T.; Hobman, J. L.; Doherty, N.; Clayton, S. R.; Iqbal, M.; Hill, P. J.; Tobe, T.; Ogasawara, N.; Kanaya, S.; Stekel, D. J. The Dynamic Balance of Import and Export of Zinc in Escherichia Coli Suggests a Heterogeneous Population Response to Stress. *J R Soc Interface* **2015**, *12* (106).

(33) Mikhaylina, A.; Ksibe, A. Z.; Scanlan, D. J.; Blindauer, C. A. Bacterial Zinc Uptake Regulator Proteins and Their Regulons. *Biochemical Society Transactions* **2018**, *46* (4), 983–1001.

(34) Brocklehurst, K. R.; Hobman, J. L.; Lawley, B.; Blank, L.; Marshall, S. J.; Brown, N. L.; Morby, A. P. ZntR Is a Zn(II)-Responsive MerR-like Transcriptional Regulator of ZntA in Escherichia Coli. *Molecular Microbiology* **1999**, *31* (3), 893–902.

(35) Outten, C. E. Femtomolar Sensitivity of Metalloregulatory Proteins Controlling Zinc Homeostasis. *Science* **2001**, *292* (5526), 2488–2492.

(36) Heinz, U.; Kiefer, M.; Tholey, A.; Adolph, H.-W. On the Competition for Available Zinc. *J Biol Chem* **2005**, *280* (5), 3197–3207.

(37) Hagenmaier, S.; Stierhof, Y. D.; Henning, U. A New Periplasmic Protein of Escherichia Coli Which Is Synthesized in Spheroplasts but Not in Intact Cells. *J Bacteriol* **1997**, *179* (6), 2073–2076.

(38) Blindauer, C. A.; Harrison, M. D.; Robinson, A. K.; Parkinson, J. A.; Bowness, P. W.; Sadler, P. J.; Robinson, N. J. Multiple Bacteria Encode Metallothioneins and SmtA-like Zinc Fingers. *Mol Microbiol* **2002**, *45* (5), 1421–1432.

(39) Petit-Härtlein, I.; Rome, K.; de Rosny, E.; Molton, F.; Duboc, C.; Gueguen, E.; Rodrigue, A.; Covès, J. Biophysical and Physiological Characterization of ZraP from Escherichia Coli, the Periplasmic Accessory Protein of the Atypical ZraSR Two-Component System. *Biochem J* **2015**, *472* (2), 205–216.

(40) Andreini, C.; Bertini, I. Zinc-Binding Proteins, Abundance. In *Encyclopedia of Metalloproteins*; Kretsinger, R. H., Uversky, V. N., Permyakov, E. A., Eds.; Springer New York: New York, NY, 2013; pp 2549–2554.

(41) Arguello, J. M.; Raimunda, D.; Padilla-Benavides, T. Mechanisms of Copper Homeostasis in Bacteria. *Front. Cell. Infect. Microbiol.* **2013**, *3*.

(42) Outten, F. W.; Huffman, D. L.; Hale, J. A.; O'Halloran, T. V. The Independent Cue and Cus Systems Confer Copper Tolerance during Aerobic and Anaerobic Growth in Escherichia Coli. *J Biol Chem* **2001**, *276* (33), 30670–30677.

(43) Changela, A.; Chen, K.; Xue, Y.; Holschen, J.; Outten, C. E.; O'Halloran, T. V.; Mondragón, A. Molecular Basis of Metal-Ion Selectivity and Zeptomolar Sensitivity by CueR. *Science* **2003**, *301* (5638), 1383–1387.

(44) González-Guerrero, M.; Argüello, J. M. Mechanism of Cu+-Transporting ATPases: Soluble Cu+ Chaperones Directly Transfer Cu+ to Transmembrane Transport Sites. *Proc Natl Acad Sci U S A* **2008**, *105* (16), 5992–5997.

(45) Drees, S. L.; Klinkert, B.; Helling, S.; Beyer, D. F.; Marcus, K.; Narberhaus, F.; Lübben, M. One Gene, Two Proteins: Coordinated Production of a Copper Chaperone by Differential Transcript Formation and Translational Frameshifting in Escherichia Coli. *Molecular Microbiology* **2017**, *106* (4), 635–645.

(46) Rae, T. D.; Schmidt, P. J.; Pufahl, R. A.; Culotta, V. C.; O'Halloran, T. V. Undetectable Intracellular Free Copper: The Requirement of a Copper Chaperone for Superoxide Dismutase. *Science* **1999**, *284* (5415), 805–808.

(47) Rensing, C.; Grass, G. Escherichia Coli Mechanisms of Copper Homeostasis in a Changing Environment. *FEMS Microbiol Rev* **2003**, *27* (2–3), 197–213.

(48) Wang, D.; Hurst, T. K.; Thompson, R. B.; Fierke, C. A. Genetically Encoded Ratiometric Biosensors to Measure Intracellular Exchangeable Zinc in Escherichia Coli. *J Biomed Opt* **2011**, *16* (8).

(49) Chung, C. Y.-S.; Posimo, J. M.; Lee, S.; Tsang, T.; Davis, J. M.; Brady, D. C.; Chang, C. J. Activity-Based Ratiometric FRET Probe Reveals Oncogene-Driven Changes in Labile Copper Pools Induced by Altered Glutathione Metabolism. *PNAS* **2019**, *116* (37), 18285–18294.

(50) Chabosseau, P.; Woodier, J.; Cheung, R.; Rutter, G. A. Sensors for Measuring Subcellular Zinc Pools. *Metallomics* **2018**, *10* (2), 229–239.

(51) Kolanowski, J. L.; Shen, C.; New, E. J. Fluorescent Probes for the Analysis of Labile Metals in Brain Cells. In *Metals in the Brain: Measurement and Imaging*; White, A. R., Ed.; Neuromethods; Springer: New York, NY, 2017; pp 51–70.

(52) Dean, K. M.; Qin, Y.; Palmer, A. E. Visualizing Metal Ions in Cells: An Overview of Analytical Techniques, Approaches, and Probes. *Biochimica et Biophysica Acta (BBA) - Molecular Cell Research* **2012**, *1823* (9), 1406–1415.

(53) Futra, D.; Heng, L. Y.; Ahmad, A.; Surif, S.; Ling, T. L. An Optical Biosensor from Green Fluorescent Escherichia Coli for the Evaluation of Single and Combined Heavy Metal Toxicities. *Sensors (Basel)* **2015**, *15* (6), 12668–12681.

(54) Carter, K. P.; Young, A. M.; Palmer, A. E. Fluorescent Sensors for Measuring Metal Ions in Living Systems. *Chem Rev* **2014**, *114* (8), 4564–4601.

(55) Ma, Z.; Faulkner, M. J.; Helmann, J. D. Origins of Specificity and Cross-Talk in Metal Ion Sensing by Bacillus Subtilis Fur. *Mol Microbiol* **2012**, *86* (5), 1144–1155.

(56) Keyer, K.; Imlay, J. A. Superoxide Accelerates DNA Damage by Elevating Free-Iron Levels. *Proc Natl Acad Sci U S A* **1996**, *93* (24), 13635–13640.

(57) Bagg, A.; Neilands, J. B. Ferric Uptake Regulation Protein Acts as a Repressor, Employing Iron (II) as a Cofactor to Bind the Operator of an Iron Transport Operon in Escherichia Coli. *Biochemistry* **1987**, *26* (17), 5471–5477.

(58) Woodmansee, A. N.; Imlay, J. A. Reduced Flavins Promote Oxidative DNA Damage in Non-Respiring Escherichia Coli by Delivering Electrons to Intracellular Free Iron. *J Biol Chem* **2002**, *277* (37), 34055–34066.

(59) Hamed, M. Y.; Neilands, J. B.; Huynh, V. Binding of the Ferric Uptake Regulation Repressor Protein (Fur) to Mn(II), Fe(II), Co(II), and Cu(II) Ions as Co-Repressors: Electronic Absorption, Equilibrium, and 57Fe Mössbauer Studies. *Journal of Inorganic Biochemistry* **1993**, *50* (3), 193–210.

(60) Marszałek, I.; Goch, W.; Bal, W. Ternary Zn(II) Complexes of FluoZin-3 and the Low Molecular Weight Component of the Exchangeable Cellular Zinc Pool. *Inorg Chem* **2018**, *57* (16), 9826–9838.

(61) Hider, R.; Aviles, M. V.; Chen, Y.-L.; Latunde-Dada, G. O. The Role of GSH in Intracellular Iron Trafficking. *Int J Mol Sci* **2021**, *22* (3).

(62) Hider, R. C.; Kong, X. L. Glutathione: A Key Component of the Cytoplasmic Labile Iron Pool. *Biometals* **2011**, *24* (6), 1179–1187.

(63) Krężel, A.; Wójcik, J.; Maciejczyk, M.; Bal, W. May GSH and L-His Contribute to Intracellular Binding of Zinc? Thermodynamic and Solution Structural Study of a Ternary Complex. *Chem. Commun.* **2003**, No. 6, 704–705.

(64) Liu, J.; Liu, H.; Li, Y.; Wang, H. Probing the Coordination Properties of Glutathione with Transition Metal Ions (Cr2+, Mn2+, Fe2+, Co2+, Ni2+, Cu2+, Zn2+, Cd2+, Hg2+) by Density Functional Theory. *J Biol Phys* **2014**, *40* (4), 313–323.

(65) Drago, R. S. (1928-1997). *Physical Methods in Inorganic Chemistry*, 3 print.; Reinhold Chemistry Textbook Series; Reinhold Publishing Corporation: New York [etc.], 1967.

(66) Krężel, A.; Wójcik, J.; Maciejczyk, M.; Bal, W. Zn(II) Complexes of Glutathione Disulfide: Structural Basis of Elevated Stabilities. *Inorg. Chem.* **2011**, *50* (1), 72–85.

(67) Handbook: Size Exclusion Chromatography Principles and Methods - Bioprocess Development Forum http://www.processdevelopmentforum.com/articles/handbook-size-exclusion-chromatography-principles-and-methods/

(68) Buszewski, B.; Noga, S. Hydrophilic Interaction Liquid Chromatography (HILIC)—a Powerful Separation Technique. *Anal Bioanal Chem* **2012**, *402* (1), 231–247.

(69) Wilschefski, S. C.; Baxter, M. R. Inductively Coupled Plasma Mass Spectrometry: Introduction to Analytical Aspects. *Clin Biochem Rev* **2019**, *40* (3), 115–133.

(70) Tsednee, M.; Huang, Y.-C.; Chen, Y.-R.; Yeh, K.-C. Identification of Metal Species by ESI-MS/MS through Release of Free Metals from the Corresponding Metal-Ligand Complexes. *Scientific Reports* **2016**, *6* (1), 26785.

(71) Ho, C.; Lam, C.; Chan, M.; Cheung, R.; Law, L.; Lit, L.; Ng, K.; Suen, M.; Tai, H. Electrospray Ionisation Mass Spectrometry: Principles and Clinical Applications. *Clin Biochem Rev* **2003**, *24* (1), 3–12.

(72) Metwally, H.; McAllister, R. G.; Konermann, L. Exploring the Mechanism of Salt-Induced Signal Suppression in Protein Electrospray Mass Spectrometry Using Experiments and Molecular Dynamics Simulations. *Anal. Chem.* **2015**, *87* (4), 2434–2442.

(73) Nguyen, T. Q.; Kim, J. E.; Brawley, H. N.; Lindahl, P. A. Chromatographic Detection of Low-Molecular-Mass Metal Complexes in the Cytosol of Saccharomyces Cerevisiae. *Metallomics* **2020**.

(74) Nguyen, T. Q.; Dziuba, N.; Lindahl, P. A. Isolated Saccharomyces Cerevisiae Vacuoles Contain Low-Molecular-Mass Transition-Metal Polyphosphate Complexes. *Metallomics* **2019**, *11* (7), 1298–1309.

(75) Ouerdane, L.; Mari, S.; Czernic, P.; Lebrun, M.; Łobiński, R. Speciation of Non-Covalent Nickel Species in Plant Tissue Extracts by Electrospray Q-TOFMS/MS after Their Isolation by 2D Size Exclusion-Hydrophilic Interaction LC (SEC-HILIC) Monitored by ICP-MS. *J. Anal. At. Spectrom.* **2006**, *21* (7), 676–683.

(76) Alchoubassi, G.; Kińska, K.; Bierla, K.; Lobinski, R.; Szpunar, J. Speciation of Essential Nutrient Trace Elements in Coconut Water. *Food Chemistry* **2021**, *339*, 127680.

(77) Cahill, J.; Young, R. Phage Lysis: Multiple Genes for Multiple Barriers. *Adv Virus Res* **2019**, *103*, 33–70.

(78) Bennett, B. D.; Kimball, E. H.; Gao, M.; Osterhout, R.; Van Dien, S. J.; Rabinowitz, J. D. Absolute Metabolite Concentrations and Implied Enzyme Active Site Occupancy in *Escherichia Coli*. *Nature Chemical Biology* **2009**, *5* (8), 593–599.

(79) Lushchak, V. I. Glutathione Homeostasis and Functions: Potential Targets for Medical Interventions. *Journal of Amino Acids* **2012**, *2012*, e736837.

(80) Masip, L.; Veeravalli, K.; Georgiou, G. The Many Faces of Glutathione in Bacteria. *Antioxid Redox Signal* **2006**, *8* (5–6), 753–762.

(81) Zborníková, E.; Knejzlík, Z.; Hauryliuk, V.; Krásný, L.; Rejman, D. Analysis of Nucleotide Pools in Bacteria Using HPLC-MS in HILIC Mode. *Talanta* **2019**, *205*, 120161.

(82) Smirnova, G. V.; Tyulenev, A. V.; Bezmaternykh, K. V.; Muzyka, N. G.; Ushakov, V. Y.; Oktyabrsky, O. N. Cysteine Homeostasis under Inhibition of Protein Synthesis in Escherichia Coli Cells. *Amino Acids* **2019**, *51* (10), 1577–1592.

(83) McCleary, W. R. Molecular Mechanisms of Phosphate Homeostasis in *Escherichia Coli*. Escherichia coli - *Recent Advances on Physiology, Pathogenesis and Biotechnological Applications* **2017**.

(84) Andrén, H.; Rodushkin, I.; Stenberg, A.; Malinovsky, D.; Baxter, D. C. Sources of Mass Bias and Isotope Ratio Variation in Multi-Collector ICP-MS: Optimization of Instrumental Parameters Based on Experimental Observations. *J. Anal. At. Spectrom.* **2004**, *19* (9), 1217–1224.

(85) Lum, T.-S.; Leung, K. S.-Y. Strategies to Overcome Spectral Interference in ICP-MS Detection. *Journal of Analytical Atomic Spectrometry* **2016**, *31* (5), 1078–1088.

(86) Heumann, K. G.; Gallus, S. M.; Rädlinger, G.; Vogl, J. Precision and Accuracy in Isotope Ratio Measurements by Plasma Source Mass Spectrometry. *J. Anal. At. Spectrom.* **1998**, *13* (9), 1001–1008.

(87) Martínez-Salas, E.; Martín, J. A.; Vicente, M. Relationship of Escherichia Coli Density to Growth Rate and Cell Age. *J Bacteriol* **1981**, *147* (1), 97–100.

(88) Hudder, B. N.; Morales, J. G.; Stubna, A.; Münck, E.; Hendrich, M. P.; Lindahl, P. A. Electron Paramagnetic Resonance and Mössbauer Spectroscopy of Intact Mitochondria from Respiring Saccharomyces Cerevisiae. *J Biol Inorg Chem* **2007**, *12* (7), 1029–1053.

(89) Schaechter, M. Escherichia Coli and Salmonella 2000: The View From Here. *Microbiol Mol Biol Rev* **2001**, *65* (1), 119–130.

(90) Kubitschek, H. E.; Friske, J. A. Determination of Bacterial Cell Volume with the Coulter Counter. *J Bacteriol* **1986**, *168* (3), 1466–1467.

(91) Imlay, J. A. The Mismetallation of Enzymes during Oxidative Stress. *J Biol Chem* **2014**, *289* (41), 28121–28128.

(92) Gu, M.; Imlay, J. A. Superoxide Poisons Mononuclear Iron Enzymes by Causing Mismetallation. *Mol Microbiol* **2013**, *89* (1), 123–134.

(93) Lindahl, P. A.; Moore, M. J. Labile Low-Molecular-Mass Metal Complexes in Mitochondria: Trials and Tribulations of a Burgeoning Field. *Biochemistry* **2016**, *55* (30), 4140–4153.

(94) O'Halloran, T. V.; Culotta, V. C. Metallochaperones, an Intracellular Shuttle Service for Metal Ions. *J Biol Chem* **2000**, *275* (33), 25057–25060.

(95) Ma, Z.; Jacobsen, F. E.; Giedroc, D. P. Coordination Chemistry of Bacterial Metal Transport and Sensing. *Chem Rev* **2009**, *109* (10), 4644–4681.

(96) Wilson, S.; Bird, A. J. Zinc Sensing and Regulation in Yeast Model Systems. *Arch Biochem Biophys* **2016**, *611*, 30–36.

(97) Jacobs, A. Low Molecular Weight Intracellular Iron Transport Compounds. *Blood* **1977**, *50* (3), 433–439.

(98) Williams, R. J. Free Manganese (II) and Iron (II) Cations Can Act as Intracellular Cell Controls. *FEBS Lett* **1982**, *140* (1), 3–10.

(99) Crichton, R. R. Iron Uptake and Utilization by Mammalian Cells II. Intracellular Iron Utilization. *Trends in Biochemical Sciences* **1984**, *9* (6), 283–286.

(100) Braymer, J. J.; Giedroc, D. P. Recent Developments in Copper and Zinc Homeostasis in Bacterial Pathogens. *Curr Opin Chem Biol* **2014**, *0*, 59–66.

(101) Petrat, F.; de Groot, H.; Sustmann, R.; Rauen, U. The Chelatable Iron Pool in Living Cells: A Methodically Defined Quantity. *Biol Chem* **2002**, *383* (3–4), 489–502.

(102) Petrat, F.; Rauen, U.; de Groot, H. Determination of the Chelatable Iron Pool of Isolated Rat Hepatocytes by Digital Fluorescence Microscopy Using the Fluorescent Probe, Phen Green SK. *Hepatology* **1999**, *29* (4), 1171–1179.

(103) Zastrow, M. L.; Huang, Z.; Lippard, S. J. HaloTag-Based Hybrid Targetable and Ratiometric Sensors for Intracellular Zinc. *ACS Chem Biol* **2020**, *15* (2), 396–406.

(104) Dziuba, N.; Hardy, J.; Lindahl, P. A. Low-Molecular-Mass Iron Complexes in Blood Plasma of Iron-Deficient Pigs Do Not Originate Directly from Nutrient Iron†. *Metallomics* **2019**, *11* (11), 1900–1911.

(105) McCormick, S. P.; Moore, M. J.; Lindahl, P. A. Detection of Labile Low-Molecular-Mass Transition Metal Complexes in Mitochondria. *Biochemistry* **2015**, *54* (22), 3442–3453.

(106) Hellberg, U.; Ivarsson, J.-P.; Johansson, B.-L. Characteristics of Superdex® Prep Grade Media for Gel Filtration Chromatography of Proteins and Peptides. *Process Biochemistry* **1996**, *31* (2), 163–172.

(107) Irving, H.; Williams, R. J. P. Order of Stability of Metal Complexes. *Nature* **1948**, *162* (4123), 746–747..

(108) Martell, A. E.; Smith, R. M. *Critical Stability Constants: Second Supplement*; Critical Stability Constants; Springer US, 1989.

(109) Hider, R. C.; Kong, X. Iron Speciation in the Cytosol: An Overview. *Dalton Trans* **2013**, *42* (9), 3220–3229.

(110) Helbig, K.; Bleuel, C.; Krauss, G. J.; Nies, D. H. Glutathione and Transition-Metal Homeostasis in Escherichia Coli. *JB* **2008**, *190* (15), 5431–5438.

(111) Piwowar, A. M.; Lockyer, N. P.; Vickerman, J. C. Salt Effects on Ion Formation in Desorption Mass Spectrometry: An Investigation into the Role of Alkali Chlorides on Peak Suppression in Time-of-Flight-Secondary Ion Mass Spectrometry. *Anal Chem* **2009**, *81* (3), 1040–1048.

(112) Akiyama, M.; Crooke, E.; Kornberg, A. An Exopolyphosphatase of Escherichia Coli. The Enzyme and Its Ppx Gene in a Polyphosphate Operon. *J Biol Chem* **1993**, *268* (1), 633–639.

(113) Ma, Z.; Chandrangsu, P.; Helmann, T. C.; Romsang, A.; Gaballa, A.; Helmann, J. D. Bacillithiol Is a Major Buffer of the Labile Zinc Pool in Bacillus Subtilis. *Mol Microbiol* **2014**, *94* (4), 756–770.

(114) Glover, C. N.; Bury, N. R.; Hogstrand, C. Zinc Uptake across the Apical Membrane of Freshwater Rainbow Trout Intestine Is Mediated by High Affinity, Low Affinity, and Histidine-Facilitated Pathways. *Biochim Biophys Acta* **2003**, *1614* (2), 211–219.

(115) Daly, M. J.; Gaidamakova, E. K.; Matrosova, V. Y.; Kiang, J. G.; Fukumoto, R.; Lee, D.-Y.; Wehr, N. B.; Viteri, G. A.; Berlett, B. S.; Levine, R. L. Small-Molecule Antioxidant Proteome-Shields in Deinococcus Radiodurans. *PLoS One* **2010**, *5* (9), e12570.

(116) Sharma, A.; Gaidamakova, E. K.; Matrosova, V. Y.; Bennett, B.; Daly, M. J.; Hoffman, B. M. Responses of Mn2+ Speciation in Deinococcus Radiodurans and Escherichia Coli to γ-

Radiation by Advanced Paramagnetic Resonance Methods. *PNAS* **2013**, *110* (15), 5945–5950.

(117) Higgins, K. A.; Carr, C. E.; Maroney, M. J. Specific Metal Recognition in Nickel Trafficking. *Biochemistry* **2012**, *51* (40), 7816–7832.

(118) Miki, K.; Atomi, H.; Watanabe, S. Structural Insight into [NiFe] Hydrogenase Maturation by Transient Complexes between Hyp Proteins. *Acc Chem Res* **2020**, *53* (4), 875–886.

(119) Moncrief, M. B.; Maguire, M. E. Magnesium Transport in Prokaryotes. *J Biol Inorg Chem* **1999**, *4* (5), 523–527.

(120) Sargent, F. The Model [NiFe]-Hydrogenases of Escherichia Coli. *Adv Microb Physiol* **2016**, *68*, 433–507.

(121) Lacasse, M. J.; Douglas, C. D.; Zamble, D. B. Mechanism of Selective Nickel Transfer from HypB to HypA, Escherichia Coli [NiFe]-Hydrogenase Accessory Proteins. *Biochemistry* **2016**, *55* (49), 6821–6831.

(122) Krężel, A.; Bal, W. Studies of Zinc(II) and Nickel(II) Complexes of GSH, GSSG and Their Analogs Shed More Light on Their Biological Relevance. *Bioinorg Chem Appl* **2004**, *2* (3–4), 293–305.

(123) Musiani, F.; Zambelli, B.; Bazzani, M.; Mazzei, L.; Ciurli, S. Nickel-Responsive Transcriptional Regulators. *Metallomics* **2015**, *7* (9), 1305–1318.

(124) Diederix, R. E. M.; Fauquant, C.; Rodrigue, A.; Mandrand-Berthelot, M.-A.; Michaud-Soret, I. Sub-Micromolar Affinity of Escherichia Coli NikR for Ni(II). *Chem. Commun.* **2008**, No. 15, 1813–1815.

(125) Huang, H.-T.; Maroney, M. J. Ni(II) Sensing by RcnR Does Not Require an FrmR-Like Intersubunit Linkage. *Inorg Chem* **2019**, *58* (20), 13639–13653.

(126) Carr, C. E.; Musiani, F.; Huang, H.-T.; Chivers, P. T.; Ciurli, S.; Maroney, M. J. Glutamate Ligation in the Ni(II)- and Co(II)-Responsive Escherichia Coli Transcriptional Regulator, RcnR. *Inorg. Chem.* **2017**, *56* (11), 6459–6476.

(127) Aron, A. T.; Ramos-Torres, K. M.; Cotruvo, J. A.; Chang, C. J. Recognition- and Reactivity-Based Fluorescent Probes for Studying Transition Metal Signaling in Living Systems. *Acc. Chem. Res.* **2015**, *48* (8), 2434–2442.

(128) Dodani, S. C.; He, Q.; Chang, C. J. A Turn-On Fluorescent Sensor for Detecting Nickel in Living Cells. *J Am Chem Soc* **2009**, *131* (50), 18020–18021.

(129) R. J.P. Phillips, C. S. G. & W. *Inorganic Chemistry Volume II: Metals*; Oxford University Press, 1966.

(130) Brawley, H. N.; Lindahl, P. A. Low-Molecular-Mass Labile Metal Pools in Escherichia Coli: Advances Using Chromatography and Mass Spectrometry. *JBIC* **2021**.

(131) Kopaciewicz, W.; Regnier, F. E. Nonideal Size-Exclusion Chromatography of Proteins: Effects of PH at Low Ionic Strength. *Anal Biochem* **1982**, *126* (1), 8–16.

(132) Zhang, Y.; Akilesh, S.; Wilcox, D. E. Isothermal Titration Calorimetry Measurements of Ni(II) and Cu(II) Binding to His, GlyGlyHis, HisGlyHis, and Bovine Serum Albumin: A Critical Evaluation. *Inorg. Chem.* **2000**, *39* (14), 3057–3064.

(133) Xu, Z.; Wang, P.; Wang, H.; Yu, Z. H.; Au-Yeung, H. Y.; Hirayama, T.; Sun, H.; Yan, A. Zinc Excess Increases Cellular Demand for Iron and Decreases Tolerance to Copper in Escherichia Coli. *J Biol Chem* **2019**, *294* (45), 16978–16991.

APPENDIX I

RECIPES FOR LC AND ICP-MS

ICP-MS

1. Aqueous ICP-MS tuning solution
    a. Use Aqueous tune-labeled 50 mL volumetric flask; store in 50 mL conical tube
    b. 5.5 µL tuning solution (Agilent – ICP-MS Stock Tuning Solution)
    c. 1 mL trace-metal grade (TMG) Nitric acid (2% HNO_3)
    d. Raise to 50 mL with high-purity water (HPW)
        i. If tuning in He-high or H_2, add 100 µL of standard stock (TEXASAM-15REV3) solution

2. Organic ICP-MS tuning solution
    a. Use Organic tune-labeled 50 mL volumetric flask; store in 50mL conical tube
    b. 50 µL tuning solution (Agilent – ICP-MS Stock Tuning Solution)
    c. 1 mL TMG Nitric acid (2% HNO_3) – *optional*
    d. 0.1% HPW (50 µL for 50 mL total volume)
    e. Raise to 50 mL with choice of organic solvent for mobile phase
        i. If tuning in He-high or H2, add 100 µL of standard stock (TEXASAM-15REV3) solution

3. Aqueous Internal standard
    a. Use Aqueous iSTD-labeled 50 mL volumetric flask; store in 50 mL conical tube
    b. 1 mL internal standard (Inorganic Ventures – IV-ICP-MS 71-D)
    c. 1 mL TMG Nitric acid (2% HNO_3)
        i. The [HNO_3] of iSTD should match standards and samples; adjust as necessary

d. Raise to 50 mL with HPW

4. Organic Internal standard
    a. Use organic iSTD-labeled 50 mL volumetric flask; store in 50 mL conical tube
    b. 1 mL internal standard (Inorganic Ventures – IV-ICP-MS 71-D)
    c. 1 mL TG Nitric acid (2% HNO_3) – *optional* (this will be dependent on organic solvent of choice as not all organics are compatible with this strong acid)
    d. 0.1% HPW (50 µL for 50 mL total volume)
    e. Raise to 50 mL with choice of organic solvent for mobile phase

LC

Special notes

- All buffers should be made with the highest quality reagents (i.e., HPLC-grade, HPW, LC-MS grade, etc.)
- All buffers should be filter through a 0.2 µm Stericup filter into an acid-washed bottle prior to degassing (organics such as ACN, MeOH, and IPA **cannot** be filtered)
- All buffers for LC must be degassed

1. Acid Washed Bottle (all bottles used for LC mobile phases must be acid-washed)
    a. Add 10% TMG HNO_3 (in HPW) to the glass bottle and let soak overnight
    b. Rinse with HPW 3X before use

2. 100mM Ammonium (Amm.) acetate (pH 6.5)

a. 1L HPW

b. ~7.7 g of Amm. acetate (LC-MS grade) in fridge 2

c. Once dissolved, adjust pH to 6.5 with TMG HCl

3. 100mM Ammonium bicarbonate (pH 8.5)

a. 1 L HPW

b. ~7.9 g of Amm. bicarbonate in fridge 2

c. Adjust pH with TMG HCl or NaOH

4. 1X chelator buffer

a. 1 L HPW

b. 0.198 g ascorbic acid

c. 14.6 mg ethylenediaminetetraacetic acid (EDTA)

d. 19.0 mg ethylene glycol-bis(β-aminoethyl ether)-N,N,N′,N′-tetraacetic acid (EGTA)

e. 9.0 mg 1,10-phenanthroline

f. 7.81 mg 2,2-bipyridine

g. 18.0 mg bathocuproinedisulfonic acid (BCS)

h. 33 mg deferoxamine

i. 21.25 mg N,N,N′,N′-tetrakis(2-pyridinylmethyl)-1,2-ethanediamine (TPEN)

5. 10X chelator solution

a. 1 L HPW

b. All chelators' mass x10

6. 20mM ammonium acetate + dithionite ($Na_2S_2O_4$) (pH 6.5) – the dithionite at this pH is only stable for ~ 1 week
    a. Prepare 1M dithionite stock (store in LC box for 1-3 months)
        i. Weigh out 1.74 g dithionite into Eppendorf or 15 mL falcon tube
            1. *Caution:* loose powder
        ii. Bring into box
        iii. Add 4 mL of 0.5 M NaOH (cleaning solution inside LC box)
        iv. Vortex until >90% powder dissolves
        v. Dilute to 10 mL mark with HPW
        vi. Vortex until all dithionite is in solution
    b. ~1 L of HPW
    c. 1.554 g of Amm. acetate (LC-MS grade)
    d. Once dissolved, adjust pH to 6.5 with TMG HCl
    e. Once degassed, dilute dithionite into buffer (dilute such that minimal dithionite (1M) is introduced to the buffer to keep the desired pH)

APPENDIX II

ICP-MS TUNING INSTRUCTIONS

Tuning in Aqueous mode

1. Ensure that the correct torch is installed in the ICP-MS (if unsure, please ask)
    a. 2.5 mm for aqueous
    b. 1.0 or 1.5 mm for organics
2. Attach the gas regulator to the liquid or ultra-high-purity (UHP) argon (Ar) tank; open main gas valve; open back pressure valve
    a. Output of Ar tank should be between 500 - 700 kPa
    b. Back pressure output should be between 100 - 300 Psi
        i. Please refer to the troubleshooting manual if either of these conditions are not met
3. Attach the drain tubing to the ICP-MS T-splitter if not already connected
    a. Attach the drain tubing to the ICP-MS peristaltic pump
        i. Use the tube position closest to the ICP-MS
    b. Check to make sure the drain tube is not flat
        i. To determine if the tube is flat, compare the (to be) compressed section to one of the ends of the tubing; if significantly compressed, please replace and/or seek assistance
4. Connect the autosampler tubing to the ICP-MS T-splitter
    a. Attach the autosampler tubing to the ICP-MS peristaltic pump in the first position (closest to glovebox)

5. The other port of the splitter should be plugged with a blank nut (i.e., do not connect the internal standard)
6. Make sure to ground the splitter with the small, black conductive piece of the T-splitter (this is not the blank nut)
7. Turn on the circulator/chiller
    a. If low on fluid, replenish with: PolySci coolant
        i. The chiller has an indicator light that will turn on in the event of low on fluid
8. Open the ICP-MS Masshunter workstation in <u>administrator mode</u> by right-clicking the icon and selecting 'Run in Admin Mode'
9. Select the hardware tab
    a. Make sure autosampler appears under hardware of ICP-MS
        i. If it does not, right click sample introduction, select 'Properties,' toggle to the Sample Introduction drop-down, ensure 'Peripump' is chosen and check the box that states 'use autosampler'
10. Move the autosampler to the tuning solution (*please see Recipes for LC/ICP-MS google document*)
11. Click the tune icon
    a. 5 gas modes should appear (no gas, He-low, He-high, H_2, and Organic_Helow)
    b. Ensure 'override hardware settings' is NOT selected
    c. Ensure 'set as global tune' is NOT selected
12. Click the hardware icon, right-click on the plasma, select 'Properties'
    a. Set ignition mode for 'Aqueous'

13. Under Instrument tab, select configuration ignition sequence followed by selecting: ‘Standard Tune’ and checking: (1) run start-up on ignition and (2) wait for warm-up
14. Click on the Startup tab, select ‘Select Custom Settings’ (this will allow for automatic tuning and then go back to the Startup tab and select ‘Startup Configuration’ to ensure the proper configurations are checked (with the proper elements denoted):
    a. Torch axis (7, 89, 205)
    b. EM (80)
    c. Plasma correction (n/a)
    d. Standard lenses tune (7, 89, 205)
    e. Resolution/axis (7, 89, 205)
    f. Performance report (Oxide: 140; Doubly charged: 140)
    g. Full spectrum (n/a)
        i. Ensure the correct vial is set for these configurations (i.e., the vial with the tune solution)
15. Turn on the ICP-MS (Standby (yellow) to Analysis mode (green) will take some time, be patient):
    a. Click the drop-down area on the plasma tab and select ‘Plasma On’
        i. Make sure drain tube is connected!
        ii. Make sure the duct fan is <u>on</u>
            1. The fan should always be on, if the duct is not pulsating check if the fan is switched on (the fan switch is located behind the instrument table within a metal wall switch box)
    b. A warm-up period prior to the startup configurations will occur: ~23 min

i. The autosampler probe should be in the tune solution during this time

c. When the instrument is in analysis mode:

i. Forward power: 1550 W

ii. Reflected power: 0-10 W

iii. IF/BK pressure: 250 -270 Pa (<300 is acceptable; >300, check the cones followed by the roughing pump)

iv. Analyzer pressure: 3.3 - 4 Pa

16. Tune the instrument

a. Click on the tune tab

i. Select the appropriate tune tab by highlighting the tune file name and checking the appropriate box to the left of the name

1. all our tune files are after the collision gas/configuration used)
2. Nogas
3. He- low
4. He-high
5. H_2
6. Organic_Helow (only shown when organics are in use)

a. Do not change any parameters as from the 'Cell gas' section

i. Standard flow rates:

1. He (best for most transition metals except Fe); check 'Use Cell Gas' and then select 'He'

a. Flow: 3.6 ml/min

i. Higher flows (8.0 ml/min) are more optimal Cu, S, and Co)

2. H_2 (best for Fe); check 'Use Cell Gas' and then select 'H_2'

a. Flow: 4.0 ml/min (standard)

i. 5.0 ml/min = best for Fe

3. No gas (best for Na, K, Cl); do <u>not</u> check 'Use Cell Gas'

ii. If the appropriate tune file is not listed, add a new tune file by clicking the tab with (+) (this will copy all the settings from the current tune file select to the newly created file

b. Send the tune parameters to the ICPMS ('Send to ICPMS' button)

i. Make sure autosampler is still in the tune solution

c. Select monitor signal

i. Monitor element levels appropriate to each tune (set by HB) until stabilized (RSD% <5, preferrably <3) for 10-20 min

1. Nogas: 7, 51, 59, 78, 89, 205

2. He-low: 7, 51, 59, 78, 89, 205, 56/59

a. Same for Organic_Helow

3. He-high: 7, 51, 59, 78, 89, 205, 63, 65, 34

4. H_2: 7, 51, 59, 78, 89, 205, 56

5. If you are changing the collision gas from a previous setting, let the stabilization occur for 20 - 30 min

d. Once stabilized, stop signal monitor and then select for the instrument to autotune with the 'start auto tune' button

e. The system will automatically generate a tune report (only when in administrator mode).

    i. Analyze for the following modes:

        1. He mode checks:

            a. 59 (63 for He-high) counts: > 2400

            b. RSD (%) < 5 for all elements analyzed

            c. Gaussian shapes for resolution

            d. Oxide: < 1%

            e. Doubly Charged (70/140): < 2.5%

                i. If these are not obtained, adjust He flow; check carrier gas filter on back of instrument; prepare fresh tune solution; or see troubleshooting manual

                ii. If the oxide levels are high, re-perform plasma correction

        2. H_2 mode checks:

            a. 205 counts: > 6000 (with RSD(%) < 5)

                i. If not, adjust H_2 flow; check H_2 carrier gas filter on the back of the instrument; or see troubleshooting manual

3. Nogas mode checks:
    a. 79 counts: 3000
    b. 89 counts: 10000
    c. 205 counts: 6000
    d. RSD (%) < 5 for all elements analyzed

ii. If the tune is not successful, try the suggested tasks or defer to the troubleshooting manual

f. Save the tune report with the date, mode tuned, and initials (example: ICPMS-TuneReport 040521 He-low HNB)

g. Select for the tune to be global by selecting 'set as global tune' button

i. This will allow the tuning of the instrument to carry over into individual batches (i.e., you will <u>not</u> have to tune individually for each batch you create)

ii. You must ensure that the tune file in your batch is named the exact same as the global tune

Tuning in Organic Mode

1. Ensure that the correct torch is installed in the ICP-MS (1. 0 or 1.5 mm diameter torch)
2. Ensure that the Platinum sampler and skimmer cones are installed
3. Ensure the brass lens base is installed
4. Attach the gas regulator to the liquid or ultra-high-purity argon tank; open main gas valve; open back pressure valve
    a. Output of Ar tank should be between 500 - 700 kPa

b. Back pressure output should be between 100 - 300 Psi

    i. Please refer to the troubleshooting manual if either of these conditions are not met

5. Make sure 20% O_2/ 80% Ar tank is setup on the option gas line

    a. Output pressure should not exceed >100 kPA

6. Determine if you will be either self-aspirate the tune solution or feed in the tune solution via peristaltic pump (requires specific autosampler tubing)

    a. Self-aspirate if performing LC-ICP-MS

    b. Use peristaltic tubing if performing offline (need to condition the tubing)

7. Attach the drain tubing to the ICP-MS T-splitter if not already connected

    a. Attach the drain tubing to the ICP-MS peristaltic pump

        i. Use the tube position closest to the ICP-MS

    b. Check to make sure the drain tube is not flat

        i. To determine if the tube is flat, compare the (to be) compressed section to one of the ends of the tubing; if significantly compressed, please replace and/or seek assistance

8. Connect the autosampler tubing to the ICP-MS T-splitter if need be; if self-aspirating, disconnect autosampler tubing from the nebulizer tubing

    a. Attach the autosampler tubing to the ICP-MS peristaltic pump in the first position (closest to glovebox)

9. The other port of the splitter should be plugged with a blank nut (i.e., do not connect the internal standard)

10. Make sure to ground the splitter with the small, black conductive piece of the T-splitter (this is not the blank nut)
11. Turn on the circulator/chiller
    a. If low on fluid, replenish with: PolySci coolant
        i. The chiller has an indicator light that will turn on in the event of low on fluid
12. Open the ICP-MS Masshunter workstation in *ADMINISTRATOR MODE* by right-clicking the icon and selecting 'run in admin mode'
13. Ensure all the proper hardware/configurations are – click the hardware icon
    a. Sample introduction
        i. Either connect or disconnect the autosampler in the hardware of the ICP-MS
            1. Right click Sample Introduction, select 'Properties', toggle to the Sample Introduction drop-down, ensure Peripump is chosen and then either select or deselect 'Use Autosampler'
        ii. Ensure that the Micromist nebulizer is selected
            1. Right click Sample Introduction, select 'Properties' and toggle to 'Nebulizer'
    b. Plasma: right-click on the plasma, select 'Properties' and then set ignition mode as 'Organic'
    c. Ion Lenses: right-click on the ion lenses and ensure under 'Properties' that the model 'x-lens' appears
14. Configure user tune

a. Click tune gadget
    i. Select IPA from organic solvent parameters pull down menu (even if IPA is not the organic solvent being used)
b. Highlight and check the appropriate Organic_collisiongas tune file (or create if necessary)
    i. Currently only Organic_Helow created
c. Set this tune file as set base tune for startup

15. Click on Instrument tab, select 'Configuration Ignition Sequence followed by selecting 'User Tune'
16. Click on the Startup tab and select 'Select Custom Settings' (this will allow for automatic tuning and then go back to the Start-up tab and select 'Startup Configuration' to ensure the proper configurations are checked (with the proper elements denoted):
    a. Torch axis (7, 89, 205)
    b. User lenses tune (7, 89, 205)
    c. Resolution/axis (7, 89, 205)
    d. Performance report (Oxide: 140; Doubly charged: 140)
    e. Full spectrum (n/a)
        i. Ensure the correct vial is set for these configurations (i.e., the vial with the tune solution)
17. Turn on the ICP-MS (Standby (yellow) to Analysis mode (green) will take some time, be patient):
    a. Click the drop-down area on the plasma tab to toggle the plasma on
        i. Make sure drain tube is connected!

ii. Make sure the duct fan is ON

1. The fan should always be on, if the duct is not pulsating check if the fan is switched on (the fan switch is located behind the instrument table within a metal wall switch box)

iii. DE-SELECT Startup Configurations

b. When the instrument is in analysis mode:

i. Forward power: 1600 W

ii. Reflected power: 0-10 W

iii. IF/BK pressure: 250 -270 Pa (<300 is acceptable; >300, check the cones followed by the roughing pump)

iv. Analyzer pressure: 3.3 - 4 Pa

v. Option gas: 20-30%

vi. Peltier cooling: -5 degrees C

vii. Nebulizer gas: 0.55 L/min

18. Either by self-aspiration or via autosampler/peristaltic, rinse with 1:1 HPW/organic to condition the nebulizer and tubing for 30 minutes

a. A slower ramp of HPW (100%) to Organic (99%) may have to take place to condition the nebulizer

19. Once the nebulizer/tubing is properly conditioned, begin uptake of tune solution

20. Tune the instrument

a. Click on the tune tab

i. Make sure the appropriate tune file is highlighted and selected

b. Ensure:

i. Forward Power: 1600 W
ii. Torch depth: 8 mm
iii. Nebulizer flow: 0.55 L/min
iv. Option gas flow: 20-30%
v. Makeup flow: 0.1 L/min
    1. The more volatile the solvent, the more you should increase your option and makeup gas flow

c. Select monitor signal (same as aqueous tune files)
    i. Monitor element levels until stabilized (RSD% <5, preferably <3) for 15-20 min
d. Once stabilized, stop signal monitor and then select for the instrument to autotune by selecting the 'start auto tune' button
e. The system will automatically generate a tune report so long as in admin mode
    i. Analyze for the appropriate tune mode checks (see aqueous tuning above)
    ii. Do not worry about oxide levels in tune report (you are supplying O_2 into the system, the oxides will be higher)
f. If the tune is not successful, try the suggested tasks (per the aqueous section) or defer to the troubleshooting manual
g. Save the tune report with the date, mode tuned, and initials
h. Select for the tune to be global by selecting the 'set as global tune'
    i. This will allow the tuning of the instrument to carry over into individual batches (i.e., you will not have to tune individually for each batch you create)

Perform P/A factor tuning once/week

1. Prepare P/A factor tuning solution (50 mL): 1 mL of PA Tuning 1 (Agilent); 1mL PA Tuning 2 (Agilent); 5% TMG HNO_3; fill to 50 mL mark with HPW
    a. Prepare fresh monthly
2. Once all other Startup configurations have been completed, send the autosampler probe to the vial containing the P/A factor tuning solution
3. Once the solution has reached the nebulizer and has become an aerosol, click on Startup tab in Masshunter, deselect all other Startup configuration tasks except for the P/A factor tune
    a. Ensure the proper vial is selected
    b. Ensure the following elements are selected: As, Be, Cd, Zn, Mg, Ni, Pb, Al, Ba, Bi, Co, Cr, Cu, In, Li, Lu, Mn, Na, Sc, Sr, Th, Tl, U, V, Y, Yb
4. Select ‘add to queue’; once finished, proceed to send the autosampler vial back to the tune solution to prepare the day’s tune.

To change which masses are monitored for sensitivity when in the tune tab

1. Click tune tab
2. Select ‘Set acq parameters for sensitivity’ button

To determine the optimal cell gas flow for element of interest

1. Create a blank and standard containing element of choice (it is best if it contains a known interference of the element)

2. Click on the tune tab -
3. Select ‘Set acq parameters for sensitivity’ button to select the element of interest
    a. Be sure to return these values back to their previously monitored elements (see aqueous tuning steps above)
4. In the graphics window of the tune tab, right-click
5. Toggle to ‘advanced’ and select ‘ramp cell gas’.
6. Parameters:
    a. Select which gas by selecting the appropriate checkbox
    b. Choose desired range (step by 0.25 or 0.5 is recommended)
    c. Acquisition time should be approximately 200 s (this allows enough time for the liquid to traverse the autosampler tubing into the nebulizer).
    d. Ensure the proper vials have been selected for the blank and the standard
7. Click start when ready
8. When the ramp is finished, click print result
    a. save the result as a pdf -> save to the ‘cellgasramps’ folder on the desktop
    b. BEC = background equivalent concentration (want to minimize)
9. Update the tune files as necessary to reflect these optimal flow rates

Important note: At certain flow rates, the deflect of the octopole of the CRC has to be adjusted (there is no way to do this while ramping). To see if the deflect plays a role, find the optimal flow and then adjust the deflect slowly to see if there is an improvement in the sensitivity of the element (this is done just be monitoring the signal in the tune tab and adjusting the deflect under tune parameters by changing the value or using the arrows).

APPENDIX III

LC AND LC-ICP-MS INSTRUCTIONS

Contents:

1. Sample-Prep

- a. Filter all samples
    - i. 0.45 or 0.2 μm filter
    - ii. Molecular weight cutoff filtration is acceptable (Centricon or Amicon stir cell)
- b. Use either the 54-vial plate or 27 Eppendorf plate for loading sample vials
    - i. Eppendorf plate is also compatible with fraction collector
        1. When using the Eppendorf plate, use only 1.5 mL tubes (specifically the Surelock brand)
    - ii. When using the 54-vial plate, use vials with rubber septum screw cap
        1. 2 mL, 700 μL, and 300 μL vial options available

2. **Prior to analysis**

    a. Sign up for a time to use the instrument by sectioning off a date/time through the lab's LC/ICP-MS Google calendar

        i. Sign-up at least 24 hours in advance

        ii. Designate method (online in this case)

            1. If a heavy user, please use designated day of week

            2. If a light user, use one of the designated days of the week for light users

    b. Attach the gas regulator to the liquid or ultra-high-purity (UHP) argon (Ar) tank; open main gas valve; open back pressure valve

        i. Output of Ar tank should be between 500 - 700 kPa

        ii. Back pressure output should be between 100 - 300 Psi

            1. Please refer to the troubleshooting manual if either of these conditions are not met

        iii. If the liquid Ar tank is running low (there is an indicator in the middle of tank at the top), inform the instrument manager so that a new one can be ordered ASAP

        iv. UHP Ar gas tank can be purchased from the stockroom

            1. 1 <u>FULL</u> UHP Ar gas tank can be used for ~ 4-5 hours

    c. Ensure there is enough mobile phase for your analysis as well as for post-analysis cleaning (refer to LC/ICPMS recipes if you need to prepare more)

    d. Load the multisampler tray

i. Load your sample into sample container (vial plate or fraction collector tray)
    1. Add excess volume of desired injection volume (example: if the injection volume is 100 µL, then load 150 µL of sample)
    2. Smaller injection volume results in more resolute peaks
ii. Must push on multisampler drawer to open
    1. Sampler container will snap into place on the white collection tray
    2. Correctly orient the tray (align A1 in multisampler with A1 on the tray of choice)

3. Cleaning and Re-equilibration:

a. Every column should be free of residual metals prior to analysis
b. To assess if the column needs to be cleaned, perform ghost column (PEEK tubing in lieu of column) analysis
    i. If the ghost column shows adsorption onto the column of >20% or 250+ samples have been run, it is time to clean the column with a chelator buffer
c. To clean, run 1X chelator buffer through the column for 3 column volumes (CVs) followed by high-purity water (HPW) rinsing of 3 CVs
    i. 10X chelator should mainly be used as an injection (too much chelator results in discoloration of the column and thus, harsher cleaning methods with HCl or NaOH)
    ii. Monitor Zn-67 counts (these should decrease over time)

d. Once the column has been cleaned, it must be loaded with Zn-67 isotope
e. A de-gassed solution of 10μM Zn-67 isotope in 20mM AA pH6.5 should be used as a buffer
    i. First rinse the column with 3 CVs of HPW
    ii. Rinse the column with the Zn-67 loading buffer with 5 CVs
    iii. Rinse the column with 3 CVs of HPW
    iv. Re-equilibrate column to desired mobile phase (3-4 CVs)
        1. <u>This the proper number of CVs to effectively re-equilibrate the column with the desired mobile phase</u>
f. All cleaning and re-equilibration can be conducted via LC standalone (preferred) or LC-ICP-MS
g. To ensure the column is properly cleaned, inject 100-500 μL of HPW or mobile phase onto column with desired mobile phase
    i. If the column is clean, a flat baseline should be achieved during this injection
        1. Monitor such via LC-ICP-MS

4. LC Standalone:

a. Log into the LC-ICP-MS computer
    i. Login credentials are located on the desktop tower on a sticker
b. Disconnect the communication cable connecting the LC to the ICP-MS
    i. Beige colored line; plugs into the “remote” port on the back of the ICPMS
c. Launch OpenLab CDS software:

i. On the computer desktop, launch the shortcut Control Panel

ii. In control panel, the instrument configurations will be located on the left-hand side

iii. Select the instrument LC01

1. Launch online

2. Launch Offline should be used for data processing when the system is being used, such as during yours or a colleague's analysis

d. Open Lab CDS will launch and may take time to fully load

i. Wait 5 min before taking any other actions such as force closing the application

ii. a pop-up window will come up, select 'Download the Last Method' option

e. On the left side of the screen, ensure you are in the 'Method and Control' tab (all LC modules should be visible)

i. All six modules should be online (i.e., no grey status bars)

1. Multisampler, quat pump, 2 valve drivers, DAD, and fraction collector

f. Ready all modules by either selecting the 'on' button on the lower right of the module screen or by selecting the 'on' button for each individual module

i. Do NOT ready the quaternary pump unless the method loaded has the desired column in the flow path with the correct mobile phase conditions

ii. See troubleshooting document if a module does not ready

g. Load a method:

i. In OpenLab CDS select your desired method from your folder or load in a default method

1. There are default methods for ghost column, Superdex peptide (SP), dual Superdex peptide (DP), Superdex 200 (SD), and HILIC
2. Go to Method tab (top of screen) and select 'Load Method'
    a. Search through the file directory
        i. folder (1) (d drive)
        ii. <u>If using a default method be sure to resave the method under a new filename and place it into your sub-directory</u>

h. Edit a method (also used to check that all parameters of a default method are to your liking):

i. Under the Method tab, select 'Edit Entire Method'

1. Check 'Method Information' and 'Instrument/Acquisition' as the method sections to edit
2. In the 'Method Information' pop-up window, enter all pertinent method information details (column type, fraction collection method, flow rate, etc)
3. In the 'Injection Source/Location' pop-up window, ensure that HipAls is selected
4. In the 'Setup Method Window'…
    a. Quat Pump tab:
        i. Set flow rate for quat pump

1. Max flow rates (for 4 degrees C):
    a. Dual peptide: 0.25 ml/min
    b. Single peptide: 0.6 ml/min
    c. High mass: 0.6 ml/min
    d. HILIC: 0.5 ml/min
    e. Ghost column: n/a

ii. Select which solvent/buffer percentages you would like to use:

1. A= HPW (bottom MGCV port) – do <u>not</u> ever change!
2. B= organic (top MGCV port)
3. C= organic (top MGCV port)
    a. B and C can be changed to aqueous when organic solvents are not common use, but these ports need to be purged with organic solvent prior to use
4. D=100mM Amm. acetate pH6.5 or other aqueous based buffer (top MGCV port)

iii. Ensure pressure limits are correct

1. Minimum = 2 bar

2. Look at column manuals to ensure proper max pressure limits or see troubleshooting manual

iv. Set analysis time (dependent on column volume- check column manuals) in the Stoptime box

v. The timetable is only used when gradients are employed

b. Multisampler tab:

i. Input injection volume

ii. Needle wash: standard

1. Injection path cleaning -> set wash time between 3-15 s

iii. Sampling speed:

1. Draw speed: 100uL/min
2. Eject Speed: 500uL/min
3. Wait Time After Draw: 10 s

iv. Needle Height Position:

1. Offset: 0mm
2. Either select or deselect ‘use vial/well bottom sensing’ (not necessary)

v. High throughput

1. Sample flush out factor: 5
2. Do not select either 2 remaining boxes

c. Multisampler Injector Program tab: no additions
d. Valve tab:
    i. Valve 1 (reverse from LC-ICP-MS) refers to switch 1 or switch 2 (unnecessary if not flowing out of position 4
    ii. Set position switch at end of run to ‘do not switch’
e. Valve 2 tab:
    i. Valve 2 refer to flow paths 1- 4 (main columns)
    ii. Flow path is on the desktop for reference
    iii. Set position switch at end of run to ‘do not switch’
f. DAD tab:
    i. No change unless need to assess a particular wavelength
g. Fraction Collector tab:
    i. Design fraction collector program if necessary
        1. best to use timetable on right side
h. Instrument Curve tab:
    i. keep all selected

5. Select ‘OK’ once finished
6. Click Method tab and select ‘Save Method As’ if not saved to personal folder yet or ‘Save Method’ if already saved

i. Make a sequence (can do this through sequence -> sequence table or via sample entry):

i. For sample entry, select the Sample Entry tab in the main window of Open Lab
    1. This panel is divided into 4 panels:
        a. Multisampler plate location (top left)
        b. Selected plate well positions (top middle)
        c. Sample type (top right)
        d. Sequence list (bottom)
    2. Select the sample plate
        a. In the multisampler plate location, select the plate with your loaded samples
            i. Ensure that the multisampler is configured to the appropriate sample container you are using (to do this in the main module control screen, right click on the multisampler -> assign well plates -> scroll and select correct type)
    3. Sample Type: Select where your sample is loaded and its sample type
        a. Right click where your sample is located in the well/plate
        b. Click Append Samples and select 'Sample Type'
            i. For 'Sample type', select if it is a sample, blank, calibration, or control sample (sample is the main choice)
    4. Fill in sample information in the 'Sequence List':

a. In the sequence list, a new line should have been generated containing the container location and sample location
    i. Fill in the information for ‘Sample Name’ and ‘Sample Info’
    ii. Insert the desired method to be used for the sampler
        1. Select the column for the method name
        2. Click on the box to the left of the dropdown arrow in the ‘Method Name’ box and search the directory for your method

5. Set the directory your sequence will save to (save to the d drive):
    a. In the sequence list panel tool bar select the gear cog icon on the far right
        i. A new window will open up
        ii. Select the sub-directory that the sequence data will be stored in post-run (typically date_initials)
            1. You can make a subdirectory for the analysis performed on the date of analysis or by experiment, this is a user choice. Lab norms are to make a folder based on the experiment date (date you injected the sample into the LC system) as it is easier to search for a date than various experiment folders.

6. Append more samples if necessary
7. Save your sequence (save to the d drive):
    a. In the Sample Entry panel tool bar select save and save your sequence and give it a name

ii. To make a sequence via the sequence table, click the sequence tab and then select the sequence table

1. Fill in the sample location: D1F-(row)(number) (example: D1F-A2)
    a. (D1F) refers to the first plate, so do not change this nomenclature
    b. Each row in the vial plates is designated with a letter and then each position has a corresponding number
2. Fill in the sample name
3. Injection source: 'As method' should be selected
4. Fill in the injection volume in µL
5. Fill in the Inj/Loc
    a. This is asking how many injections per this location
        i. Typically, this is '1' but if you have multiple sequential injections, they can be loaded into one vial and use this function instead of creating multiple lines
6. Fill in the Sample Type
7. Fill in the Sample Amount

8. Fill in Sample Information
9. Select the correct Method Name from the drop-down list or via browsing through methods
10. If running a method that uses the fraction collector, the start and end positions of the fraction collection method can be set in the sequence table (optional)
11. All other fields can be left blank
12. Append additional samples by right clicking the in the table and either ‘insert’ (adds one line directly following the position you have highlighted) or ‘append’ (adds X lines to the end of the sequence)
13. Select ‘OK’ once finished

iii. Click the sequence tab and select ‘sequence parameters’

1. Create a subdirectory folder where the data will be stored (typically date_initials)
2. Add a comment on the data (add all pertinent details regarding sample type, column, conditions, etc)
3. Click ‘OK’ when finished

iv. Save the sequence table by clicking the sequence tab and selecting ‘Save Sequence Template As’ (save to the d drive)

j. When the sequence has been saved, you can add the sequence to the queue by:

i. Select ‘Add to Queue’ in the ‘Sample Entry’ box

1. Two popups will appear

a. Save the sequence
    i. Give the sequence a name and click ‘OK’
b. The second is the option to append the sequence to either the back or the front of the queue
    i. If this is the first run of the day, select ‘front of the queue’
    ii. If another run is already in progress, select ‘back of the queue’

ii. Click the Sequence tab, select ‘Sequence Table’, and click the ‘Run’ button
    1. Two popups will appear
        a. The first is the sequence parameters again
        b. The second is the option to append the sequence to either the back or the front of the queue
            i. If this is the first run of the day, select ‘front of the queue’
            ii. If another run is already in progress, select ‘back of the queue’

iii. Sample sequence will be located in the RunQueue tab located to the left of the Sample Entry tab

k. Once all sequences are queued in OpenLab main toolbar, do the following two things:

i. Queue a sequence to run 2-3 CV of HPW (the mobile phase) only down the column you have chosen to use (this washes the buffer out of the column/system to prevent degradation and clogging)

1. Set the injection amount to 0 and select the needle to pull from an empty vial

a. You must have a dud vial in the tray to do this

ii. Click the RunControl tab and select 'Queue Command'

1. Click the drop-down box arrow
2. Select for the quaternary pump to turn off

a. This will turn the flow rate to 0 ml/min once the run is done

b. This keeps the pump from potentially running dry of solvent

3. Repeat this step for turning off the lamp

a. The lamp should only be on during analysis to prevent pre-mature burnout

5. **LC-ICP-MS:**

a. Log into the computer

i. The computer credentials are located on a sticker on the desktop tower

b. Launch Services app of the LC computer; ensure that Windows update is disabled

i. If it shows as enabled, right click on the service, select properties, and from the drop-down select 'disable'

c. Assemble the ICP-MS in correct configuration (aqueous vs. organic)

d. Tune the ICP-MS in the appropriate mode (see ICP-MS tuning protocol)
e. Close the ICP-MS Masshunter and Chemstation softwares and re-open once the communication cable between LC and ICP-MS has been plugged in

OpenLab CDS:

a. Open the Open Lab CDS software
    i. On the computer desktop select the shortcut Control Panel
    ii. In control panel select the instrument LC_ICP_MS01
        1. Select 'Launch Online'
        2. 'Launch Offline' should be used for data processing when the system is currently in analysis
        3. Launching OpenLab CDS will take time to fully load
            a. Wait 5 min before taking any other actions such as force closing the application
    iii. A popup will ask you to confirm what modules are in LC_ICP_MS01 configuration
        1. Ensure that the valves, fraction collector, and diode array are the only modules in this configuration
    iv. A second popup will ask you to select a method, select 'download last method'
b. Ready the modules once they are loaded (see above LC standalone for how to ready the modules and/or see troubleshooting guide for assistance)
c. Load/save a method in OpenLab CDS:
    v. In OpenLab, select your desired method or default method

1. Click the Method tab and select ‘Load Method’ (warning: methods for LC-ICP-MS and LC-Standalone are NOT the same)
    a. LC methods have the start command triggered via the “HiALPS” selection; this is a start command coming from the multisampler whereas LC-ICP-MS methods have a start command triggered via a “Manual” selection
        i. The manual start occurs from the start command coming from the pump/multisampler that is controlled via Masshunter
2. Search through the file directory (2)
    a. Methods for each instrument selection are located in different root folders
        i. LC-ICP-MS: (2)
        ii. LC standalone: (1)
3. If using a default method, be sure to resave the method (Method tab -> select ‘Save Method As’) under a new filename and place it into your sub-directory
    a. NOTE: OpenLab CDS Methods for LC-ICP-MS are less specific than OpenLab CDS methods for LC standalone; thus, methods for LC-ICP-MS can be re-used time and time again (with only a new sequence needing to be created)

d. Making a sequence

vi. On the left-hand bar in OpenLab select Method and Run Control (if not already in this main window)

vii. Click the Sequence tab and select 'Sequence Table'

1. This brings up the sequence table, which can be modified (previous samples may be present); if so, lines can be deleted/cleared by selecting a line and right clicking the highlighted line
2. A single sample line should be present at the end which is left blank (the sequence table requires a dummy line at the end)

viii. In the new sequence line fill in the following columns:

1. Sample Location
    a. Insert the value "1" to the sample location field
        i. Note: The multisampler is NOT configured in this instrument configuration
        ii. Note: A value of "1" tells the instrument that it will not be a blank run and will come from location 1
            1. Location 1 is an arbitrary location that has no meaning in the current instrument configuration
            2. if 0 then the system registers the sample type as a blank and the system will automatically initiate a start command even if the injection profile is set to "Manual"

2. Sample Name
3. Select the Method from the dropdown list/directory
    a. Search through the directory window that appears and select your desired method
4. Injection Source: Use “As Method”
5. Injection and Sample volume
    a. Can put in a value, but the system will take the injection volume from the method used in Masshunter
6. Sample Information
    a. Scroll to the right to find this column
    b. Describe your sample in a meaningful way that will still be useful years in the future

ix. Once finished, select ‘OK’

x. Adjust sequence parameters by clicking the Sequence tab and selecting ‘Sequence Parameters’

1. Select or create the sub-directory that the sequence data will be stored in post-run (typically a date_initials)
2. Fill in sample description (please be descriptive; this will help you and those who follow you)

e. Save the sequence table by clicking the Sequence tab and selecting ‘Save Sequence Template As’

f. Run the sequence table by clicking the Sequence tab, selecting ‘Sequence Table’ and clicking the ‘Run’ button

xi. The system will transition into “waiting for injection”

g. Appending sample to sample queue (a new sequence must be created if a different mobile phase or injection volume is desired)

xii. Click RunControl (main toolbar) tab, select ‘Queue Sequence

1. A popup window will appear for you to select which sequence you would like to append
    a. If the sequence has not been created yet (but another sequence has been queued), you will need to launch offline LC_ICP_MS01 to create this sequence prior to queueing in the online software
2. A second popup window will appear for the sequence parameter of the sequence
3. A third popup window will appear asking if you would like to add the sequence to the back or front of the queue
    a. Add the sequence to back of queue if appending a run to a current run queue
    b. Add the sequence to front of queue if no other sequence is running

h. Once all runs are queued, perform the following as an added precaution (typically the shutdown of the ICP-MS when connected to LC will trigger shutdown of the LC):

xiii. Click the RunControl tab and select ‘Queue Command’

xiv. Click the drop-down box arrow

xv. Select for the quaternary pump to turn off

1. This will turn the flow rate to 0 ml/min once the run is done
2. This keeps the pump from potentially running dry of solvent

xvi. Repeat this step for turning off the lamp

1. The lamp should only be on during analysis to prevent pre-mature burnout

Masshunter:

a. After relaunching Masshunter, click the Hardware icon, right click on the Sample Introduction, select 'Properties', deselect 'Use Autosampler', select 'Agilent LC' from the Sample Introduction drop-down box (still within 'Properties')
    a. The multisampler and quat pump will now be controlled by Masshunter and will under the Agilent LC tab
b. Ready the modules when they are loaded
c. Prepare a batch file in Masshunter
    a. Open a default batch file that corresponds to the method loaded in OpenLab CDS by clicking the Batch tab (specifically the drop-down arrow) and selecting 'Open Batch folder'
    b. Save the batch under a new file name in your folder (d drive)
        i. Example: BatchName_Date
    c. In the Batch tab, select 'AcqMethod' tab
        i. In the sub-tabs, select 'Acq Parameters' tab
            1. Acquisition type = time resolved analysis (TRA)
            2. Do not select:

a. ‘Auto/Semi Auto Tune before Batch’
b. ‘Generate Tune Report’
c. ‘P/A Factor Adjustment’

3. Add all necessary elements and remove those that are unnecessary for your analysis
    a. The number of elements affects the cycle time (also known as the settling time of the quadrupole)
4. Set the integration time for all elements at 0.3 s; this will update the cycle time for the batch file
    a. Unlike offline, where the acquisition type is spectrum, time resolved analysis is limited in isotope ratio
    b. Want 20-40 points per peak
        i. If a peak is spread across 2 mL and 20 elements are analyzed, the cycle time would be 20*0.3 s = 6 s ; at 0.6 ml/60 s (flow rate of SP), 2 mL = 200 s spread, so the number of points per peak would be 33
5. Input the desired acquisition time in min (taking into account flow rate and CV)
    a. If a CV is 24 mL and the flow rate is 0.6 ml/min, the amount of time to for a run = 24/0.6 = 40 min; however, an additional 15-20 min (a void volume)

should be added to a run to account for any potential species interaction with the column

ii. In the sub-tabs, select ‘Agilent 1200 LC’ tab
    1. In the sub-tabs, select ‘Quaternary pump’
        a. Adjust the mobile phase percentages
        b. Adjust flow rate
        c. Adjust system pressure limits
        d. Acquisition time should match ‘AcqMethod’ tab’s acquisition time
    2. In the sub-tabs, select ‘Wellplate Sampler’ (first one)
        a. Change the sample volume to the desired amount
        b. Make sure to have:
            i. Draw speed: 100 µL/min
            ii. Ejection speed: 500 µL/min
            iii. Wait time post draw: 10 s
            iv. Check the box for the needle head vial bottom detection
            v. Under the ‘Advanced’ tab, keep the washing to 3-15 s in the flush port
    3. In the sub-tabs, select ‘Wellplate Sampler’ (second one)
        a. Injection programming panel
            i. Do <u>not</u> mess with this unless you really need it

1. if you are running normal viscosity (like water) aqueous samples you don't need it

ii. You might use to make your own injection program:

1. Utilizing the analytical sampling head for automatic dilutions/mixing
2. When you have an incredibly sticky/viscous analyte that then requires a special needle washing sequence

d. Click 'Send to LC' button

i. This will send the batch parameters for the pump and multisampler to the LC system

e. In the Batch tab, select 'Data Analysis Method' tab:

i. In the sub-tabs, select 'Basic Information'

1. Ensure analysis mode is 'Chromatogram'

f. In the Batch tab, select 'Sample List' tab

i. Match the samples according to the sequence queued in OpenLab CDS

ii. Insert the following information, match as best as possible to OpenLab CDS sample list:

1. Sample type

a. Decide on the sample type
b. Select sample unless you are running something specific

2. Sample Name
3. Comment
    a. Describe your sample in a meaningful way that will still be useful 1-3 years in the future
4. File Name
    a. Can make the same as sample name for simplicity
5. Vial#
    a. Example: P1-X
        i. P1 is tray 1
        ii. X = A1 or B1 or …
            1. If vial is in location B5 the vial# = P1-B5
            2. You can view the labeling system - select the Agilent 1200 LC tab under the instrument status panel and select the icon of the hotel draws in the multisampler module

g. When finished inserting/validating all the above information, click ‘Validate Method’ button followed by the ‘Save Batch’ button

h. When the batch has been verified select Add to Queue when you are ready to initiate analysis
    i. *Be sure your samples and LC methods/queues are setup appropriately prior to adding the batch to the queue in Masshunter*
    ii. *Ensure outlet of LC is attached to the T-splitter of the ICP-MS*
        1. *Ensure iSTD is attached to the T-splitter of ICP-MS if desired*
i. Always queue a sequence and subsequent batch to run 3 CV of HPW (mobile phase, not injection) down the column you have chosen to use last (this washes the buffer/system out of the column to prevent degradation and clogging)
    i. Set the injection amount to 0 and select the needle to pull from an empty (dud) vial
j. Select for the plasma to turn off once you have queued all batches for the day by clicking the 'Turn Off Plasma Button' in the Queue Icon
    i. This prevents the instrument from running continuously and using liq. Ar when not necessary

6. Appending sequences/batches:

a. A sample sequence/batch may be appended at the end of another analysis while the instruments are running, and the appropriate software is in use

OpenLab CDS

a. Open the “Offline” version of the software to make your sequence/adjust your methods while another analysis is running
b. When your sequence and/or method(s) are complete, you can queue them in the “online” software

Masshunter

a. Create a new batch as previously described above and then click ‘Add to Queue’ button to add the new batch after validating and saving
    i. All batches must be prepared sequentially

APPENDIX IV

LC, LC-ICP-MS, AND ICP-MS DATA ANALYSIS

LC-ICP-MS:

1. *To determine void cut-off in chromatograms (to understand which peaks are of importance):*
    a. Must calculate column void volume- need column diameter, length, and pore volume
        i. Example:
            1. Superdex peptide:
                a. Dimensions: 10 (d) x 300 (l) (mm)
                b. Porosity 7 µl
                    i. Average pore vol= 0.70
                c. Equation: vol (mL)= (d^2(pi)(l)(pv))/4)
                    i. d and l must be in cm
                d. Vol= 14.94 mL
                    i. Corresponds to ~25700 Da
    b. Divide void volume by flow rate to get column void in min
    c. To confirm this experimentally, run a high-mass standard such as Blue Dextran or Thyroglobulin on the Superdex peptide column

2. *To obtain raw LC-ICP-MS data*
    a. Launch ICP-MS (offline) data analysis software
    b. Click the down-drop arrow of the batch icon

c. Select open batch results

d. Navigate to your folder and your subsequent batch file you wish to analyze

e. The chromatogram is displayed on the lower half of the window

f. The green up and down arrow keys allow for toggling between different samples within a batch

g. The purple left and right arrow keys allow for toggling between different elements analyzed within a single sample

h. To extract the data, right-click within the chromatogram, select 'tabulate chart', followed by 'raw data to csv'

    i. This will bring up a separate excel window with the elution time (in seconds) versus all elements analyzed for that single sample

    ii. This process must be repeated for each sample

i. To change x-axis from time to volume eluted: (time point (in sec) * (1 min/60 s) * (flow rate in mL/1min))

3. *To determine molecular weight of peaks in chromatogram:*

    a. Determine the elution time of the peak of interest (converting seconds to minutes if necessary)

    b. Use the most recent LC-ICP-MS calibration curve to input minutes and receive molecular weight

        i. Keep in mind that these are APPARENT masses

ii. The calibration curve must be operated under the same conditions under which the sample was run (mobile phase concentration, pH, flow rate, temperature, etc)

4. *To extract the area under the curve from a chromatogram:*
    a. Launch ICP-MS (offline) data analysis software
    b. Click the down-drop arrow of the batch icon
    c. Select open batch results
    d. Navigate to your folder and your subsequent batch file you wish to analyze
    e. Click the DA method tab at the top of screen and select 'edit'
    f. Under 'set up analyte', select 'open data file'
        i. This will allow you to select which sample within the batch you would like to extract the area under the curve from
    g. In the chromatogram window, select the element you are interested in from the TIC/EIC drop-down box
    h. Typically, if a strong peak is present (S/N 3+), the software will immediately draw a line under the curve and list the area under the curve on top of the peak
    i. If this is not the case, click on the icon of a green peak with an informational "I" in the upper right (also found in the chromatogram window)
        i. A pop-up screen will appear with different chromatogram information that can be displayed
        ii. Check the box 'Area' in the EIC/TIC window and then select 'Ok'

j. Select the ‘start/end manual integration’ button (green chromatographic peak with an arrow cursor)
k. Now, drag the cursor on the chromatogram from baseline to baseline, encompassing the peak
l. Once finished dragging, the area under curve will appear above the peak
m. This area under the curve must be recorded manually as there is no way to export this number from the software. This must be down for each analyte of interest.
n. Once finished, select ‘return to batch-at-a-glance’
    i. Do <u>not</u> update the data analysis method

LC:

1. *To extract fraction collector start and stop times:*
    a. Launch OpenLAB CDS in the configuration in which you collected the data (either LC standalone or LC-ICP-MS)
    b. Click on data analysis tab in lower left corner
    c. Navigate to folder on the date in which the data was collected and select the appropriate sample sequence
    d. Double click on sample
    e. Click the ‘purify’ button
    f. Times should appear as a chart in lower right corner
    g. Screenshot an image of this chart for your records and store in word file or manually record

2. *To export diode array signals:*
    a. Launch OpenLAB CDS in the configuration in which you collected the data (either LC standalone or LC-ICP-MS)
    b. Click on data analysis tab in lower left corner
    c. Navigate to folder on the date in which the data was collected and select the appropriate sample sequence
    d. Double click on sample
    e. Click file -> export -> csv file
    f. Select data source as “signal”
    g. Check copy to clipboard
    h. Select which signal you desire to export (can only do one/time)
    i. Launch excel and paste the data into excel
        i. X data = time (min)
        ii. Y data = Abs (mAU)

ICP-MS:

1. *To extract offline data:*
    a. Launch ICP-MS (offline) data analysis software
    b. Click the down-drop arrow of the batch icon
    c. Select open batch results
    d. Navigate to your folder and your subsequent batch file you wish to analyze
    e. In the screen that opens…
        i. Internal standard stability graph will be on the lower left
        ii. Calibration curves each element on lower right

1. Data points shown in blue were collected in ‘pulse’ mode
2. Data points shown in green were collected in ‘analog mode

iii. The table of CPS or Concentrations for each element is at the top

1. Toggle between CPS and Concentration by selecting the buttons ‘Conc’ or ‘Count’ in the Full Quant batch table

f. Right-click in the batch table and select export to CSV file to open in excel

i. All elements will appear for all samples analyzed but only for CPS or concentration (i.e., this process will need to be repeated twice with a toggle between CPS/Conc)

2. *To analyze samples against a previously obtained standard curve:*

a. Launch ICP-MS (offline) data analysis software

b. Click the down-drop arrow of the batch icon

c. Select open batch results

d. Navigate to your folder and your subsequent batch file you wish to analyze

e. Click the DA method tab at the top of screen and select ‘edit’

f. On the left-hand side panel, select import DA method and STD data

g. Select file from which you’d like to pull standard information

h. On the left-hand side panel, select validate and then to return to batch-at-a-glance

i. When asking to update method, select yes

i. Reject old standards by check marking the boxes under the reject panel corresponding to those standards

j. Hit the process button to re-process that data with the previously obtained standards

APPENDIX V

ICP-MS STANDARD AND SAMPLE PREPARATION

General Considerations

- For moderate - low protein-containing samples, samples should be digested in minimal 70% trace-metal grade (TMG) nitric acid (HNO_3) for 24 hours (hrs) at 80 degrees Celsius
    - The current laboratory standard is 5% TMG HNO_3 (such that the final [HNO_3] is 0.5%)
- For high protein containing samples, samples should be digested in minimal TMG HNO_3 for 48 hrs at 80 degrees Celsius
- For samples that contain no protein, digestion is not necessary
- For a concentrated sample (ex, whole cells), less sample volume is needed to prepare offline samples (ex., 50 -100 µL)
- For a less concentration sample (i.e., cytosol, FTS, nuclei), more sample volume will be necessary. (i.e., 100 - 200 µL)
    - If limited volume of sample exists, calibration curve of standards will need to be adjusted to be within the range of sample

E. coli Samples

Whole cells (WC)

1. Spin down *E. coli* cells as directed by growth/isolation protocol
2. Obtain weight of cells
    a. Mass of cells / density of *E. coli* (~1.1 g/mL) / packing efficiency (~0.77)
        i. References:

1. https://www.ncbi.nlm.nih.gov/pmc/articles/PMC216012/
2. http://book.bionumbers.org/what-is-the-density-of-cells/

3. Dilute the aliquot of WC (i.e., aliquot of lysate from cytosol isolation prep or resuspended WC in buffer), 1:1 with high-purity water (HPW)
4. In triplicate, add 100 µL of WC resuspension to a 15mL (metal-free) falcon tube
5. Add TMG HNO_3 such that the final [HNO_3] will match the laboratory standard
6. Seal each falcon tube well with electrical tape
    a. Wrap tape in the same direction as the way the top tightens (in a clockwise direction when looking down)
7. Digest in oven at 80 degrees Celsius for 48 hrs
8. Once finished digesting, take the samples out of the oven and let cool to room temperature (RT)
    a. Check for particulate matter (further digestion may be necessary)
9. Dilute to final volume (5 -10 mL, depending on which elements are desired to be analyzed and how many potential times you would like to analyze these samples) with HPW

Cytosol/flow-through-solution (FTS)

1. In triplicate, add 50 - 100 µL of cytosol or FTS to a 15mL (metal-free) falcon tube
2. Add TMG HNO_3 such that the final [HNO_3] will match the laboratory standard
3. Seal each falcon tube well with electrical tape
4. Digest in oven at 80 degrees Celsius for 24 hrs
5. Once finished digesting, take the samples out of the oven and let cool to RT

    a. Check for particulate matter (further digestion may be necessary)
6. Dilute to final volume (5 -10 mL, depending on which elements are desired to be analyzed and how many potential times you would like to analyze these samples) with HPW

Yeast Samples

Whole cells

*Note: ensure excess metals have been washed off of cells by this point: 2x wash with 5 mL of 1mM ethylenediaminetetraacetic acid (EDTA) per g of cell pellet followed by 2x wash with 5 mL of deionized (DI) water per g of cell pellet. Remove wash supernatant each time by centrifugation at 5000 *xg* for 5 minutes (min).

Day 1

1. Pre-weigh a clean labelled Eppendorf tube
2. Resuspend DI water-washed cell pellet in HPW and add to pre-weighed tube
3. Centrifuge at 12000 *xg* for 10 min in minicentrifuge and discard HPW supernatant
4. Weigh Eppendorf tube and record difference as cell pellet mass
    a. For calculations: Cell packing efficiency is 0.7 g yeast/g pellet; cell pellet density is 1.1029 g pellet/mL pellet (Bryan, Andrea et al. PNAS 2010)
5. Resuspend pellet in known volume of HPW
    a. Leave a little headspace in the Eppendorf after adding HPW; otherwise, resuspension will take longer, and you risk overflow when trying to aliquot
    b. As a general rule aim for at least 2:1 ratio of HPW:pellet
6. Aliquot equivalent volumes into 3+ falcon tubes PER sample (triplicate is standard)

a. Depending on the initial volume of pellet and HPW added the suspension may be too viscous to properly draw via (micro)pipette
    i. P1000/P200 tips can be cut with scissors to better enable flow
b. Shake the Eppendorf tube before each aliquot as cells will settle over time

7. Add TMG HNO_3 to each falcon tube
    a. Volume needed will depend on final volume of offline sample; aim for 0.5% final [HNO_3]
    b. Offline sample volume is dependent on the number of elements to be analyzed along with the desired number of replicates analyses (i.e., you want all of these samples to be analyzed independently at least times)
        i. use plastic, serological pipette or designated micropipette for TMG HNO_3
8. Seal falcon tube tops with electrical tape
    a. Wrap tape in the same direction as the way the top tightens (in a clockwise direction when looking down)
9. Incubate in the oven at 80 degrees Celsius and for 48 hrs.

<u>Day 2:</u>

10. Remove samples from the oven and allow them to cool to RT
11. Adjust the temperature of oven down to 65 degrees Celsius
12. Unseal the samples (within a fume hood) and add equivalent volumes of undiluted (~35%) hydrogen peroxide
    a. Aim for 2.5% of final volume of offline sample
13. Reseal and incubate in oven at 65 degrees Celsius for 2 hours
14. Remove the samples from the oven and allow them to cool to RT

15. Dilute to desired final sample volume with HPW and store in at 4 degrees Celsius until analysis
16. Filter samples into fresh falcon tubes (optional)

Controls (designated as QCs in the batch files)

1. QC1 - blank (0.5% HNO_3)
2. QC2 - aliquot of standard level 2 or 3 (these serve as checks to monitor instrument stability and reproducibility throughout the analysis)
    a. Ideally, you want to run these at the beginning and end of a run in addition to in between different types of samples (ex., WC and FTS)

Standards

1. Use stock solutions: Inorganic ventures (TEXASAM-15 or TEXASAM-15REV3)
    a. REV3 contains 2x P and salts as compared to TEXASAM-15 to closely mimic cellular conditions
    b. TEXASAM-15 contains Fe-57
    c. Both stocks are prepared in 5% HNO_3
    d. High-purity standards ICP-MS-ISC-2 (in 2% HNO_3) is the stock solution for Ni analysis
2. 2 blanks (0.5% HNO_3)
3. Serial dilutions (5- at 5/0.5%):
    a. Level 5: stock -> 5 mL (this will be your only standard at 5%)

b. Level 4: 10-fold dilution of stock (no need to add extra HNO_3 as the concentration will be 0.5%)
c. Level 3: 10-fold dilution of standard level 4 (final [HNO3] = 0.5% HNO3)
d. Level 2: 10-fold dilution of standard level 3 final [HNO3] = 0.5% HNO3)
e. Level 1: 10-fold dilution of standard level 4 2final [HNO3] = 0.5% HNO3)

4. Arrange standards from least to most concentrated for analysis (b1, b2, 1, 2, 3, 4, 5)
5. If you add, H_2O_2 to samples, the same concentration must be added to all standards/blanks/iSTD

Wash

1. Create wash solution (0.5% HNO_3) from (70%) TMG HNO_3
    a. Use labeled 250 mL plastic bottles in autosampler tray

Internal Standard (iSTD)

1. Recipe can be found in LC/ICP-MS recipes
    a. Match [HNO_3] and if necessary [H_2O_2] from samples/standards to iSTD

APPENDIX VI

OFFLINE ICP-MS OPERATIONAL INSTRUCTIONS

ICP-MS Pre-analysis

1. Sign up for a time to use the instrument by sectioning off a date/time through the lab's LC/ICP-MS Google calendar
    a. Sign-up at least 24 hours (hrs) in advance
    b. Designate method (offline in this case)
        i. If a heavy user, please use designated day of week
        ii. If a light user, use one of the designated days of the week for light users
2. Attach the gas regulator to the liquid or ultra-high-purity (UHP) argon (Ar) tank; open main gas valve; open back pressure valve
    a. Output of Ar tank should be between 500 - 700 kPa
    b. Back pressure output should be between 100 - 300 Psi
        i. Please refer to the troubleshooting manual if either of these conditions are not met
    c. If the liquid Ar tank is running low (there is an indicator in the middle of tank at the top), inform the instrument manager so that a new one can be ordered ASAP
    d. UHP Ar gas tank can be purchased from the stockroom
        i. 1 <u>FULL</u> UHP Ar gas tank can be used for ~ 4-5 hours
3. For offline analysis, please make sure the communication cord (beige cord) that allows communication between the LC and ICP-MS is UNPLUGGED
4. Tune the ICP-MS in the appropriate tuning mode(s) *(see ICPMS tuning google document prior to launching Masshunter for analyses)*

5. Prepare trace-metal grade (TMG) nitric acid (HNO_3) wash (0.5 - 5% HNO_3) fresh using HPW
    a. Laboratory standard is currently 0.5% HNO_3
6. Once the tune is complete, move the autosampler probe to the position of this wash
    a. Make sure autosampler is in correct configuration (i.e., 21, 60, 60 ,60)
        i. Click the hardware icon, right-click on the autosampler icon, select 'Properties', toggle to the Rack tab, select the correct racks, and click 'OK' when finished
        ii. Allow ICP-MS to rinse in this wash for 30 min prior to analysis
7. If using internal standard (iSTD), connect to T-splitter with 15 minutes (min) left of HNO_3 pre-analysis wash
    a. Recipe for internal standard found in LC/ICP-MS recipes
    b. The T-splitter will have all three ports occupied (one with autosampler; one with internal standard; and one with drain tubing)
    c. The internal standard tubing should be positioned in the middle position of the peristaltic pump

ICP-MS Analysis

1. Create/load a method (i.e., batch)
    a. Click the Batch tab drop-down tab
    b. Create a new batch file from scratch or load in a default offline analysis batch file from default ICPMS methods in d drive

i. Default files have been created for the two main standard stocks (TEXASAM-15 and TEXASAM-15REV3) and for the three different CRC tune files (He-low, He-high, and H_2)

c. If loading in from default, click on the Tune tab (PRIOR to saving the default as your own), and select the appropriate tune file from the 4 possible files (selecting means highlighting the tab and clicking the check in the box)

i. At this point, now that the tune mode matches for the default file, you can save the file as your own in your own folder **(you must save this batch to your personal folder prior to editing the batch)**

ii. Fill in the sample list under the Sample List tab

1. Must indicate sample type, sample name, vial #, and level if a STD (*see offline sample/standard preparation for more detail*)

2. *Recommended*:

a. Sample name should match data file name

b. Add a comment about the types of samples (when isolated, dilution factors, etc)

iii. Under the Acq Method tab, toggle to the 'PeriPump/ISIS' sub-tab

1. Ensure the appropriate rinse vial (where the X% TMG HNO_3 wash is) is selected under Post Run: Rinse 1 vial #

iv. Click the 'Validate Method' button to check for any potential errors (i.e., renaming a sample the same name twice or listing an incorrect vial number, etc)

v. Click the 'Save Batch' button to save the file

d. If creating a new batch file (i.e., new standard stock purchased or new conditions necessary),
    i. Click Acq Method tab and select ‘Acq Parameters’ sub-tab:
        1. Acquisition mode: spectrum
            a. Spectrum mode options:
                i. Peak pattern: 3 pts
                ii. Replicates: 5
                iii. Sweeps/Replicates: 100
                    1. This number can be increased to achieve increased isotopic ratio precision
                iv. Tune mode: no quick scan
                v. Stabilization time: 30 s
                vi. Integration time/mass: 0.1 for main isotopes/elements
                    1. Int time should be adjusted for less abundant isotopes (for example, if Fe-56 = 0.1 s int; Fe-57 should be 4.3 s int)
        2. Acquisition options: highlight none
    ii. Click Acq Method tab and select ‘PeriPump/ISIS’ sub-tab:
        1. Uptake speed: 0.35 rps
        2. Uptake time: 60 s
        3. Stabilization time: 30 s

4. Rinse Vial: _ (select 1-4, depending on which position you place your X% TMG HNO_3 wash)
5. Rinse Speed: 0.35 rps
6. Rinse time: 120 s
7. No after acq rinse port, intelligent rinse, or execute pre-emptive rinse
    a. the rinse port is not setup for this autosampler

iii. Click Data Analysis Method tab and select 'Basic Information' sub-tab:

1. Check full quant analysis
2. Analysis mode: spectrum
3. Bkg subtraction if exists: count subtraction except for ISTD
4. Interference correction: acq. Defined

iv. Click Data Analysis Method tab and select 'Analyte' sub-tab:

1. Make sure all desired elements are listed for the appropriate tune files
    a. Possible analytes: 31P, 32S, 34S, 45Sc, 48Ti, 55Mn, 56Fe, 57Fe, 59Co, 63Cu, 64Zn, 65Cu, 66Zn, 67Zn, 68Zn, 89Y, 95Mo (these should match all analytes present in the standards)
    b. These analytes must match the analytes found in the Acq method tab
2. Select the appropriate tune mode for each analyte (see ICP-MS tuning protocol)

v. Click Data Analysis Method tab and select ‘Full Quant’ sub-tab:

1. Make sure appropriate tune mode is selected for each element
2. Units = user defined
3. Fill in appropriate concentrations for calibration standards
    a. These are listed on the stock bottle
    b. Ensure these concentrations are in the appropriate units defined
4. Select Sc and Y as internal standards (see LC/ICPMS recipes)

vi. Fill in the sample list under the Sample List tab:

1. Must indicate sample type, sample name, vial #, and level if a STD (*see offline sample/standard preparation for more detail*)
2. *Recommended*:
    a. Sample name should match data file name
    b. Add a comment about the types of samples (when isolated, dilution factors, etc)

vii. Click the ‘Validate Method’ button to check for any potential errors (i.e., renaming a sample the same name twice or listing an incorrect vial number, etc)

viii. Click the ‘Save Batch’ button to save the file

2. Add to queue (i.e., begin analysis) after the appropriate time has passed for the X% TMG HNO_3 pre-analysis wash by clicking the ‘Add to Queue’ button
3. Click the queue icon

a. If you would like the ICP-MS to shut off afterwards, in the queue, select the button ‘plasma off at end’
b. Select which vial you would like the autosampler to end in by (preferably wash solution or home) by clicking ‘vial # at end’ and selecting the appropriate vial

Shut-Down and Clean-up

1. Select the drop-down box next to the plasma icon and select ‘Plasma Off’ (if not previously queued by ‘plasma off at end’ button)
2. Turn off chiller/circulator
3. Unclamp the peristaltic pump
    a. Remove tension from the tubing (autosampler tubing, internal standard tubing, drain tubing)
4. Disconnect internal standard line from T-splitter
    a. Re-connect the blank net
5. Close back pressure valve on liquid Ar tank if regulator is on a liquid Ar tank
6. Re-cap all samples and standards and discard/store properly
7. Discard any additional HNO_3 wash down the sink

APPENDIX VII

TROUBLESHOOTING GUIDE FOR LC AND ICP-MS

LC

1. Identifying instrument errors:
    a. View logbook in OpenLab CDS (you will need to launch LC standalone or LC-ICP-MS01 from the OpenLab Control Panel) for details on why modules errored out
        i. To open the logbook, click on the View tab, select 'Logbook' followed by 'Current Logbook'
        ii. A new window will appear in the Methods and Control panel
        iii. View the logbook for an error (both error code and description)

2. Communication (or lack thereof) errors: When switching between LC standalone and LC-ICP-MS, the LC modules will error out as you are switching communication when swapping different instrument configurations; the modules can only communicate with one software at a time.
    a. Should be able to just clear error by pressing 'on' buttons in software
    b. Double check the communication cable that connects LC and ICP-MS is plugged in (if trying to run online)
    c. If there is no communication between the software and the instruments
        i. Check the router that the instruments are connected
        ii. Ping the instruments via command prompt

1. IP for LC: 192.168.254.11
2. IP for ICP-MS is 192.168.254.12
3. Local is 192.168.254.10
4. Computer: 165.91.176.17 (use this IP address when trying to connect to the LC computer remotely)

iii. Make sure the BootTable is active

1. BootTable is located under the "ICP-MS Masshunter…" folder in the windows start pane
2. MAC addresses are located on the desktop along with default IP addresses for LC and ICP-MS

d. If control panel states no connection to local server, navigate to the 'Services App' in Windows, find Agilent Openlab Shared Services, right click and select 'Start'; this will change the status to active (will change status to active)

e. If Masshunter goes unresponsive while running LC-ICP-MS, this is likely due to Window update being enabled

i. Navigate to 'Services App,' scroll down to Windows update, right click and select 'Properties' and then select 'disable'

ii. If this does not resolve the issue or Windows update was already disabled:

1. Open the Control Panel, specifically the Network and Internet settings; select 'Network Connections'
    a. Two connections: Ethernet (CHEM) and localhost
2. Disable the localhost and re-enable

3. Right click on the localhost connection, select ‘Properties’ followed by ‘Internet protocol version 4’
    a. Make sure the IP address is the local above
    b. Ensure the subnet mask is 255.255.255.0

3. To hard reset the LC system:
    a. Launch Agilent’s LabAdvisor and close OpenLab CDS
    b. Unplug each module via outlets on back of glovebox (3)
        i. Keep unplugged from ~10 s
    c. Re-plug in all outlets
    d. Press the power button on each module manually inside the box
    e. Connect the modules via LabAdvisor via the ‘Connect’ button on the main home screen

4. To cold reset the LC system (this requires access to the back of the LC multisampler):
    a. Unplug the two CAN cables (beige-colored, right next to each other)
    b. Unplug the power cable (black)
    c. Look at the original setup of the 6-labeled switches (small, illuminated by green light)
        i. All should be in the down position
    d. Turn off all modules
    e. Using a flathead screwdriver, place switch 1 and 6 in the ‘UP’ position and switches 2-5 in the ‘DOWN’ position.

f. Plug the power cable and CAN cables back in.

g. Turn the module on by pressing the front power button

h. Perform autoreferencing of multisampler (through LabAdvisor under 'Instrumental Control' by toggling to the Multisampler tab and clicking 'Control' followed by 'Special Commands')

i. Turn off module (and all other modules) if autoreferencing is a success

j. Flip all switches back to the original position

    i. Ensure all cables are correctly installed

k. Turn all modules back on

    i. Ensure the system goes into Standby

5. Multisampler-specific errors:

    a. Never reaches ready state (yellow indicator status):

        i. Make sure the door of module is correctly installed

        ii. Make sure both well plates are installed correctly and logged in the system

    b. Error 25235 and 25121 (OpenLab CDS) along with a "Z2 index missing" (Masshunter) error (potential solution from ND):

        i. Disconnect the LC from the ICP-MS via removing the COM cable from the ICP-MS

        ii. Shut down all software (Masshunter, OpenLab CDS, and Agilent LabAdvisor)

        iii. Hard reset the LC system (see above)

iv. Reconnect LC to the ICP-MS via the COM cable with no software open
v. Hard reset LC system
vi. Open Masshunter, configure the sample introduction with Agilent 1200 LC
vii. Hard reset LC system
viii. Open Masshunter, configure the sample introduction with Agilent 1200 LC
ix. Clear multisampler error in Masshunter by clicking the green 'On' button in the multisampler module display
x. Reset Multisampler injector by right clicking in the multisampler module display and selecting 'Reset Sampler'
xi. Close the Masshunter software and perform a multisampler autoreferencing in Agilent's LabAdvisor (see above)
xii. Close LabAdvisor and re-launch Masshunter

c. Clog in needle seat (this can be observed when a high pressure results upon injecting a sample)
    i. Remote unclogging (first attempt)
        1. Switch the valves of the LC to the ghost column (position 4, switch 2, position 4)
        2. Adjust the max pressure limit to 150 bar
        3. Send HPW (100% A) through the ghost column in Mainpass mode at a low flow rate (~0.1 ml/min)

a. The pressure should spike initially >100 bar and slowly begin to decrease

4. Gradually keep increasing the flow rate (0.25 or 0.5 ml/min at a time) until the clog has been cleared out
    a. This should take no more than 10 - 15 minutes to complete
5. Flush the system (in mainpass mode, flowing through ghost column) at 1.0 ml/min with HPW for 5 minutes
6. Set the LC back to desired mobile phase and flow rate
7. Set the LC valves back to desired column and **reset the pressure limits**
8. Ensure at the desired flow rate that the pressure is within column limits for the column

ii. For a more persistent clog (i.e., remote unclogging was not successful), a backflush of the needle seat is necessary)

1. Switch the LC valves to ghost column (position 4, switch 2, position 4)
2. Adjust the pressure limits to between 0 bar and 50 bar
3. Set the pump flow rate to 3 mL/min of HPW (100% A) through OpenLab CDS (LC standalone) or LabAdvisor
4. Open the purge valve of the quaternary pump (only quarter of a turn)

5. In LabAdvisor, navigate to the Maintenance tab, highlight the multisampler, and select ‘Maintenance Positions’ followed by ‘Replace Needle’
    a. The door to the module must be properly installed
    b. The sample handler will move the needle out of the needle seat (so as to allow you to replace the needle)
6. Perform the following steps while the multisampler is in ‘Service Mode’:
    a. Disconnect the seat capillary from port #5 of the injector valve
    b. Connect the needle seat capillary to port # 6
    c. Close the purge valve for 10 s
        i. You should observe flow through the seat capillary
    d. Open the purge valve for 10 s
        i. Have Kimwipes or paper towels on hand to collect the mobile phase flow at the needle seat so as to not trigger the leak sensor
    e. Continue to alternate opening and closing the purge valve for 5 – 10 minutes to rid the clog
    f. Open the purge valve
    g. Reinstall the needle seat capillary into port #5, return the capillary to the column or TCC to position #6

7. End the maintenance position (the sample handler will return the needle to the needle seat and perform an autoreferencing)
8. Either through OpenLab CDS or LabAdvisor, set the flow rate to desired rate to test the pressure of the system (remember to close the purge valve) rates.
    a. If pressure is normal, the procedure has worked
    b. Return pressure limits to normal limits
    c. If there is no flow out the needle seat and/or the pump pressures out, then the procedure was not successful, and the seat capillary will need to be replaced.

d. Pressure drops/spikes upon injection

During an injection, when the needle moves to the sample vial, the injection valve switches from mainpass to bypass mode (i.e., the flow is now going directly from the quat pump to the column instead of through the needle/needle seat). *When the injection valve switches from mainpass to bypass, there will be a slight pressure drop (this is dependent on flow rate as to exact pressure difference).*

i. When the needle returns from 'drawing up' sample and goes to switch from bypass mode back to mainpass (i.e., pressure should return to normal), the following malfunctions are possible:
    1. Pressure drop to 0 bar
        a. When this happens, no sample is drawn up

b. Stop the queued run immediately as the system does not know that a malfunction has occurred (there are 'Stop' button in both the Queue icon of Masshunter and the Method and Run Control tab of OpenLab CDS)
c. Once you observe green 'ready' status indicators for all modules, reset the multisampler in Masshunter by right-clicking in the module's graphic display and selecting 'Reset Sampler'
    i. This will take 2 - 3 minutes to complete
d. Once complete, requeue your batch beginning on the sample that was not successfully injected

2. Pressure spike such that the pressure limit was exceeded and the quat pump was triggered off
    a. This spike could have resulted from a clog; if the below steps below do not resolve the issue, please see the above steps to clear a clog (5c)
    b. Your batch will immediately terminate as the pressure will have exceeded the limit for the quat pump
    c. Reset the multisampler as stated in 5d1c
        i. You should immediately notice the pressure reading from the quat pump module decrease
    d. Allow the quat pump to flow through desired column at desired mobile phase for 5 - 10 minutes prior to re-

queueing the sample on which the run terminated (most times the sample is not drawn up during this malfunction; however, it is important to always add additional sample volume to vials)

i. It is recommended to perform a water injection once this malfunction has occurred to re-equilibrate the column and flow path since the quat pump had been shut off.

6. Water sensor detected a leak:
    a. Find the module that detected the leak
        i. Logbook records actions per module model number
    b. Clean up the leak and **determined what caused the leak**
        i. Check ferrules, tube connections, waste ports (i.e., check waste bottles; if these are full, the lines cannot properly drain)

7. No pressure over the system:
    a. Double check for leaks in ferrules or at unions
    b. If a mobile phase has run low, air has likely been sucked into the quat pump
        i. Set the flow rate to 0 mL/min in LC standalone
        ii. Open the purge valve (quarter of a turn)
        iii. Set the flow rate to 5 ml/min of HPW (100% A) for 10 minutes

1. You should be able to observe an air bubbles flushing out of the quat pump

iv. Set the flow rate to 0 mL/min and close the purge valve

v. Set to desired flow rate and test if pressure has returned to normal limits. If not,

1. Set the flow rate to 0 mL/min
2. Unscrew the quat pump outlet valve using LC wrenches inside the glovebox (loosen by unscrewing to the left)
3. Open the purge valve
4. Set the flow rate to 5 mL/min for 10 minutes
5. Set flow rate to 0 mL/min
6. Close the outlet valve and the purge valve
7. Test desired flow rate with HPW (100%)

8. Fluctuating pressure over the system (the pressure ripple should be < -2%; you can find this value under the quat pump tab in OpenLab CDS):

a. If the pressure ripple is > -2%, these following steps should be taken:

i. Check all ferrules of the LC system

ii. If no loose ferrules, the fluctuations could be caused by an air bubble

1. Set the flow rate to 0 mL/min
2. Unscrew the quat pump outlet valve using LC wrenches inside the glovebox (loosen by unscrewing to the left)
3. Open the purge valve

4. Set the flow rate to 5 mL/min for 10 minutes
5. Set the flow rate to 0 mL/min
6. Close the outlet valve and the purge valve
7. Test desired flow rate with HPW (100% A) for 15 - 30 min. If the fluctuations do not improve, re-perform the above steps for longer than 10 min.

9. High pressure over the system:
    a. Check for blockage in the LC flow path and isolate the blockage (do this by disconnect all parts of the flow path, starting with the DAD, then move to the valves, then the column, and finally the multisampler, leaving only the pump)
        i. For most blockages, the following will help:
            1. Flush IPA through the system (do **NOT** send IPA down the SEC columns) at a low flow rate (~0.3 mL/min) for 15 min
                a. Please keep in mind that organic solvents are to be placed on mobile phase lines B and C.
            2. Flush warm HPW water (bottle kept of HPW for warming in glovebox) through the system for 15 min (start at low flow rate and slowly increase, but do not exceed 1 mL/min)
            3. Rinse the LC system with glovebox temperature HPW (100% A) for 15 min at a normal flow rate

10. Determining the pressure limits for columns:

a. Refer to the column manuals to see the recommended flow rates for specific mobile phases
b. Flow desired mobile phase at assumed flow rate for 15 min
c. Monitor the pressure for the system as a whole (Quat pump, multisampler, column, and DAD). Record the total pressure of the system
d. Take the DAD out of the flow path by removing the tubing leading to the inlet. Be sure to have paper towels on hand to soak up the flow. Allow the system to flow for a few minutes. Record the pressure – DAD
    i. Total pressure - (pressure - DAD) = pressure of DAD
e. Take the column out of the flow path (this can be done by removing the tubing that leads to the valve, the column, or the outlet of the multisampler). Allow the system to flow for a few minutes. Record the pressure – Column
    i. Total pressure - (pressure - DAD) - (pressure - column) = pressure of column
    ii. Ensure the pressure drop over the column does NOT exceed the limits of the column
f. Take the multisampler out of the flow path by removing the tubing that flows from the top of the purge valve on the quat pump into the inlet of the multisampler valve (will need to remove the multisampler door to accomplish this). Allow the system to flow for a few minutes. Record the pressure – Multisampler
    i. Total pressure - (pressure - DAD) - (pressure - column) - (pressure - multisampler) = pressure of the pump

1. Equivalent to minimum pressure of the system

g. To set the max pressure limit: pressure of quat pump + pressure of multisampler + pressure of DAD + pressure limit of column
    i. These settings will need to be updated when the flow rate or temperature of the system is changed

11. Updating LC Firmware:
    a. Close all ChemStation/OpenLab CDS software, and launch LabAdvisor
    b. Connect the modules by pressing the 'Connect' button in the main screen
        i. The COM cable between the ICP-MS and LC should be unplugged
    c. Click on the Firmware Update tab (left side of the screen)
    d. Lock the system by clicking the 'lock' button
    e. Select firmware for desired modules (**resident should match main**)
        i. Use firmware files from 'Firmware_set_710' folder on the LC/ICP-MS computer desktop
        ii. All modules should not be disparate in terms of firmware updates (i.e., do not constantly update the multisampler without updating the other modules)
    f. Select 'Update' once all firmware files have been selected (this begins the download process)
        i. Do NOT power off any modules/computer during this time
        ii. Modules will blink red while updating
    g. Once finished, unlock the system and close LabAdvisor

i. As a precaution, restart the computer and power off-on each module

12. Updating LC drivers (only in case of software crash or malfunctioning equipment due to faulty software):
    a. Close ChemStation/OpenLab CDS and Masshunter softwares
    b. Ensure the remote COM cable between the two instruments is unplugged
    c. Click the Windows tab at the bottom left of the home screen, navigate to Agilent technologies, and launch OpenLAB Additional Software and Drivers Deployment Wizard
    d. Under component, select LC and CE Drivers, click next
        i. Uninstall if troubleshooting and no new updates from Agilent
        ii. Install if updating to a new patch
    e. To install, select 'Browse' and navigate to the 'Chemstation' folder on the LC/ICP-MS computer desktop; select the .xml file (if performing troubleshooting; if Agilent sends a new patch, store it in a folder on the desktop with ChemstationX (1,2, etc) for every new patch received); Select 'Agree to Terms/Conditions'
    f. The system will go through a verification process afterwards
        i. Ensure that it passes (a popup window will appear with the results)
    g. Once finished, close out of the wizard, restart the computer, and power off-on the modules
    h. Perform a test injection in LC standalone to ensure the drivers were properly installed and the system is functioning

ICP-MS

1. Identifying instrument errors:
    a. In Masshunter, click the Help tab, click the Search sub-tab, and type the error number into the search box; the error description along with suggested fixes will appear for the error code (and closely related codes)

2. Error 1220 (plasma shut off during analysis mode)
    a. Inspect the torch, torch shield, and bonnet
        i. If any piece looks damaged or dirty, replace/clean as necessary
    b. Ensure that no air is getting into the sample introduction system
        i. Systematically, cover inlets/outlets of sample introduction pieces with parafilm to isolate potential air leak
    c. Check the Argon flow rate and pressure building
        i. Try igniting with a secondary source of Ar in the event that a tank is contaminated
    d. Ensure that the RF coil is properly aligned by using the tool that measures the distance between coils
    e. Continuous appearance of 1220 error is indicative of issues surrounding the radio frequency generator

3. Error 1445 (low Argon flow rate)

a. If the pressure is not building in the liquid Ar tank, the small knob on the pressure building inlet, can be turned to the right (clockwise) to build pressure
    i. A specific wrench for this knob is located near the tank
    ii. This knob needs to only be turned one-quarter of a rotation
    iii. It will take ~ 5 - 10 minutes for the tank to "respond" and appropriately build pressure
        1. The pressure building vale should read between 100-300 PSI
b. Output pressure of the liquid or gas argon should be between 500 – 700 kPa

4. To allow Ar gas to flow into the instrument (recommended when switching argon sources)
    a. In Masshunter, click Hardware tab and right click on Sample Introduction icon, select 'Maintenance' followed by checking the box to 'Open the Ar gas valve'
        i. This valve will only stay open so long as you present on this maintenance screen

5. To hard reset the ICP-MS system:
    a. Inside the ICP-MS (lifting up the main hood that covers the vacuum portion of the ICP-MS), there is a small button on the lower righthand side. This automatically turns off the turbo pump.
    b. Press this button and allow the turbo to pump down for 5 -10 minutes before continuing to the next steps
    c. Push the power switch on the front of the instrument

d. Turn off the foreline pump switch on the back of the instrument
e. Flip the power switch for the instrument on the back of the instrument
f. After waiting for 5 minutes, turn on all switches in the reverse order
    i. Do **not** re-press the button on the inside of the machine to turn the turbo back on
    ii. The power button should turn green, and the instrument status indicator should turn grey (shutdown mode).
        1. Launch Masshunter software
        2. If the ICP-MS shows as offline (red X), right click on the mainframe section under the Hardware tab, select 'Communication Settings', click for the instrument to be online under the designated IP address.
        3. The instrument should come back online at this point
g. Turn the vacuum back on and wait for instrument to go into standby mode (yellow)

6. If the autosampler probe is not fully extending into solution (i.e., the probe tip is sitting above the desired solution)
    a. Confirm this a hardware and not a software issue by:
        i. Click the 'Autosampler' button and selecting for the autosampler to move to home by clicking the 'Home' button within this window (Masshunter)
        ii. Click the Click the 'Autosampler' button and select for the autosampler to move to a vial by clicking the on the vial's location (Masshunter)

b. If the probe still sits above the solution after 6a, inspect the back of the autosampler
    i. You will see a white, plastic thread that feeds through a loop on the back of the autosampler; this loop is responsible for the up-down position of the probe
    ii. If a small portion of this white thread is visible at the beginning of the loop (left side), push the remaining visible portion of the white thread through the loop
        1. This will push the probe down into the solution
        2. Confirm the probe tip is sitting just above the bottom of the vial
        3. Confirm the autosampler probe proper pulls the probe up and moves about the stage by repeating step 6a.
    iii. If no thread is visibly caught through the loop on the back of the autosampler, power the autosampler off and on, and repeat step 6a

7. If the nebulizer is clogged:
    a. Turn the instrument to Standby mode
    b. Carefully remove the nebulizer from the sample introduction system
    c. Remove the carrier gas line (you will need to press inwards on both sides of the union junction (black/yellow piece) to remove this piece (do so carefully so as to not break the nebulizer)
    d. The nebulizer can either be backflushed for a quick fix or soaked overnight for more stubborn clogs

i. Backflushing

1. Remove the autosampler probe tubing from the clear peristaltic tubing (leave the clear peristaltic tubing connected to the ICP-MS T-splitter)
    a. The T-splitter should have the autosampler introduction line, draining tubing, and a blank nut installed
2. Orient the clear peristaltic tubing such that the tubing is pulling sample away from the nebulizer (opposite from feeding sample into the nebulizer)
    a. As always, place the clear tubing in the first position of the peristaltic pump (position closest to the glovebox)
    b. Fasten the clamp (not too tight)
3. Gently place the nebulizer into a 50 mL falcon tube of 10% TMG HNO_3 in HPW
4. Place the loose end of the clear peristaltic tubing into an empty 50 mL falcon tube
5. In Masshunter, click on the Hardware icon, right click on Sample Introduction, and select 'Maintenance.'
6. Under Peripump settings, change the 'Nebulizer Pump' from 0 to 0.3 rps and press 'Enter'
    a. Do not exit out of the Sample Introduction Maintenance panel

b. You should begin to notice fluid dripping from the clear peristaltic tubing into the waste tube

7. Allow the nebulizer to backflush for 5 – 10 min
    a. If limited fluid goes into the waste, it is likely there is a more stubborn clog or worse, a broken nebulizer
    b. Once backflushing is complete, change the 'Nebulizer Pump' parameter to 0 rps and press 'Enter' in the Sample Introduction Maintenance panel
8. Dispose of the waste from backflushing but keep the waste tube
9. Carefully place the nebulizer inside of the waste tube (orient such that the tip of the nebulizer is not touching the bottom of the tube)
10. Place the open end of the clear peristaltic tubing into the 10% TMG HNO_3
11. Re-orient the clear peristaltic tubing such that fluid is feeding into the nebulizer
12. Once again, under Peripump settings in the Sample Introduction Maintenance panel, change the 'Nebulizer Pump' from 0 to 0.3 rps and press 'Enter'
    a. Allow flow out of the nebulizer for 2 minutes
13. In the Sample Introduction Maintenance panel, select to 'Open Ar Gas Valve' followed by setting the 'Nebulizer Gas' to 0.5 L/min
14. Take the nebulizer out of the waste tube and reattach the carrier gas line to observe:

a. A spray of liquid is coming from the nebulizer; the nebulizer is no longer clogged
    i. Set the ‘Nebulizer Gas’ to 0 L/min and the ‘Nebulizer Pump’ to 0 rps
    ii. Reattach the carrier gas line to the nebulizer and assembled the nebulizer back into the sample introduction system
    iii. Reattach the autosampler probe line back to the clear peristaltic tubing
b. No spray is coming from the nebulizer; the nebulizer is still clogged
    i. you can either backflush for a longer period of time or soak the nebulizer overnight and replace with a spare nebulizer

ii. Overnight soaking
    1. Prepare 500 mL of 10% TMG HNO_3 in HPW (designated bucket in LC/ICP-MS maintenance cabinet)
    2. Remove the white adapter that connects the nebulizer to the T-splitter of the ICP-MS
    3. Gently place the nebulizer inside the bucket with the solution
    4. Let soak overnight (~12 – 24 hrs)
    5. Once finished soaking, rinse the nebulizer with HPW
    6. Let air dry or heat dry in the oven

a. Set the temperature of oven to ~100 degrees Celsius
b. Carefully place the nebulizer on a watch glass
c. Let the nebulizer dry for 30 – 60 min

8. If the Startup configurations fail to due to lack of sensitivity:
    a. Confirm the autosampler probe is fully submersed in tune solution
    b. If the autosampler probe is in the tune solution, confirm:
        i. The autosampler tubing is correctly oriented/not flatten/securely fastened in the peristaltic pump
            1. Be careful not to overtight the peristaltic as the tubing will become flat rather quickly resulting in low uptake
        ii. An aerosol is visible in the sample introduction system
            1. If aerosol is not visible, ensure the correct nebulizer gas flow rate is applied
                a. If the flow rate is accurate and no aerosol is present, there is likely a blockage in the nebulizer
    c. If all physical checks have been performed:
        i. Prepare a 10X concentrated tune solution (50 mL)
        ii. Send the autosampler probe to this solution and allow enough time for solution to be nebulized and then perform the Startup configurations
            1. This is a way of tricking the instrument so as to properly align the sample introduction for sensitive measurements

iii. Send the autosampler probe to the standard 1X tune solution and re-perform the Startup configurations

9. If the tune lacks sensitivity:
    a. Confirm the autosampler probe is fully submersed in the tune solution
    b. Ensure the nebulizer is not clogged by visual affirmation of an aerosol in the sample introduction system
    c. Ensure the carrier gas filter for particular CRC gas is not contaminated with moisture or air
        i. See the GasCleanFilterSystem_manual.pdf for replacing the filter
    d. Prepare fresh tune solution with freshly aliquoted TMG HNO_3
    e. Check the IF/BK pressure meter of the ICP-MS
        i. If IF/BK pressure ~ 300+ Pa, the cones need to be inspected
            1. There may be a potential orifice clog, or the orifice is too large (> 1.0 mm for sampler and 0.4 mm for skimmer)
                a. If orifice is too large, the cone will need to be replaced
                b. See the 7700ICPMS Hard Maintenance Manual or Coneperfomancemanual_ICPMS.pdf for cone cleaning
    f. Inspect the lenses stack and polish if necessary (see 7700ICPMS Hard Maintenance Manual)

10. In the case of a **flood** (due to LC quat pump not shut off while in tandem with ICP-MS or faulty drain tubing):

a. Turn off the quat pump in OpenLab CDS/Chemstation and disconnect the LC from the ICP-MS
b. Disassembled all piece of the sample introduction system including torch, bonnet, and spray chamber
c. Rinse with glass pieces HPW and 10% HNO_3 (if applicable)
d. Dry all pieces (overnight in air or in oven at high temperatures for ~ 1 hr)
e. Clean torch box and all wet surfaces with Kimwipes
f. Leave torch box top open 12+ hrs to dry
g. Assemble sample introduction/torch box once all pieces are dry
h. Place the autosampler probe in a 1 - 2% TMG HNO_3 (in HPW) solution
i. Allow the instrument to "purge" with HNO_3 wash for 2-3 hours to gain sufficient sensitivity
    i. Test via tuning (fresh tune solution)